UNIVERSITY OF CALIFORNIA, SAN DIEGO

Seasonal Sand Level Changes on Southern California Beaches

A dissertation submitted in partial satisfaction of the
requirements for the degree Doctor of Philosophy
in
Oceanography

by

Marissa L. Yates

Committee in charge:

R.T. Guza, Chair
Scott A. Ashford
Neal Driscoll
Sarah T. Gille
Tara C. Hutchinson
Richard J. Seymour
Clint Winant

2009

The dissertation of Marissa L. Yates is approved, and it is acceptable in quality and form for publication on microfilm and electronically:

_____

_____

_____

_____

_____

_____

_____

Chair

University of California, San Diego

2009

To Mr. Lumbra and Mr. Tolle, who inspired me to be a scientist.

"Although nature begins with the cause and ends with the experience, we must follow the opposite course, namely, begin with the experience and by the means of it investigate the cause."

— *Leonardo da Vinci, (1452-1519), Notebooks*

"The outcome of any serious research can only be to make two questions grow where one grew before."

— *Thorstein Velben*

TABLE OF CONTENTS

LIST OF FREQUENTLY USED SYMBOLS

H	Wave height
T	Wave period
L	Wave length
E	Wave energy
S_{xx}	Radiation stress, cross-shore directed cross-shore component
S_{xy}	Radiation stress, cross-shore directed alongshore component
β	Beach slope
w_s	Sediment fall velocity
Ω	Dean's parameter

LIST OF FIGURES

LIST OF TABLES

ACKNOWLEDGMENTS

Many people have helped me reach this point, and it's hard to describe how much I've appreciated their support.

I owe my growth as a young scientist to my advisor Bob Guza, who had the patience, firm editing hand, and insistence on conciseness to guide me along the way. He taught me to pause and "cogitate," instead jumping to conclusions, and I am grateful that he shared his knowledge and energetic devotion to his work with me. His subtle encouragement was greatly appreciated, and his sense of humor brought me many laughs.

I would like to thank my committee members for their discussions and support along the way. Clint Winant encouraged me starting in my first year Fluid Mechanics class, teaching me how to think through problems. Dick Seymour provided insight, background knowledge, and suggestions on how to understand our observations. Sarah Gille gave useful assistance with data analysis techniques and has been thoughtful in her advice regarding future scientific positions. I am grateful to Neal Driscoll for trying to turn me into a geologist by taking me on a lab field trip and for teaching me to think about the beach as a highly interconnected system from the cliffs to the shelf. I would like to thank Scott Ashford for his encouragement and his desire to remain on my committee even after leaving UCSD to become the department head at Oregon State University. Finally, I especially appreciate Tara Hutchinson's gracious willingness to join my committee when I was more than halfway through my work, never hesitating to ask probing questions or to provide clarifications of our sediment analysis interpretation.

My work wouldn't have been possible without the sleepless survey nights, hours on the ATV, cold jetski rides, tough dolly pushes, and always-work-harder attitude of the survey crew. I owe many thanks to Bill Boyd, Dennis Darnell, Ian Nagy, Kent Smith, Brian Woodward, and all of the volunteers who have helped collect the in situ survey data. Roberto Gutierrez, from the University of Texas

at Austin, completed the lidar surveys.

Bill O'Reilly coupled this tremendous set of sand level observations with wave data, and all of the members of CDIP (Coastal Data Information Program), including Julie Thomas, Randy Bucciarelli, Grant Cameron, Darren Wright, and Corey Olfe have supported and made these data sets available.

I've appreciated support from Nate Huffnagle and Jerry Wanetick, who kept my computer running when it tried to crash on me in the final writing stages, and from all of those who have provided entertainment in the "dungeon" of Coast.

My family has supported and encouraged me along the road to my Ph.D., and I hope to make them proud. I thank my friends for all of the fun moments we've shared during first-year study sessions, dinner parties, and our backpacking trips. I especially thank Sébastien for sharing these last five years together, opening my eyes to a world beyond my own, and welcoming me to be part of his family.

I am grateful to have received a year of funding from the T.R. and Edith Folsom Graduate Fellowship, three years of funding from the National Defense Science and Engineering Graduate Fellowship, and one year of additional support from the ARCS Foundation.

The text of Chapter 2 contains some material that has been reformatted from the paper "Overview of Seasonal Sand Level Changes on Southern California Beaches," *Shore & Beach*, **77**(1), 1-8, which was awarded the 2008 American Shore & Beach Preservation Association Educational Award. The dissertation author was the primary researcher and first author with guidance provided by R.T. Guza, W.C. O'Reilly, and R.J. Seymour.

The text of Chapter 3, in full, is a reprint with minor modifications of the paper "Seasonal Persistence of a Small Southern California Beach Fill," *Coastal Engineering*, doi: 10.1016/j.coastaleng.2008.11.004 (in press). The dissertation author was the primary researcher and first author with guidance provided by R.T. Guza, W.C. O'Reilly, and R.J. Seymour.

The text of Chapter 4, in full, is a reprint with minor modifications of

the paper "Equilibrium Shoreline Response: Observations and Modeling," to be submitted for publication to the *Journal of Geophysical Research*. The dissertation author was the primary researcher and first author with guidance provided by R.T. Guza and W.C. O'Reilly.

The text of Appendix A, in full, is a reprint with minor modifications of the paper "A Technique for Eliminating Water Returns from Lidar Beach Elevation Surveys," *Journal of Atmospheric and Oceanic Technology*, **25** (9), 1671-1682, doi: 10.1175/2008JTECHO561.1 (Copyright of the American Meteorological Society 2008). The dissertation author was the primary researcher and first author with guidance provided by R.T. Guza, R. Gutierrez, and R.J. Seymour.

VITA

2003	B.S., Environmental Engineering, Massachusetts Institute of Technology
2003–2009	Research Assistant Scripps Institution of Oceanography, University of California, San Diego
2009	Ph.D., Physical Oceanography Scripps Institution of Oceanography, University of California, San Diego.

PUBLICATIONS

Sanford, L.P., P. Dickhudt, L. Rubiano-Gomez, M. Yates, S. Suttles, C. Friedrichs, D. Fugte, and H. Romaine, 2005: Variability of suspended particle concentrations, sizes and settling velocities in the Chesapeake Bay turbidity maximum. *In* Flocculation in Natural and Engineered Environmental Systems. I.G. Droppo, G.G. Leppard, P. Liss, and T. Milligan, Eds. Boca Raton, Florida, CRC Press, LLC: 221-236. UMCES Contribution No. 3597.

Yates, M.L., R.T. Guza, R. Gutierrez, and R. Seymour, 2008: A Technique for Eliminating Water Returns from Lidar Beach Elevation Surveys. *J. Atmos. and Ocean. Tech.*, **25**(9), 1671-1682, doi: 10.1175/2008JTECHO561.1.

Yates, M.L., R.T. Guza, W.C. O'Reilly, and R.J. Seymour, 2009: Overview of Seasonal Sand Level Changes on Southern California Beaches. *Shore & Beach*, **77**(1), 1-8.

Yates, M.L., R.T. Guza, W.C. O'Reilly, and R.J. Seymour, 2009: Seasonal Persistence of a Small Southern California Beach Fill, *Coast. Eng.*, doi: 10.1016/j.coastaleng.2008.11.004.

Yates, M.L., R.T. Guza, and W.C. O'Reilly, 2009. Equilibrium Shoreline Response: Observations and Modeling. *J. Geophys. Res.*, to be submitted.

SELECTED PRESENTATIONS

Madsen, O.S. and M.L. Yates, 2004: On Wave Reflection from Beaches, *International Conference of Coastal Engineering*, Lisbon, Portugal.

Yates, M.L., R.T. Guza, R.J. Seymour, W.C. O'Reilly, and J.O. Thomas, 2006: Seasonal Sand Level and Wave Variability on Southern California Beaches, *International Conference of Coastal Engineering*, San Diego, California.

Yates, M.L., R.T. Guza, R.J. Seymour, W.C. O'Reilly, 2006: Seasonal Sand Level and Wave Variability on Southern California Beaches, *California and the World Ocean*, Long Beach, California.

Yates, M.L., R.T. Guza, R.J. Seymour, and W.C. O'Reilly, 2008: Seasonal Beach Changes and Equilibrium Concepts, *AGU, Ocean Sciences Meeting*, Orlando, Florida.

Yates, M.L., R.T. Guza, R.J. Seymour, and W.C. O'Reilly, 2008: Sand Level Changes and Beach Equilibrium Concepts, *International Conference of Coastal Engineering*, Hamburg, Germany.

Yates, M.L. and R.T. Guza, 2008: Seasonal Sand Level Changes on Southern California Beaches: Observations and Modeling, *Physical Oceanography Dissertation Symposium*, Honolulu, Hawaii.

Yates, M.L., R.T. Guza, W.C. O'Reilly, and R.J. Seymour, 2008: Overview of Seasonal Sand Level Changes on Southern California Beaches, *American Shore and Beach Preservation Association National Coastal Conference: Sustainable Shorelines*, Chicago, Illinois.

Yates, M.L., R.T. Guza, R.J. Seymour, W.C. O'Reilly, and A. Young, 2008: Alongshore Variability of Shoreline Change and Geologic Factors, *AGU, Fall Meeting*, San Francisco, California.

FIELDS OF STUDY

Major Field: Oceanography (Physical Oceanography)

Studies in Descriptive Physical Oceanography
Professors Myrl C. Hendershott, Paul E. Robbins, Dean H. Roemmich, and Lynne D. Talley

Studies in Fluid Mechanics:
Professors Clint Winant, Richard Salmon, and Paola Cessi

Studies in Data Analysis and Statistics:
Professors Robert Pinkel, Daniel Rudnick, and Sarah Gille

Studies in Applied Mathematics:
Professors Glenn Ierley, Stefan G. Llewellyn-Smith, and William R. Young

Studies in Waves:
Professors Myrl C. Hendershott, R.T. Guza, and Ken Melville

ABSTRACT OF THE DISSERTATION

Seasonal Sand Level Changes on Southern California Beaches

by

Marissa L. Yates
Doctor of Philosophy in Oceanography
University of California, San Diego, 2009
Professor R.T. Guza, Chair

Seasonal airborne and ground-based observations of sand level changes were made along the coast of southern California from 2001 to 2008. Hourly, high alongshore spatial resolution wave estimates from a network of wave buoys and a spectral refraction wave model complement the sand level change data. Water returns from the ocean surface were removed from the airborne lidar elevation observations with a new method using tide and wave data, which was validated with concurrent in situ surveys. The resultant sand levels show high alongshore variability in seasonal shoreline position change along the 120-km survey region. Alongshore variability in wave energy, geologic factors, and sand grain size are hypothesized to control the alongshore variability of the seasonal shoreline change magnitude.

Monthly or more frequent ground-based surveys at four selected focus sites show seasonal shoreline and bathymetry change, with winter shoreline erosion and offshore bar development, and summer shoreline accretion and the loss of the

offshore bar. Analysis of surveys completed after a small beach nourishment at Torrey Pines Beach showed the presence of the nourishment through more than one full seasonal cycle.

Observations from Torrey Pines Beach show the dependence of shoreline change on the initial shoreline position and the wave forcing. The observations motivated the development of an equilibrium shoreline change model, which accurately reproduces the observations with four free parameters. With at least two years of monthly surveys or multiple years of appropriately-timed biannual observations used to determine the free parameters, the model accurately predicts withheld observations and is applied at the additional survey sites. Ongoing work includes applying the model at additional locations and investigating the relationship between the tuned parameters and geologic factors.

1

Introduction

Beaches respond to waves, wind, and currents with changes spanning a wide range of temporal and spatial scales. From grain-to-grain interactions occurring over seconds and millimeters, to the reshaping of kilometers of coastline during storms, to hundreds of years of slow progression, a variety of processes interact to cause coastal change. Understanding beach change is necessary for understanding the future of coastlines and for making informed beach management decisions. Efficient tools are needed to model large-scale beach change over monthly to yearly time periods, and observations are critical for understanding the dominant forces controlling large-scale beach change.

Using unique observations of sand levels and waves, this dissertation explores seasonal beach change in southern California. Large-scale, biannual lidar observations spanning tens of kilometers show significant alongshore variability in the magnitude of the shoreline change seasonal cycle, and the importance of geologic factors in controlling the observed alongshore variability are discussed in Chapter 2. High temporal resolution change is observed at selected in situ focus sites spanning a few kilometers each. Monthly and more frequent shoreline surveys and nominally quarterly bathymetry surveys resolve beach profile change between about -10 m water depth and the backbeach. At one of the focus sites, a beach

nourishment project was monitored and showed seasonal persistence even though the nourishment volume was small compared with the volume of the seasonal cross-shore exchange of sand (Chapter 3). More than five years of high temporal resolution shoreline observations at Torrey Pines Beach are used to develop and test a simple equilibrium beach change model in Chapter 4. The model is extended to the additional focus sites, and with sufficient data, the model can be applied over large spatial scales.

1.1 Sand level measurements

Beach surveys once consisted of making step measurements with a set of graduated rods (Emery, 1961) or using standard surveying techniques with a rod and level (Winant et al., 1975) or a laser-ranging total station. These methods, while reasonably accurate with beach face profile errors of a few centimeters (Emery, 1961), are time-consuming. Global Positioning System (GPS) technology has vastly decreased the time required to complete surveys on land and under water (Morton et al., 1993; Gibeaut et al., 1998). The application of airborne lidar survey systems to the coastal zone has further improved beach survey spatial resolution and alongshore coverage achievable within a short period of time (Brock et al., 2002; Sallenger et al., 2003), but the cost usually prohibits frequent surveying. In this study, lidar and in situ surveys temporally and spatially resolve the seasonal sand level changes in southern California. Ten biannual lidar surveys span 80 km of coastline between Point La Jolla and Dana Point, with the four most recent surveys extending approximately 120 km from the Mexican Border to Los Angeles (Figure 1.1). Within this region, four additional in situ focus sites spanning 2 to 8 km each were surveyed more frequently for at least one year (Figure 1.2).

The lidar elevation surveys provide spatially dense (multiple points per square meter, Figure 1.3) observations of the cliffs, beach, and ocean surface (for lidar specifications, see Appendix A). A spatially-defined backbeach contour was

manually identified from aerial photography along the entire coastline, removing cliffs, revetments, and buildings from all lidar surveys. The near infrared laser does not penetrate the water column and instead gives returns from the ocean surface. A technique to remove water points from the lidar data set using the tide level and wave data is described in Appendix A. The final product is a high resolution elevation map of the subaerial beach (e.g. Figure 1.4c). Multiple surveys can be used to estimate changes in shoreline (Stockdon et al., 2002) and beaches and dunes (Saye et al., 2005; Woolard and Colby, 2002).

At the in situ focus sites (Figure 1.2), monthly, biweekly, weekly, and

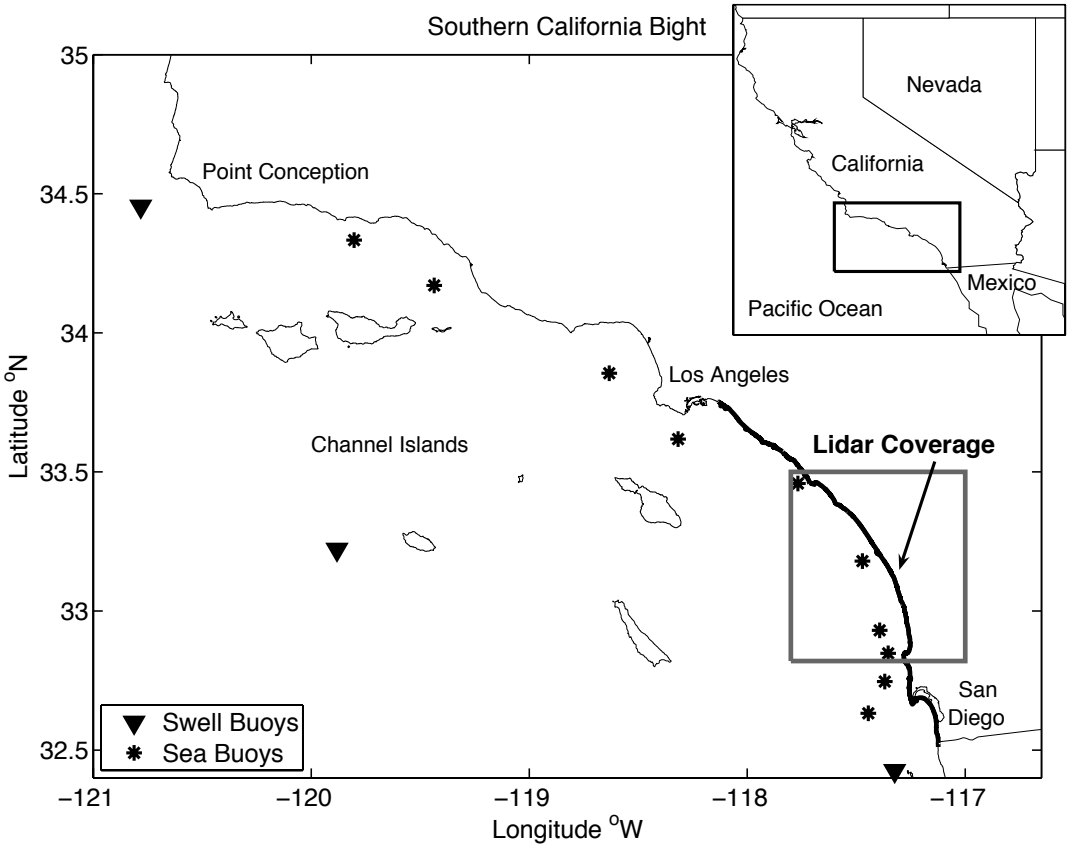

Figure 1.1: Map of the Southern California Bight showing the coastal lidar survey coverage (thick line), with the gray box identifying the most frequently surveyed 80 km reach shown in Figure 1.2. CDIP's three offshore swell buoys (triangles) and ten nearshore sea buoys (asterisks) are identified. The inset shows the map location (black rectangle).

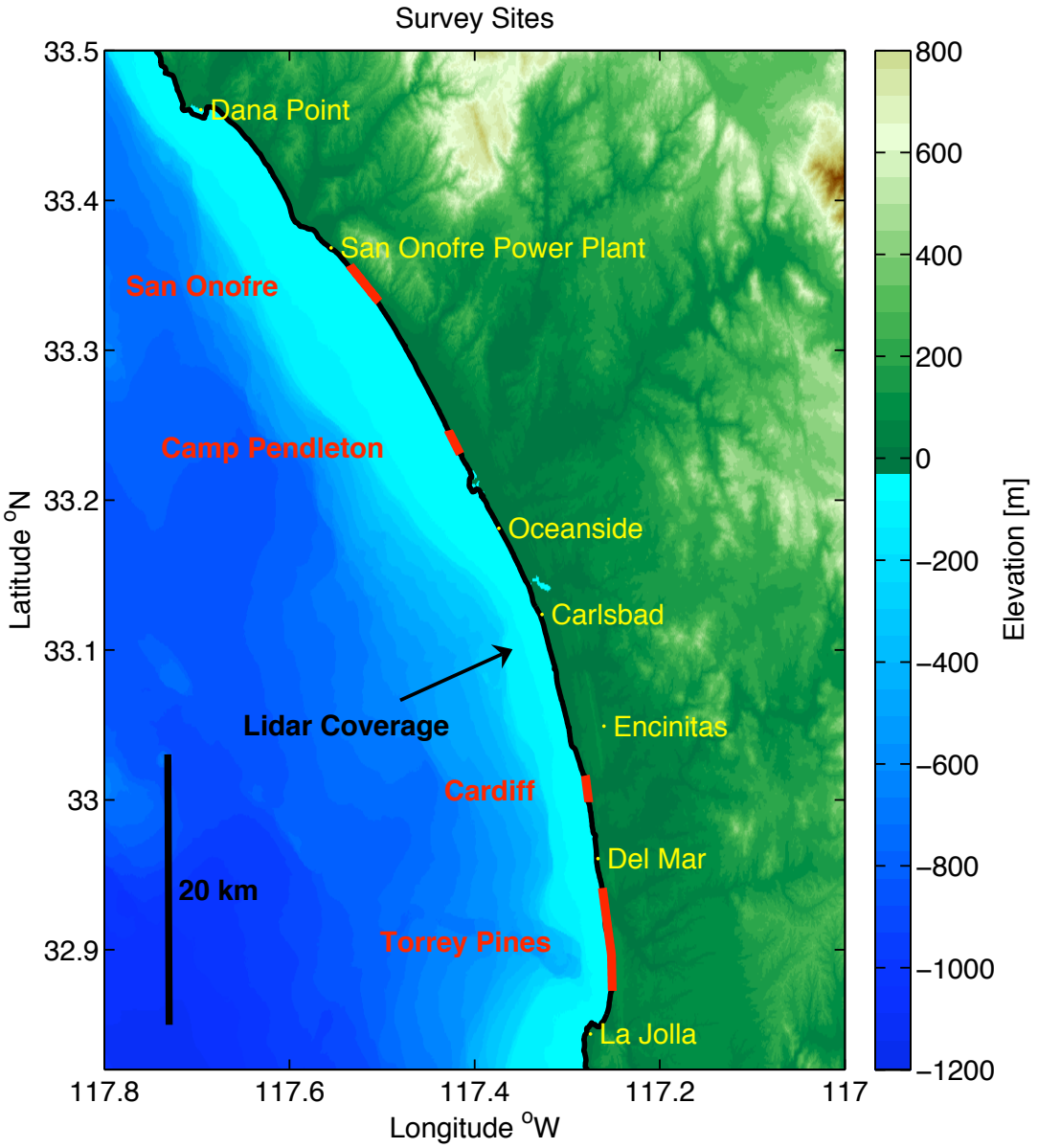

Figure 1.2: Map of lidar survey (black lines) and in situ survey (red lines) coverage. The map location is identified in Figure 1.1.

storm-response surveys of the subaerial beach are completed with a GPS-equipped all terrain vehicle (ATV), which drives alongshore-parallel tracks spaced approximately every 10 m in the cross-shore (Figure 1.4b). Approximately quarterly bathymetry surveys are completed on cross-shore transects spaced about every 50 to 100 m alongshore (Figure 1.4a). At low tide, a GPS-equipped ATV and hand-

pushed cart survey the exposed beach, and at high tide a GPS-equipped personal watercraft with an acoustic depth sounder surveys to approximately -10 m water depth. The in situ surveys supplement the lidar surveys with observations of the offshore bathymetry and with higher temporal resolution surveys to resolve better the seasonal cycle.

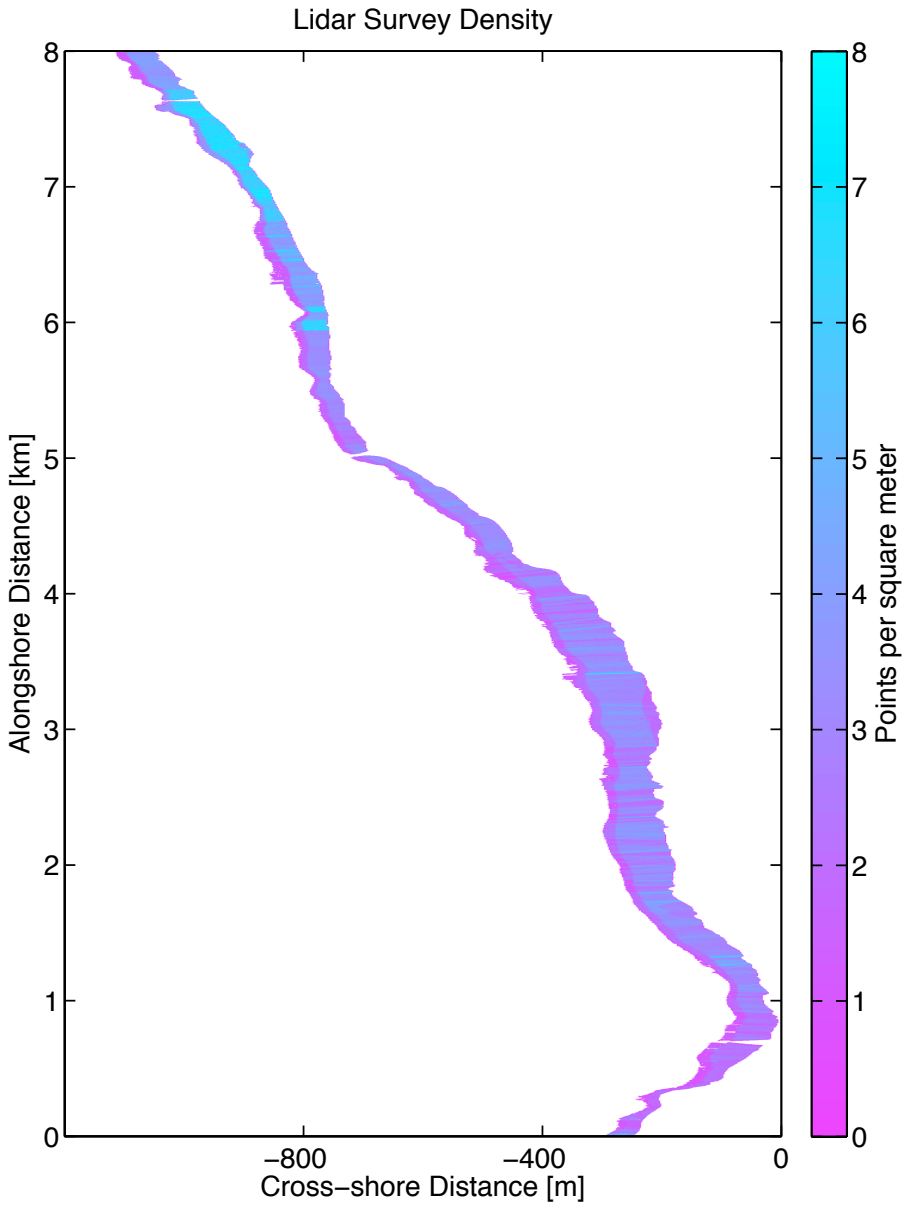

Figure 1.3: Spatial density (points per square meter) of lidar returns during the 2 April 2004 survey of Torrey Pines Beach.

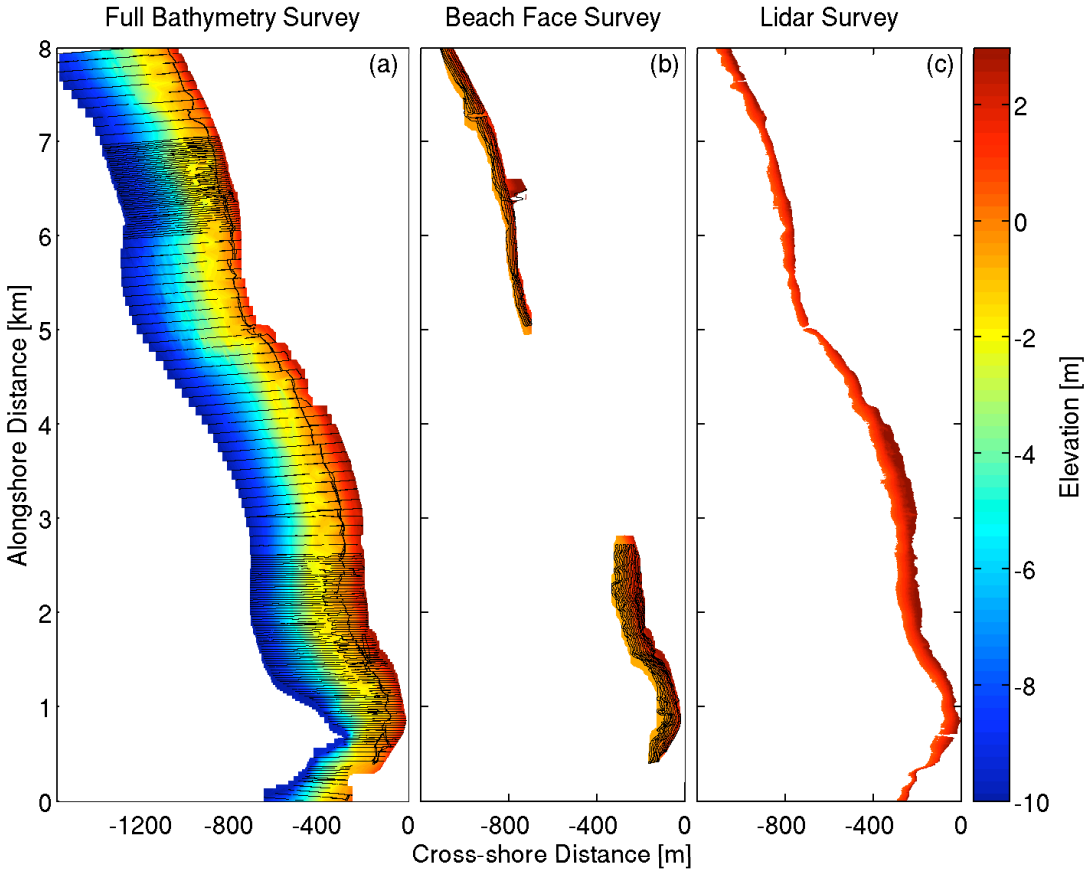

Figure 1.4: Elevation maps of in situ and lidar surveys at Torrey Pines Beach: (a) 3-6 April 2004 cross-shore, full bathymetry in situ survey, (b) 3 March 2004 alongshore, subaerial beach in situ survey, and (c) 2 April 2004 subaerial beach lidar survey. Black lines in (a) and (b) show the in situ data sampling, and the spatial density of the lidar data is shown in Figure 1.3.

1.2 Wave estimates

A spectral refraction wave model is used to make nearshore wave estimates along the reach of surveyed coastline in the Southern California Bight (O'Reilly and Guza, 1998). The model is initialized with deep sea buoys recording incoming swell and nearshore buoys measuring the local sea waves (triangles and asterisks, respectively, Figure 1.1). The Channel Islands and offshore bathymetry shelter portions of the shoreline from incoming swell, causing alongshore variability in wave exposure (Pawka, 1983). Large winter storms typically arrive from the

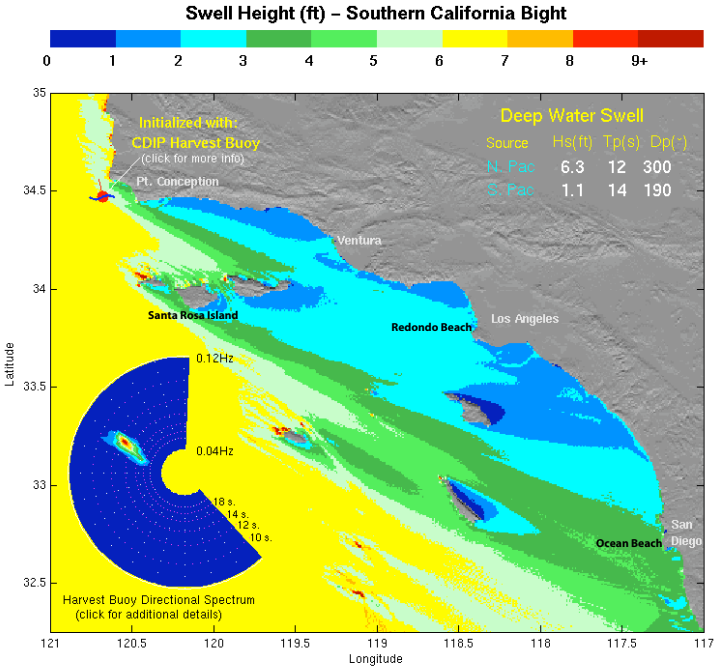

Figure 1.5: Swell model output from the California Data Information Program (CDIP) website showing northwest swell on 2 December 2008 (wave height shown in color).

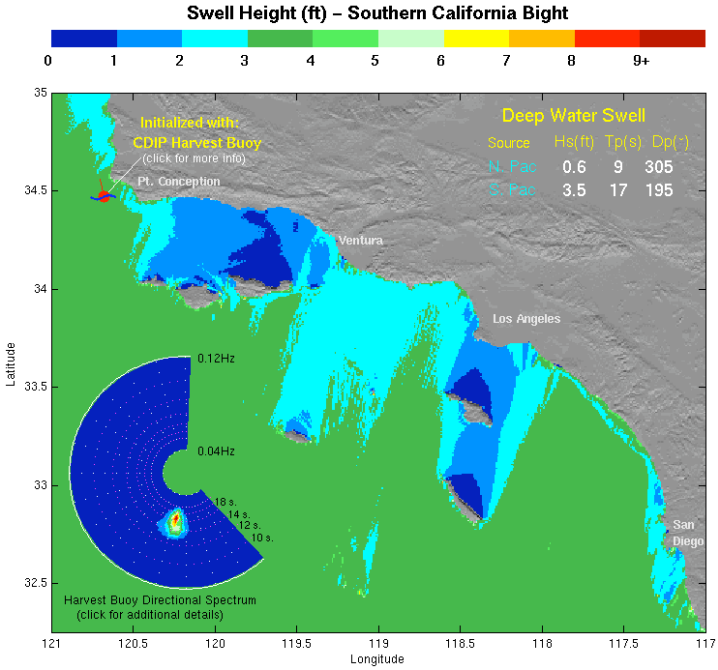

Figure 1.6: Swell model output from the CDIP website showing south swell on 21 June 2008 (wave height shown in color).

northwest Pacific Ocean (e.g. Figure 1.5), and the offshore islands shelter portions of the coastline causing smaller wave heights in regions southeast of the islands. In the summer, swell typically arrives from the south Pacific Ocean (e.g. Figure 1.6), creating wave shadows north of the Channel Islands and the headland at Point Loma. The model agrees well with observations made at several locations within the Southern California Bight (Figure 1.7).

The wave model outputs spectral wave properties every 100 m alongshore at the 10 m depth contour, providing high temporal and spatial resolution estimates of the wave field along the entire surveyed reach. The extensive sand level measurements and wave estimates are a unique and comprehensive data set to study both the large-scale spatial variability and site-specific temporal variability of sand level changes and the wave forcing.

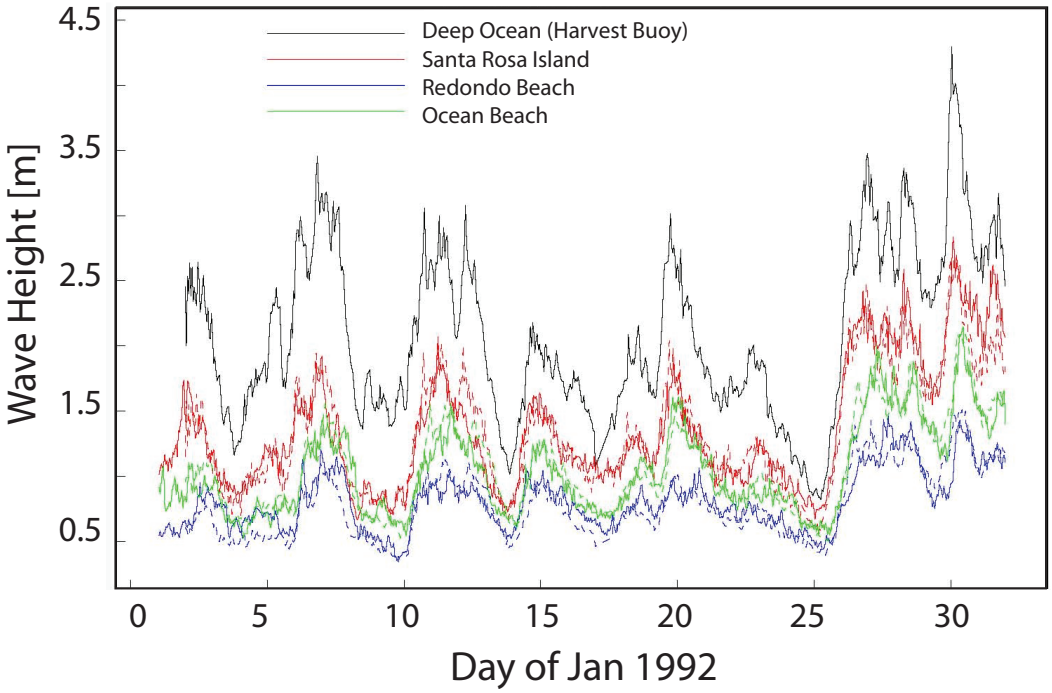

Figure 1.7: The observations (solid lines) and model outputs (dashed lines) are compared during January 1992 at Santa Rosa Island (red), Redondo Beach (blue), and Ocean Beach (green). The model is initialized with deep ocean swell from the Harvest Buoy (black). For reference, the comparison and buoy locations are identified in Figure 1.5.

1.3 Large-scale seasonal sand level changes

The first quantitative description of the seasonal cycle in southern California used empirical orthogonal functions (EOFs) to show beach profile change along three cross-shore transects at Torrey Pines State Beach (Winant et al., 1975; Aubrey, 1979). Previous work had shown seasonal vertical fluctuations of more than 2 m on beaches in southern California (Shepard, 1950), and the beach profile EOFs (Winant et al., 1975) quantified the seasonal fluctuations. In response to large wave energy events, winter shoreline erosion was coupled with offshore accretion during the formation of a winter bar (e.g. Figure 1.8a). When low energy waves persisted during the summer, the offshore bar migrated back onshore causing accretion at the shoreline (e.g. Figure 1.8b).

The Winant et al. (1975) analysis at Torrey Pines Beach is the paradigm of seasonal profile change. However, in the large-scale lidar observations, Torrey Pines stands out as a location demonstrating particularly large seasonal fluctuations in beach width (Figure 1.9). Beach width is defined as the distance from the backbeach (e.g. cliffs, revetment) to the mean sea level (MSL) contour. Subaerial beach volume change is often correlated with shoreline [e.g. mean high water (MHW) vertical datum] change (Farris and List, 2007), and seasonal beach volume and beach width change are correlated along the surveyed coastline. Therefore, beach width is discussed below.

The large-scale, airborne lidar observations in southern California show seasonal beach changes, integrating over storm-driven change and recovery periods. The biannual surveys (with quarterly surveys in the first year) could be aliasing the seasonal cycle, but concurrent monthly in situ surveys demonstrate that the lidar observations are surveying the beach near the extrema in seasonal beach width (dashed lines indicate lidar surveys in Figure 1.10). The observed seasonal cycle in beach width is present along most of the coastline (Figure 1.9). However, there is significant alongshore variability in the magnitude of seasonal beach width change,

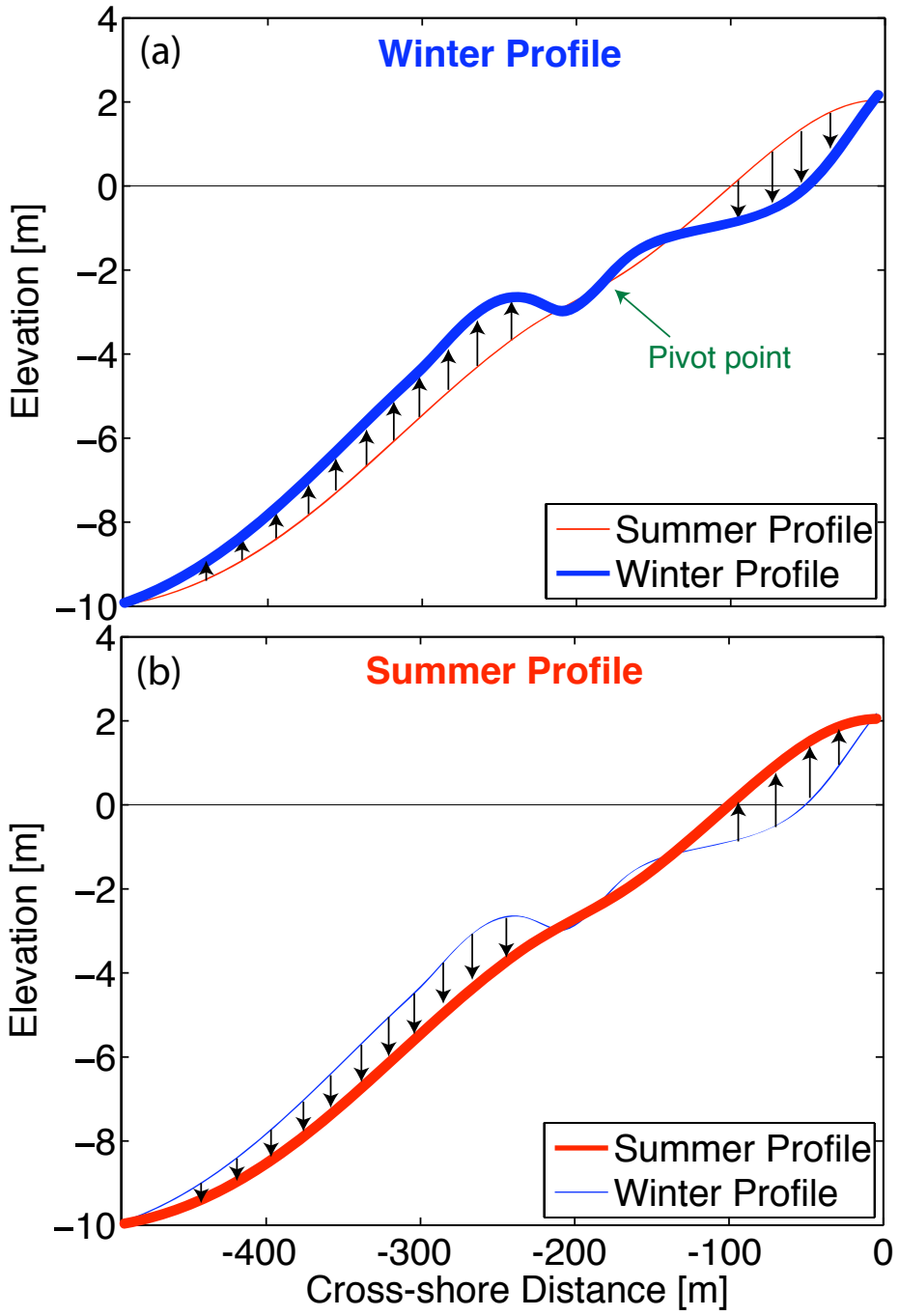

Figure 1.8: A schematic of the seasonal beach profiles shows: (a) a winter beach profile with shoreline erosion and the formation of an offshore bar, and (b) a summer beach profile with shoreline accretion and the loss of the offshore bar. The pivot point, or region showing little vertical seasonal change, is shown in (a).

ranging from less than 5 m to more than 30 m (Figure 1.9).

The processes controlling large-scale beach change are not well understood (Stockdon et al., 2002; List et al., 2006). Wijnberg and Terwindt (1995) analyzed morphological change with over 30 years of observations along 120 km of the Holland coast but were unable to explain the observed alongshore variability in morphological evolution. Overall, a lack of observations has prevented large-scale coastal change model validation (Cowell et al., 1995; Niedoroda et al., 1995).

Recent ground-based mapping of short-term, large-scale beach change was achieved with the SWASH (Surveying Wide-Area Shorelines) system, which estimated the shoreline (defined as the MHW vertical datum) position using beach slope and three-dimensional GPS position from a single alongshore survey track (List and Farris, 1999; List et al., 2003). At Cape Cod, Massachusetts and Cape Hatteras, North Carolina, List et al. (2003) predominately observed the expected beach response with the formation of winter "bar" profiles with a milder shoreline slope during storm periods and summer "berm" profiles with a steeper shoreline slope during recovery periods (Komar, 1998). They also identified "hotspots," with enhanced erosion during storms and rapid post-storm recovery. List et al. (2006) suggested several mechanisms that could control the alongshore variability in shoreline response, including the alongshore variations in wave characteristics, sand grain size, and beach slope, the influence of shore-oblique and shore-parallel bars, and the underlying geologic framework, all of which required further work to be substantiated.

Studies in the Mid-Atlantic Bight have shown that the underlying geology may strongly influence the development and morphology of sandbars (McNinch, 2004; Browder and McNinch, 2006). Further work demonstrated that shore-oblique bars may strongly impact shoreline change either directly (Schupp et al., 2006) or through the volume of available sediment in the nearshore (Miselis and McNinch, 2006). Similarly, Jackson et al. (2005) demonstrated that both the underlying geology and the nature and source of beach sand control the dissipative or reflective

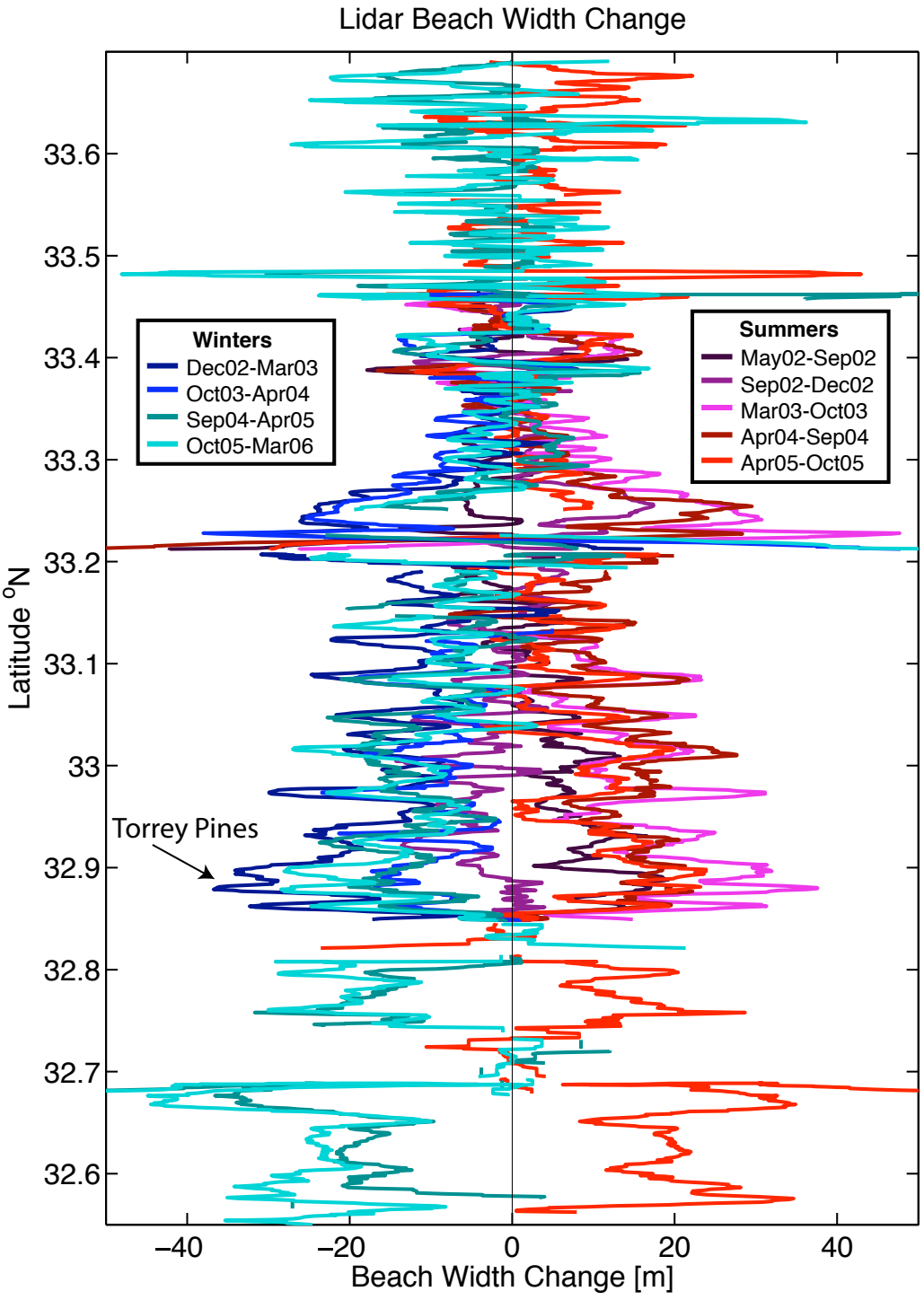

Figure 1.9: Lidar beach width change is shown between ten lidar surveys. Most of the coastline shows a seasonal cycle of beach width change with winter (blue tones) erosion and summer (red tones) accretion.

nature of beaches along the northern coast of Ireland, and Houser et al. (2008) showed that dune and shoreline erosion along an 11-km reach in northwest Florida was primarily controlled by the inner-shelf morphology. In a several kilometer study region offshore of Torrey Pines Beach in southern California, Hogarth et al. (2007) investigated the geologic control on the depth of sediment deposits in 10 m water depth, but this has not yet been related to shoreline change.

The alongshore variability of seasonal sand level changes in southern California is not well understood. The shoreline seasonal cycle is caused by seasonal variations in the wave forcing, but the alongshore variability of the seasonal shoreline change magnitude is not correlated with the alongshore variability of the seasonal wave height magnitude. Chapter 2 explores the factors controlling the alongshore variability of the seasonal beach width cycle magnitude, focusing on the importance of geologic factors and differences in sand grain size.

1.4 Focus site seasonal sand level changes

The in situ surveys supplement the lidar data with increased temporal resolution subaerial beach surveys (e.g. Figure 1.4b) and bathymetric observations to nearly -10 m water depth (e.g. Figure 1.4a) at four selected focus sites (Figure 1.2; Table 1.1). The focus sites were chosen to sample different shoreline change, wave, and geologic characteristics.

Large seasonal shoreline changes are observed at Torrey Pines Beach (Figure 1.10), in agreement with the biannual lidar observations. Additional focus sites were surveyed for at least one year to resolve shoreline changes through a complete seasonal cycle, demonstrating that the biannual lidar surveys are not aliasing the seasonal cycle at these locations (Table 1.1, Figure 1.10). The mean shoreline change (referenced to the 22 May 2002 lidar survey) at each focus site (Figure 1.10) confirms the lidar observations: Torrey Pines, Camp Pendleton, and Cardiff shorelines demonstrate large, in-phase seasonal cycles, and San Onofre shows little

shoreline change with no apparent seasonality (monthly changes are approximately 2 m, about the size of the measurement errors).

Approximately quarterly bathymetry surveys at each focus site demonstrate seasonal variability, as shown with EOFs of elevation contours ranging from -8 m depth to +3 m elevation at Torrey Pines and San Onofre (Figure 1.11). Winant et al. (1975), Clarke and Eliot (1982), and others have computed EOFs of beach profiles, resolving the cross-shore variability, but limiting the analysis to specific alongshore locations. Ruessink et al. (2000), Haxel and Holman (2004), and others have computed EOFs of mapped elevation surfaces, including both cross-shore and alongshore variability. Here, the uncertainties in interpolating the full bathymetry data between the survey transect lines led to calculating EOFs of contour position time series (Muñoz Péréz et al., 2001; Miller and Dean, 2007a). Each contour position was determined along the surveyed cross-shore transects,

Table 1.1: Focus site data collection.

Survey site	**Torrey Pines**	**Cardiff**	**Camp Pendleton**	**San Onofre**
Alongshore span (km)	8	2	2.5	4
Survey period	Feb. 2001 - Jul. 2008	May 2007 - Jul. 2008	Dec. 2006 - Jul. 2008	May 2005 - Aug. 2006
Subaerial beach survey frequency	Weekly - monthly	Biweekly - monthly	Monthly	Monthly
Number of exposed beach surveys	90	27	21	13
Full bathymetry survey frequency	Quarterly	Quarterly	Quarterly	Quarterly
Number of full bathymetry surveys	16	7	7	4

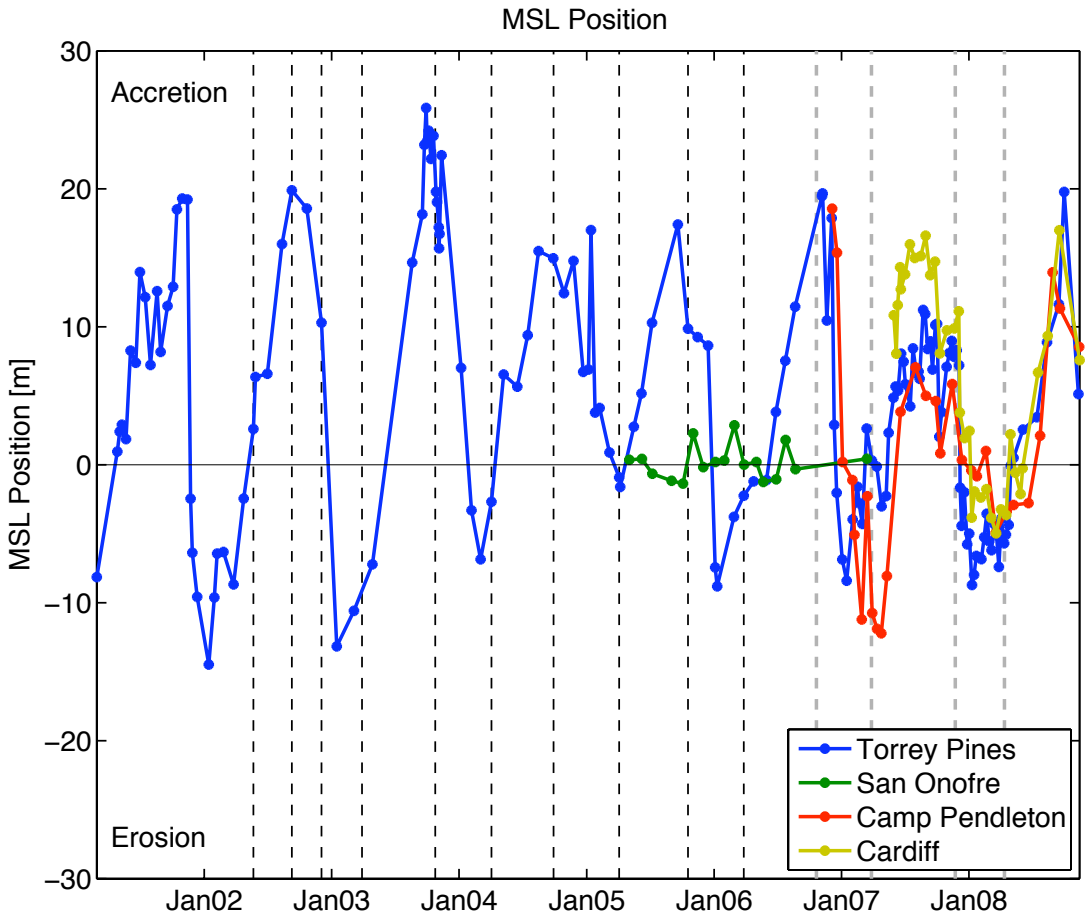

Figure 1.10: Time series of mean shoreline position, defined as the distance from the backbeach to the MSL contour (relative to a 22 May 2002 lidar survey), are shown at the four focus sites. The vertical dashed lines indicate the timing of the lidar surveys (gray lines indicate surveys not used in this analysis).

and the observations were smoothed with a 500-m alongshore running mean. The temporal mean of each contour was subtracted from the contour position time series. At each survey site, two sets of EOFs were computed: (1) with the monthly or more frequent beach face survey data (0 m to +3 m contours, spatial amplitude of the mode-1 EOF in Figure 1.11a,d), and (2) with the full bathymetry survey data (-9 m to +3 m contours, spatial amplitude of the mode-1 EOF in Figure 1.11b,e).

The mode-1 EOF temporal amplitudes of beach face and full bathymetry contours show seasonal fluctuations at the Torrey Pines and San Onofre focus sites

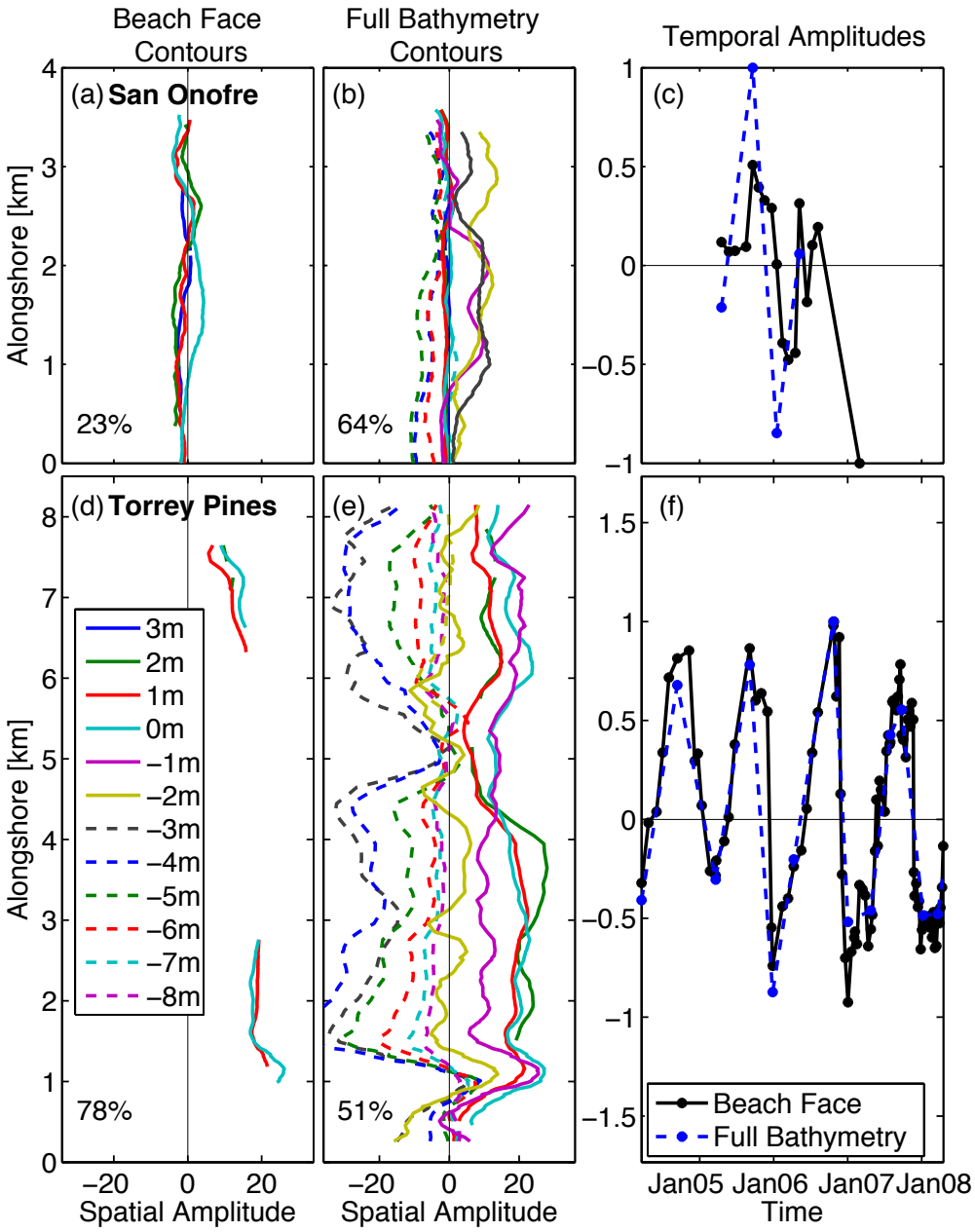

Figure 1.11: The beach face (a,d) and full bathymetry (b,e) spatial and temporal (c,f) amplitudes of the mode-1 EOFs are shown for San Onofre (top) and Torrey Pines (bottom). The percentage of variance explained by the first eigenfunction is shown in panels (a,d) and (b,e), for the beach face and full bathymetry EOFs, respectively.

(Figure 1.11c,f). However, the beach face spatial amplitudes at San Onofre show very different patterns, with little coherent beach face contour movement (Figure 1.11a), and large, in-phase contour movement at Torrey Pines (Figure 1.11d). The beach face contours (0 m and +1 m) at Torrey Pines move up to 40 m seasonally, showing erosion in winter months (landward contour movement) and accretion in summer months (seaward contour movement).

The bathymetry contours at both focus sites demonstrate large seasonal changes, and deeper water contours are out of phase with shallower contours, with the transition occurring at a pivot point in the profile where there is little seasonal contour movement (Figure 1.11b,e). At San Onofre, the beach face remains relatively stable, and the -3 m to -1 m contours are out of phase with the deeper contours (with a pivot point between -4 and -3 m depth), while at Torrey Pines, the -2 m to +1 m contours are out of phase with the deeper contours (with a pivot point between -3 and -2 m depth). The shallower contours accrete in summer and erode in winter, while the deeper water contours erode in summer and accrete in winter, with the loss and subsequent reformation of an offshore bar (shown schematically in Figure 1.8). Approximately one year of observations at the Cardiff and Camp Pendleton sites demonstrate seasonal beach face and full bathymetry contour changes similar to but slightly smaller than the observations at Torrey Pines. The cause of the observed shoreline stability and large offshore changes at San Onofre is discussed in Chapter 2.

1.5 Seasonal beach nourishment response

The observations at Torrey Pines Beach began in February 2001 to monitor the fate of a small beach nourishment. Beach nourishment response on hurricane- or storm-impacted coastlines has been studied extensively (Sorensen et al., 1988; Work, 1993; Bodge et al., 1993; Browder and Dean, 2000; Hamm et al., 2002), but nourishment evolution on coasts with large seasonal cycles is not

well understood (Marine Board, 1995; Capobianco et al., 2002). In Chapter 3, the observations from Torrey Pines Beach show the persistence of the nourishment sand through nearly two seasonal cycles even though the nourishment volume was smaller than the seasonal cross-shore volume fluxes.

1.6 Relating sand level changes and waves

The seasonal sand level changes observed along the coast of southern California are caused by seasonal variations in the wave forcing (Aubrey et al., 1980). Many authors have tried to relate beach changes (e.g. volume, shoreline location) to wave forcing (e.g. wave height, wave energy, Dean's parameter Ω) empirically through either instantaneous or short-term response to the wave forcing, or equilibrium response to the wave forcing as defined by beach or wave characteristics. Beach states may correlate with instantaneous or average wave properties [e.g. Dalrymple (1992); Masselink and Short (1993); Miller and Dean (2007b)]. However, Morton et al. (1995), Lee et al. (1998), Anthony (1998), Jiménez et al. (2008), and others have suggested that the antecedent beach state strongly impacts the response to a given wave forcing.

At Torrey Pines Beach, observations of MSL position and averaged wave energy between surveys are correlated ($R = -0.48$, Figure 1.12) due to the large seasonal cycle. However, when relating the MSL position change rate and the average wave energy between surveys, the relationship is less clear due to the importance of the antecedent state. For example, in December 2005 the beach was in an accreted state (positive MSL position), and an elevated wave energy event caused shoreline erosion (red dashed line, Figure 1.12). Six months later, in July 2006 the beach was in a neutral state (near the temporal mean of the MSL position), and a similar magnitude wave energy event caused shoreline accretion (black dashed line, Figure 1.12). The Torrey Pines Beach observations demonstrate the dependence of shoreline change on both the initial state and the wave field,

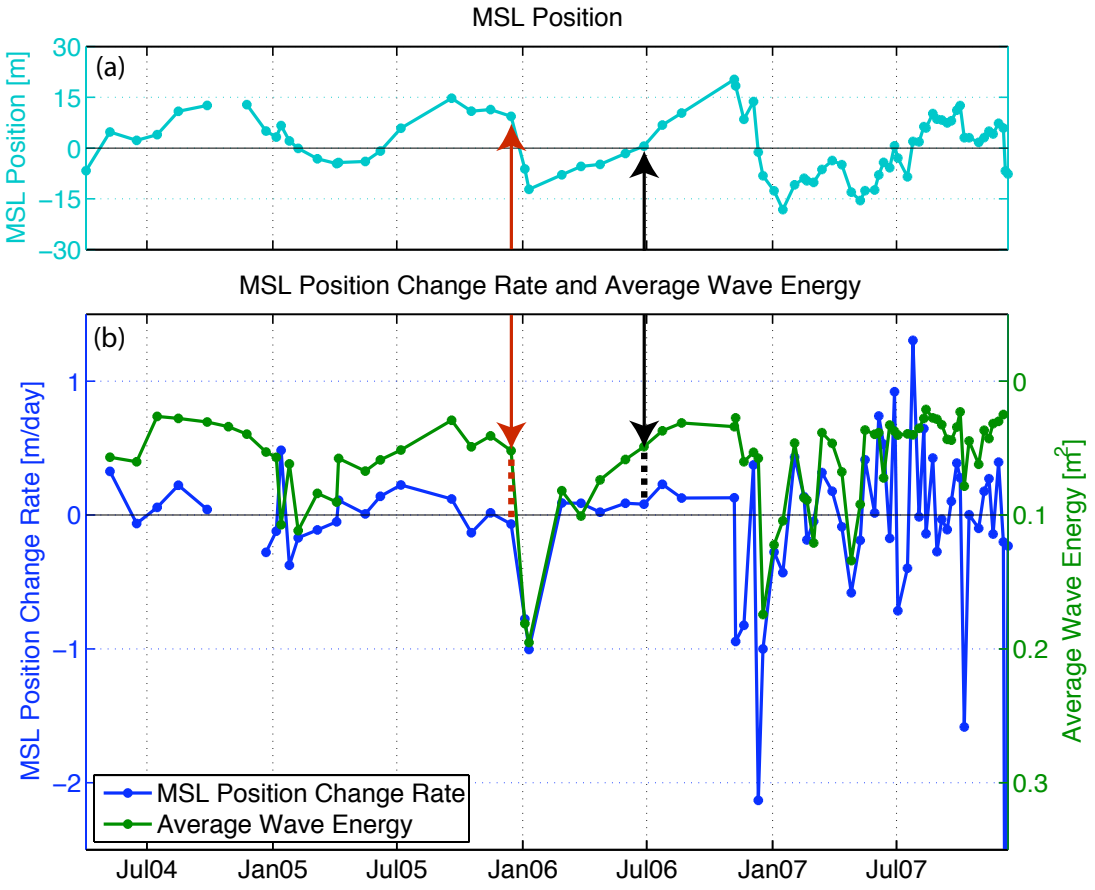

Figure 1.12: At one 500-m alongshore reach at Torrey Pines Beach, time series of (a) the mean MSL position (light blue), and (b) the MSL position change rate between surveys (dark blue) and wave energy averaged between surveys (dark green, axis positive downward for visual reference) show the dependence of MSL position change rate on both the initial MSL position and the wave energy (example highlighted with arrows).

suggesting an equilibrium-type response.

Many authors have suggested that beaches form stable equilibrium profiles for given wave and sand characteristics (Edelman, 1968; Swart, 1974; Dean, 1977). For example, a beach forced with moderate waves would respond by forming a specific equilibrium beach profile, regardless of the initial bathymetry (Figure 1.13). While the equilibrium profile is the same, the sign and magnitude of the beach change depends on the initial bathymetry. For example, with an initially accreted profile (Figure 1.13, top), the shoreline erodes in response to moderate wave

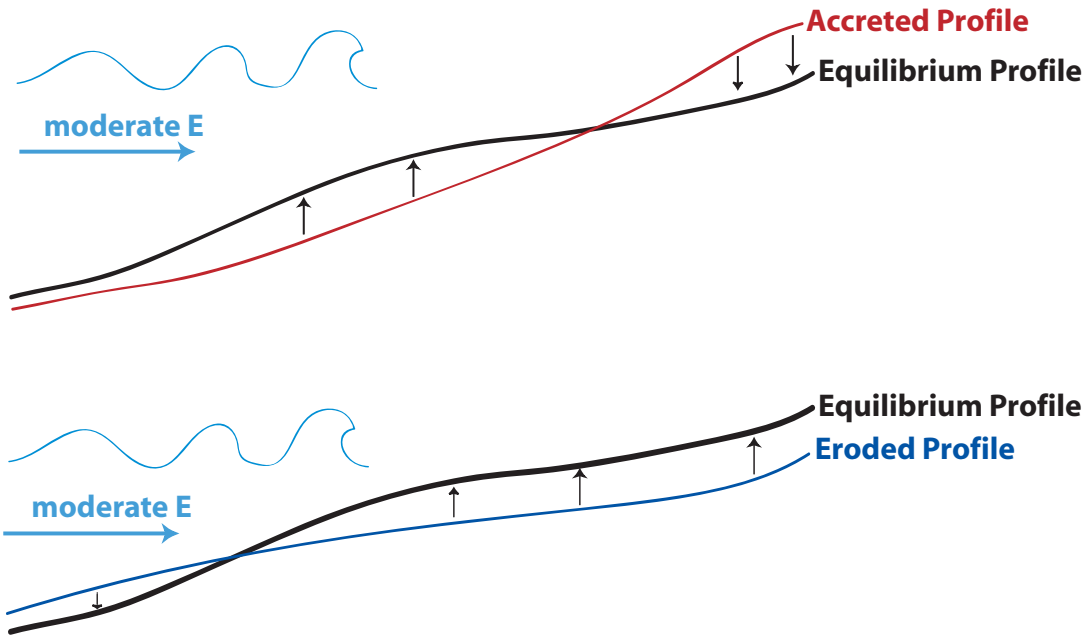

Figure 1.13: The schematic shows the equilibrium profile response (arrows) to moderate wave energy (E) forcing. The same equilibrium beach profile is attained (black lines), but the beach change is dependent on the initial bathymetry: (top) shoreline erosion for an initially accreted (or summer) profile (red line), and (bottom) shoreline accretion with an initially eroded (or winter) profile (blue line).

energy, while with an initially eroded profile (Figure 1.13, bottom), the shoreline accretes in response to the same wave energy forcing.

An equilibrium beach profile shape $h(x) = Ax^{2/3}$, where h is the water depth, x is the distance offshore, and A depends on sediment grain size (Dean, 1977), was suggested based on observations (Bruun, 1954) and the assumption of uniform wave energy dissipation per unit volume (Dean, 1977). Some applications of the equilibrium profile have included modeling beach nourishments (Dean, 1991), sea level rise (Dubois, 1990), and storm surge (Kriebel and Dean, 1993). Further adaptations of the form of the equilibrium profile have removed the infinite shoreline slope and added the presence of an offshore bar (Inman et al., 1993; Özkan Haller and Brundidge, 2007).

In Chapter 4, the equilibrium beach concept is demonstrated with shoreline and wave observations at Torrey Pines Beach and incorporated in a simple shoreline change model that assumes cross-shore transport is dominant. The model does not assume that the profile has a particular shape, but it could be extended to reproduce profile changes using EOFs. With four free parameters that must be determined from observations, and the model shows skill in reproducing observations at the additional focus sites and in predicting withheld observations at Torrey Pines Beach.

2

Large-scale alongshore variability

2.1 Abstract

The magnitude of seasonal shoreline fluctuations (the difference between winter and summer subaerial beach width), surveyed repeatedly with airborne lidar, varies considerably along 80 km of southern California coastline. The seasonally variable wave field forces seasonal sand level changes, but the alongshore variation of the magnitude of seasonal sand level changes and wave energy are not correlated. For example, along a 20 km reach with little alongshore variation in the wave field, seasonal cross-shore excursions of the shoreline vary by a factor of four. The magnitude of the seasonal beach width changes appears to be influenced by the cross-shore sand grain size difference and may also be affected by alongshore variations in cobbles, exposed bedrock, cliff inputs, and offshore sand supply.

2.2 Introduction

Beach erosion, already threatening much of the U.S. coastline, may increase if sea level rise continues, or if storm frequency or intensity increases. Beach erosion jeopardizes coastal infrastructure and reduces beach tourism. Coastal recreation expenditures in San Diego County beach communities reached $1.7 billion in 1997 (CRA, 1997), but beachgoers indicated they would decrease beach attendance by about 25% if beaches were half as wide or twice as crowded (CDBW

and SCC, 2002).

The United States Geological Survey (USGS) *National Assessment of Shoreline Change* concluded that 67% of southern California shoreline between Point La Jolla and Dana Point was eroding between 1972 and 1998 (Hapke et al., 2006). The design of beach retention and nourishment programs, which are needed to meet recreation demands and protect shoreline and sea cliff property, can be improved by understanding the mechanisms controlling beach change.

Ground-based kinematic Global Positioning System (GPS) surveys (Morton et al., 1993) enable sand level change monitoring over several kilometers on individual beaches. Airborne light detecting and ranging (lidar) systems (Brock et al., 2002) can sample hundreds of kilometers with high spatial resolution. Repeated lidar surveys are a unique resource for studying large-scale sand level change, but frequent lidar surveys are expensive. In this study, biannual lidar flights were supplemented with monthly or more frequent in situ surveys at selected focus sites to increase temporal resolution.

In southern California, seasonal fluctuations in wave energy cause large seasonal cross-shore fluxes of sediment. Winter storms erode the shoreline, forming an offshore bar, while low energy summer waves cause onshore migration of the bar and shoreline accretion, as observed at Torrey Pines Beach (Shepard, 1950; Winant et al., 1975; Aubrey, 1979). Using lidar and in situ measurements to quantify sand level variability and a regional network of directional wave buoys to monitor wave conditions, the observations show that the magnitude of sand level change varies along the southern California shoreline and that the alongshore variations are not well correlated with alongshore variations in seasonal wave energy.

In other regions of the world, the underlying geology (McNinch, 2004), nature and source of beach sand (Jackson et al., 2005), and offshore sediment availability (Miselis and McNinch, 2006) affect beach morphology. Recent work in southern California (Hogarth et al., 2007) explores the offshore geology in depths as shallow as 10 m, but the offshore geology has not yet been related to shoreline

beach morphology in southern California. This study shows that the magnitude of seasonal shoreline change in southern California likely depends on swash and surfzone geology, as well as on wave energy.

2.3 Sand level measurements

Ten airborne lidar surveys measured sand levels along 80 km of southern California coastline between May 2002 and March 2006 (Figure 2.1). The processed lidar data includes the subaerial beach, spanning from the backbeach (e.g. cliffs, seawall) to the waterline, where an algorithm using the tide level and wave height removed water data points [Appendix A, (Yates et al., 2008)]. In addition to these twice yearly, high spatial resolution surveys, sand levels were measured at four focus sites within this alongshore span (Figure 2.1, Table 1.1). Monthly or more frequent in situ surveys spanned from the backbeach to the waterline using a GPS-equipped all-terrain vehicle (ATV). Three to four times yearly full bathymetry surveys to approximately 10 m depth were obtained using a GPS-equipped ATV, hand-pushed cart, and personal watercraft with sonar. Lidar and in situ surveys both have estimated vertical root-mean-square (RMS) errors of about 15 cm.

2.4 Sand level changes

Changes in the location of depth contours are dominated by the seasonal cycle. The width of the subaerial beach available for recreation (Figure 2.2a), characterized by the location of the Mean Sea Level (MSL) contour, narrows (erodes) in winter and widens (accretes) in summer (e.g. dark and light curves, respectively, in Figure 2.2b), as observed previously at Torrey Pines beach [e.g. Winant et al. (1975)]. The magnitude of the seasonal cycle varies significantly over the 80-km surveyed reach. The standard deviation of MSL position or beach width (σ_{MSL}, roughly the RMS seasonal cycle change amplitude, Figure 2.2c), ranges from about 20 m at Torrey Pines (32.9°N) and Camp Pendleton (33.22°N), to less than 5 m at

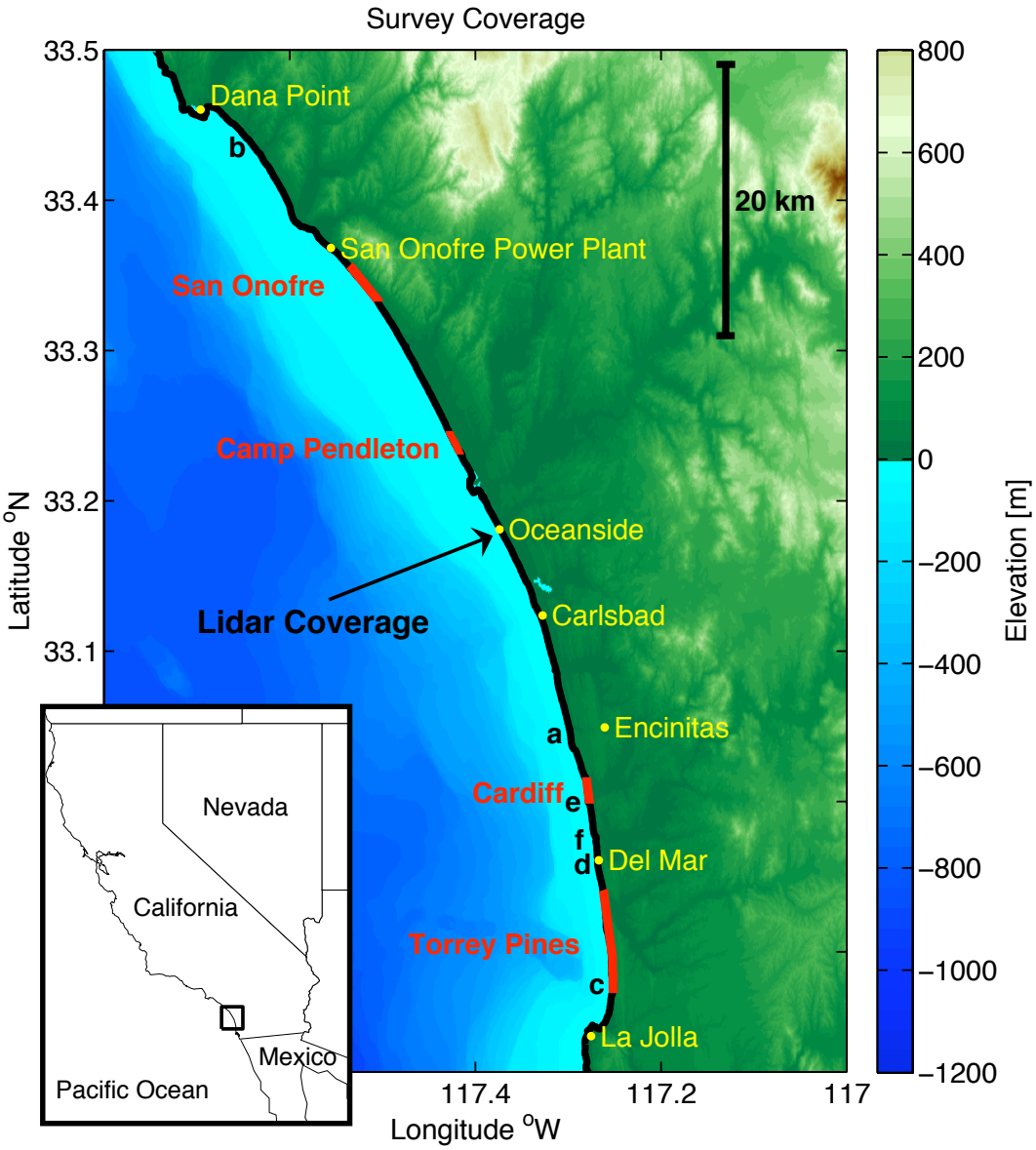

Figure 2.1: Lidar (black lines) and in situ (red lines) survey observations are shown along the southern California coastline, with the map location in the inset. The black letters (a-f) locate the images in Figure 2.5.

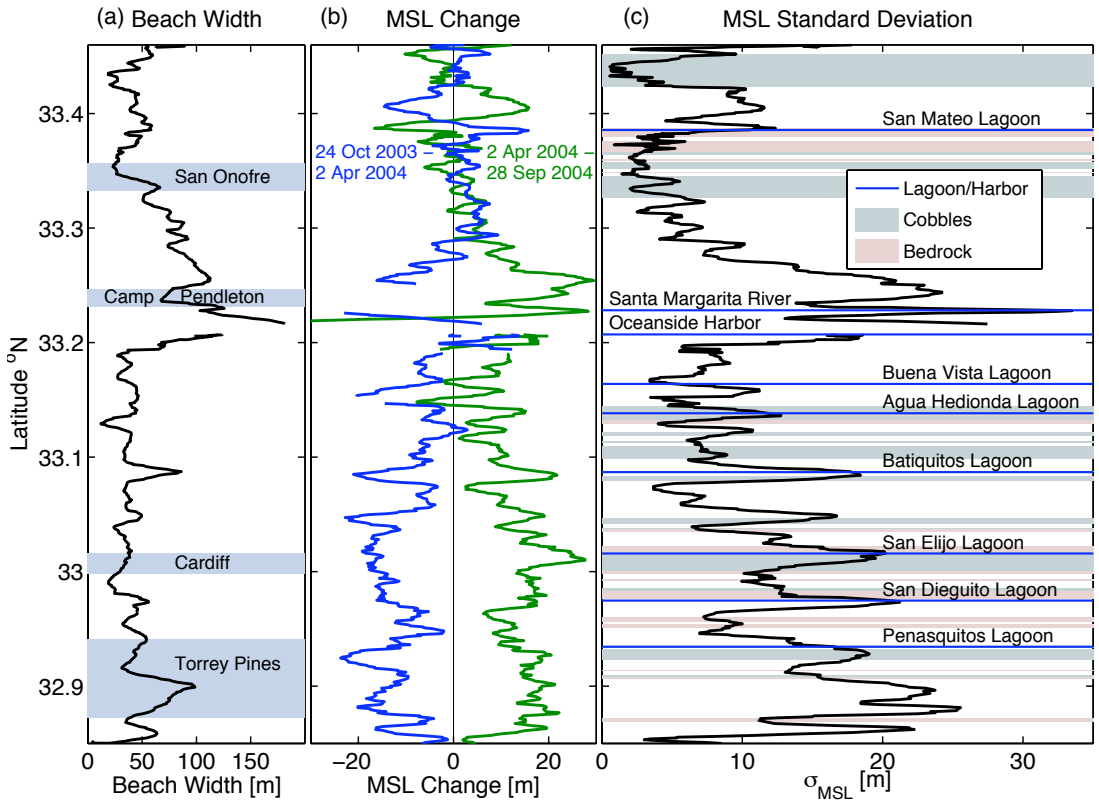

Figure 2.2: Lidar-derived beach characteristics versus alongshore location: (a) mean (ten surveys) subaerial beach width, from the backbeach (e.g. dunes, cliffs) to the MSL contour (focus sites are shaded blue), (b) example MSL changes: winter erosion (blue, 24 October 2003 to 2 April 2004) and summer accretion (green, 2 April 2004 to 28 September 2004), and (c) MSL contour location standard deviation σ_{MSL} (seasonal cycle change amplitude). Background shading and horizontal blue lines indicate beach geology (see legend).

San Onofre (33.36°N). A typical fall-spring fluctuation, about two times the MSL standard deviation, is often a significant fraction of the total beach width, and in some locations the winter MSL contour nearly reaches the backbeach.

To resolve temporally the seasonal cycle observed with biannual lidar surveys, monthly exposed beach surveys and three to four times yearly full bathymetry surveys were acquired for more than one year at selected focus sites (Figure 2.1, Table 1.1). Monthly MSL time series, averaged along a 500-m alongshore span (insets, Figure 2.3), confirm that the biannual lidar observations (Figure 2.2) are

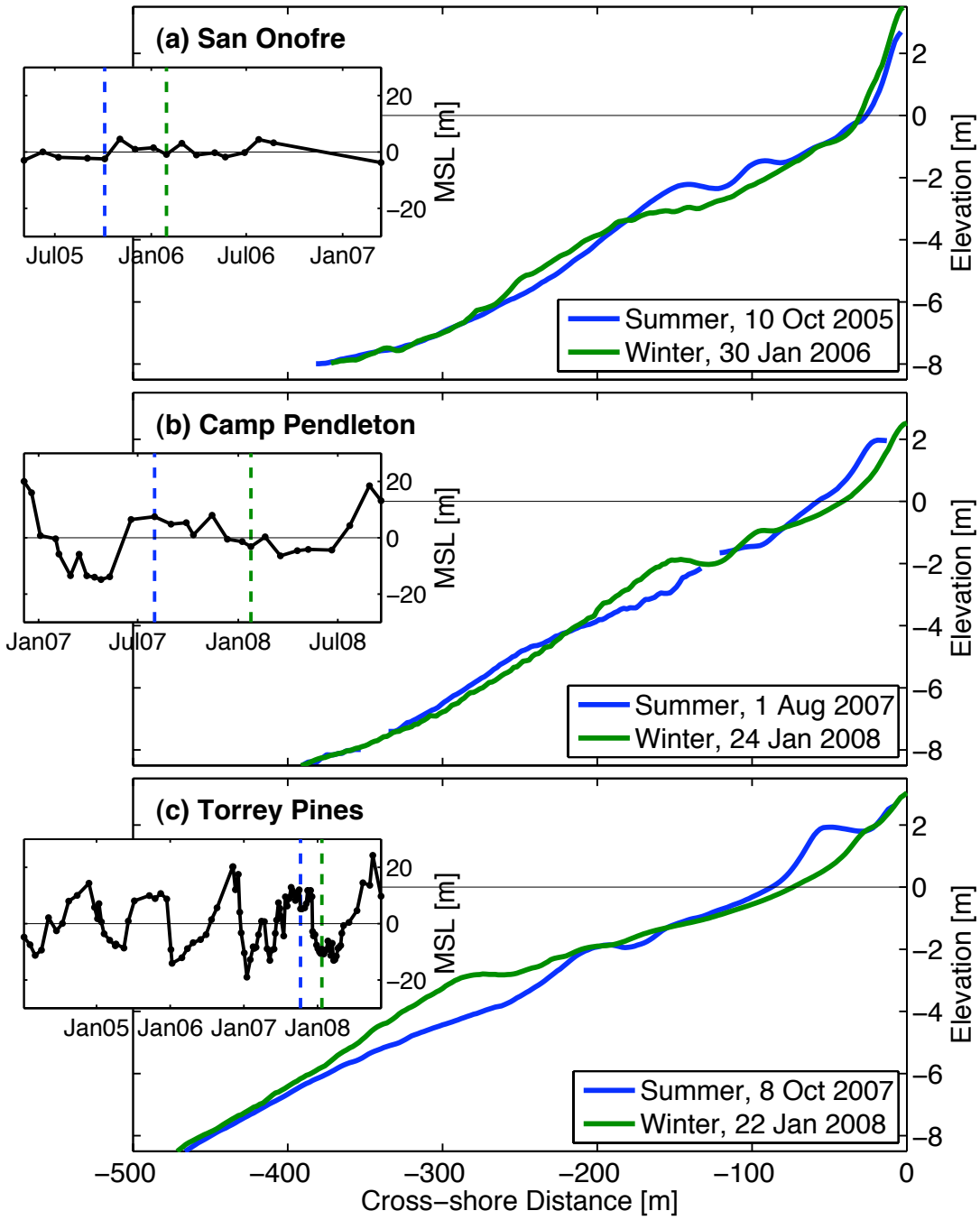

Figure 2.3: Summer (blue) and winter (green) cross-shore depth profiles at: (a) San Onofre, (b) Camp Pendleton, and (c) Torrey Pines. Insets show MSL position versus time. Blue and green vertical dashed lines indicate summer and winter profile dates, respectively.

representative of winter and summer beach width extrema. Monthly MSL position moves less than 5 m at San Onofre (inset, Figure 2.3a) and more than 20 m seasonally at Camp Pendleton and Torrey Pines (inset, Figure 2.3b,c). The shoreline at San Onofre is stable, not showing a seasonal cycle. Cross-shore profiles, extending from -9 m depth to +3 m elevation (Figure 2.3), sampled at times of approximate beach width extrema, show that although the beach face at San Onofre is stable, the seasonal cross-shore displacements of contours deeper than about -1 m are as large as 30 m (Figure 2.3a), comparable to deeper water contours at Camp Pendleton and Torrey Pines (Figure 2.3b,c). The in situ observations show large seasonal fluctuations of underwater contours at all three focus sites and verify the lidar observations of a stable beach face at San Onofre and large seasonal shoreline changes at Torrey Pines and Camp Pendleton.

2.5 Wave estimates

Hourly wave spectra are estimated every 100 m alongshore on the 10 m depth contour using a spectral refraction wave model initialized with buoy observations both seaward and shoreward of the Channel Islands (O'Reilly et al., 1993; O'Reilly and Guza, 1998). The Channel Islands and variable coastline orientation create alongshore variability in seasonal wave fluctuations (Pawka, 1983). The average significant wave height is larger in winter (December to April) than in summer (May to November) along the entire coastline, but the seasonal difference decreases from south to north, with a pronounced change around 33.1°N latitude (Figure 2.4a). Additionally, large wave events are more frequent in the southern region, again with a change around 33.1°N latitude (Figure 2.4b). The incoming wave direction of storms varies seasonally, with larger winter swell arriving from the northwest Pacific Ocean and generally smaller summer swell arriving from the south Pacific Ocean.

Large seasonal sand level fluctuations occur even on relatively sandy, long,

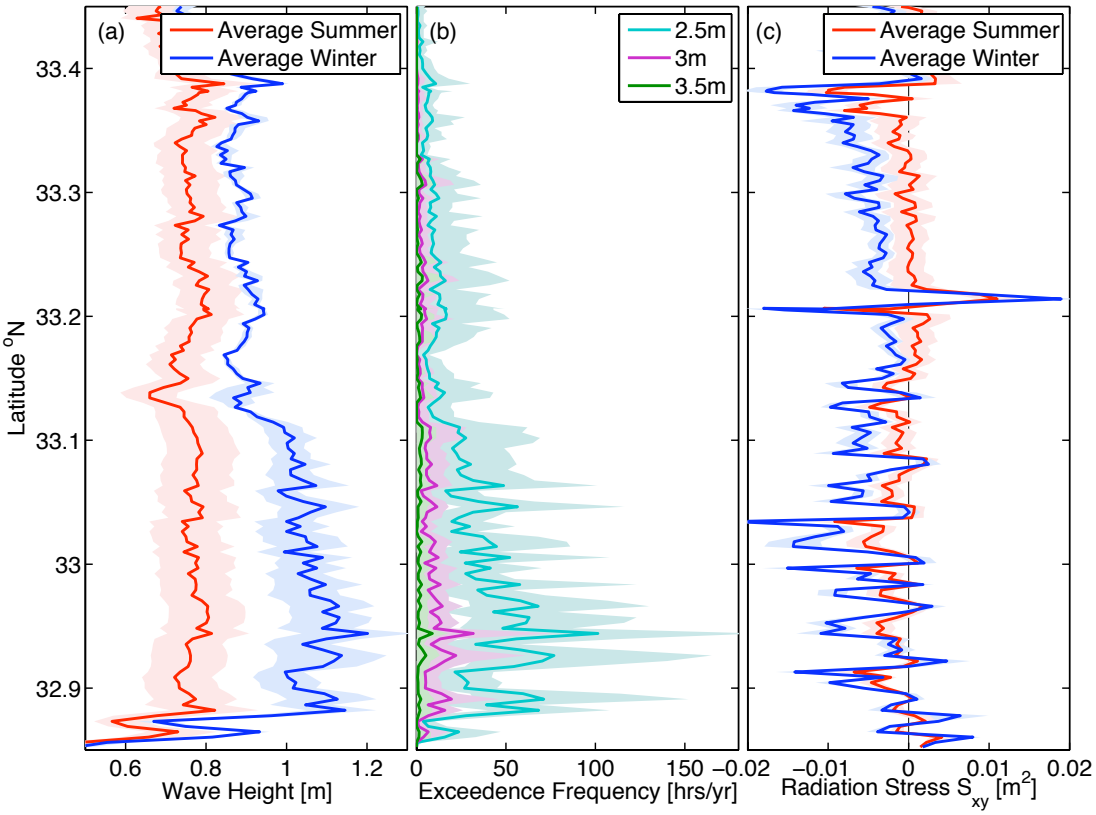

Figure 2.4: Seven-year (2001-2007) average wave properties versus alongshore position: (a) average summer (red; May to November) and winter (blue; December to April) wave height, (b) average frequency (number of hours per year) that large (2.5-3.5 m) significant wave heights are exceeded, and (c) average summer (red) and winter (blue) alongshore radiation stress component, S_{xy}. Shading shows the range of mean values in the seven-year record.

straight beaches and are believed to be caused primarily by seasonal variations in wave height and the associated cross-shore transport (Aubrey et al., 1980). However, the magnitude of seasonal beach width changes (σ_{MSL}, Figure 2.2c) has more alongshore variation than the seasonal standard deviation from the mean wave height (Figure 2.4a), and these alongshore series are not correlated (R^2 = 0.15). Correlations were also low between the magnitude of seasonal beach width changes (σ_{MSL}, Figure 2.2c) and the frequency of large significant wave height events (Figure 2.4b).

Alongshore gradients in the alongshore sediment flux, or the so-called

divergence of the drift, can also cause accretion and erosion (Kamphius, 1991). The coastline is tilted northwestward (Figure 2.1), and the radiation stress component S_{xy}, which forces alongshore currents (Longuet-Higgins, 1970), is usually directed southward (Figure 2.4c). Wave seasonal variability affects the magnitude of the seasonal S_{xy}, but alongshore gradients of S_{xy} are qualitatively similar in summer and winter, and the net alongshore transport does not have significant seasonal variation. Although quantitative analysis is needed, it seems unlikely that alongshore gradients in wave-driven sediment flux cause the observed seasonal alongshore variation in MSL displacement.

2.6 Beach geology

Visual surveys determined the location of cobbles, exposed bedrock, and lagoons along the 80-km surveyed reach. Some cobbled areas (green shading in Figure 2.2c) show reduced sand level variability, consistent with suggestions that cobbles armor the shoreline (Carter and Orford, 1984; Sherman, 1991). However, cobble coverage is both variable and difficult to quantify, ranging from dense cobble layers completely covering the sand (Figure 2.5a), to small, intermittent piles of cobbles spaced every 50-100 m (Figure 2.5b), to cobble cusps located only at the backbeach (not shown). While many beaches are sandy (Figure 2.5c), the depth of the sand layer is often unknown. In some locations, the sand layer has eroded away, exposing bedrock on the beach face (Figure 2.5d) or in the surf zone (Figure 2.5e). On beaches with limited sediment availability, bedrock (red shading in Figure 2.2c) may be exposed in winter when the overlaying sand erodes from the beach face. Additionally, lagoon and river mouths may be a sand source or sink, affecting nearby sediment transport patterns (Figure 2.5f). MSL contour motions are often large near lagoon mouths (horizontal blue lines in Figure 2.2c), perhaps owing to changes in lagoon mouth geometry. Non-sandy beach characteristics contribute to alongshore variability in shoreline and depth contour change, but the impact is not

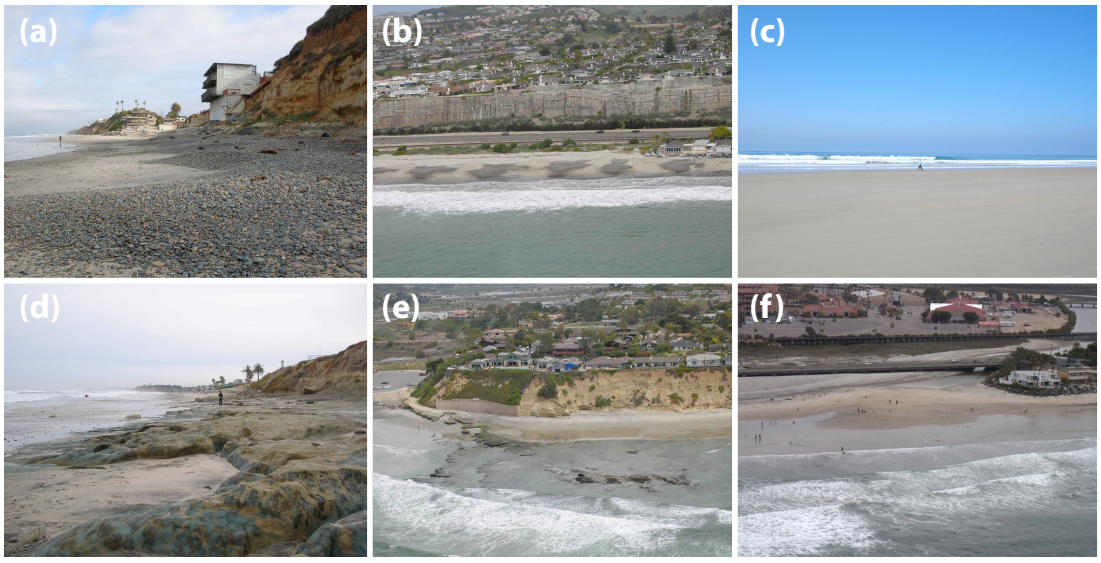

Figure 2.5: Visually identified beach features at low tide: (a) thick piles of cobbles overlaying sand, (b) intermittent cobble piles, (c) wide sandy beach, (d) exposed bedrock on the beach face, (e) exposed bedrock in the inner surf zone, and (f) wide lagoon mouth. The image locations are shown in Figure 2.1.

yet quantified.

In addition to visually characterizing beaches, sand grain size was measured approximately every kilometer along the visually located high tide line in spring 2006 (data courtesy of Jen Haas and Neal Driscoll), at three in situ survey sites in spring 2007, and between the Camp Pendleton and San Onofre focus sites in fall 2007 (Figure 2.6). Wright and Short (1984) characterized beaches as different morphodynamic states using the empirical parameter $\Omega = H_b/w_s T$ (Dean, 1973), where H_b is the breaking wave height, T is the wave period, and w_s is the sediment fall velocity, which is grain size dependent. In addition, equilibrium profile response models have included scale parameters, depending on sand grain size (Dean, 1977), suggesting that beach responsiveness to waves depends strongly on sand grain size.

The median grain size (D50) on the beach face increases from south to north along the 80-km survey region (Figure 2.6), with a break in the trend just south of the Camp Pendleton survey site near the Santa Margarita river mouth and

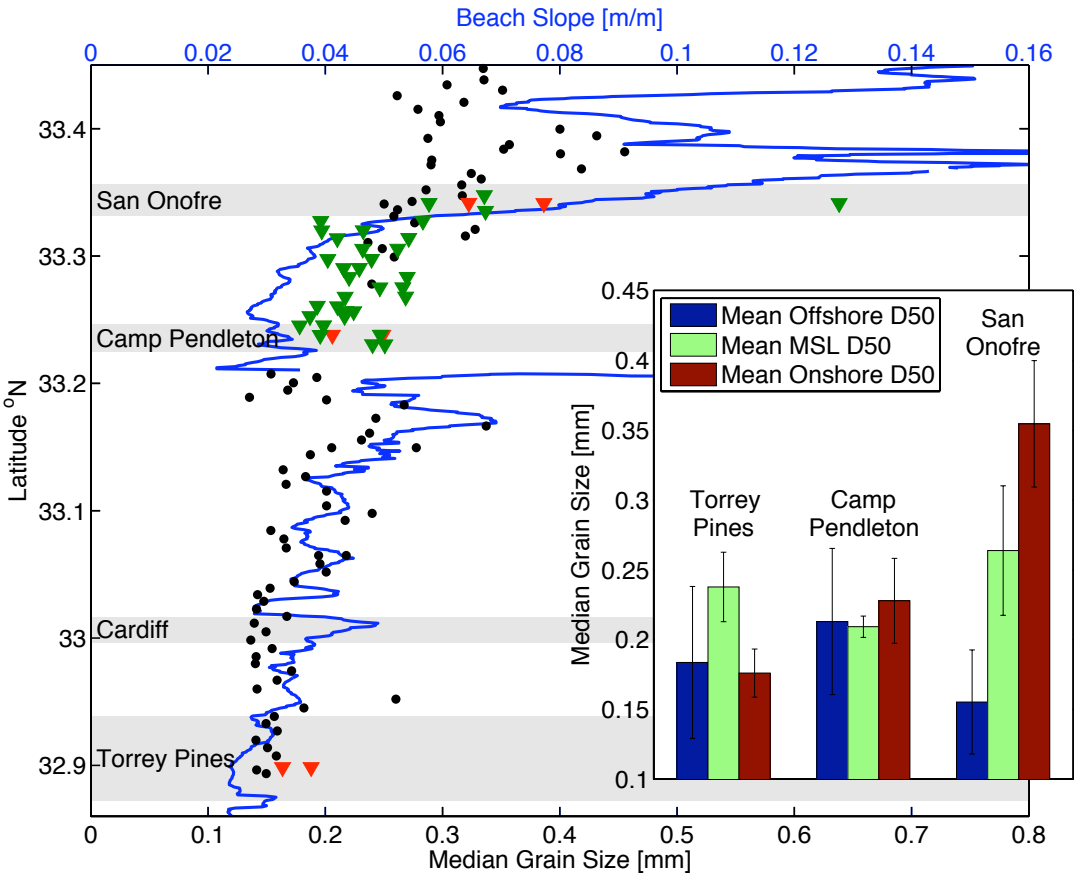

Figure 2.6: Median sand grain size [spring 2006, near the high tide waterline (black dots); spring 2007, at +1 m and +2 m elevation (red triangles); and fall 2007, at +1 m and +2m elevation (green triangles)] and beach slope (blue line) versus alongshore location. The inset shows the cross-shore variability of the median grain size (D50) at three survey focus sites.

the Oceanside harbor and jetty (identified in Figure 2.2c). Overall, sand grain size decreases with increasing wave height, opposing previous observations suggesting that grain size increases with increasing wave energy (Bascom, 1951; Bryant, 1982), but consistent with a northern source of large-grained material from the cliffs and littoral transport carrying finer grains southward (Self, 1997; Nordstrom, 1989). Cliff erosion may provide more than half of the beach sediments in the Oceanside littoral cell (Young and Ashford, 2006), and cliff sediment median grain sizes are larger in the northern portion of the study region, between Oceanside and San

Onofre, where beach grain sizes are also larger (Haas, 2006). Mean beach slope, calculated at MSL +/- 0.5 m also increases from south to north (Figure 2.6), with a break in the trend at the Oceanside Harbor, following the increase in sand grain size, as shown by Bascom (1951) and others.

In addition to the high tide samples, five sand samples (at approximately -3 m, -1 m, MSL, +1 m, and +2 m elevation) were taken on cross-shore transects at three survey sites and in the region between Camp Pendleton and San Onofre. The sand grain size distributions [including the median (D50) and spread] are shown at the three survey sites in Figure 2.7. At Torrey Pines and Camp Pendleton, most distributions have a single peak, whereas some distributions at San Onofre have two weak peaks (the resolution of the estimated distributions is limited). According to the graphical-statistical method of Folk (1974), the sediments are classified as well sorted to moderately well sorted (with two moderately sorted samples) by the grain size distribution standard deviation. At San Onofre, grains are coarser on the beach face than in the offshore, whereas the cross-shore sand size variation is weaker at Torrey Pines and Camp Pendleton (inset, Figure 2.6). A simple measure of the cross-shore grain size difference (α) is:

$$\alpha = \frac{D50_{onshore} - D50_{offshore}}{D50_{onshore} + D50_{offshore}}, \tag{2.1}$$

where $D50_{onshore}$ is the average of the +1 m and +2 m beach face samples, and $D50_{offshore}$ is the average of the -1 m and -3 m offshore samples (Figure 2.8b). When α is approximately zero, onshore and offshore grain size are equal. When α is approximately one, sand grains are much coarser onshore than offshore. Between Camp Pendleton and San Onofre, the northward decreasing trend in MSL variability is significantly negatively correlated with α (Figure 2.8c, R^2= 0.54, significant at 95%), while the seasonal wave height shows little coherent alongshore variation (Figure 2.8a). We hypothesize that the alongshore variation in beach width change, without corresponding alongshore variation in waves, is related to alongshore variation in α imposed by the sediment source location and character-

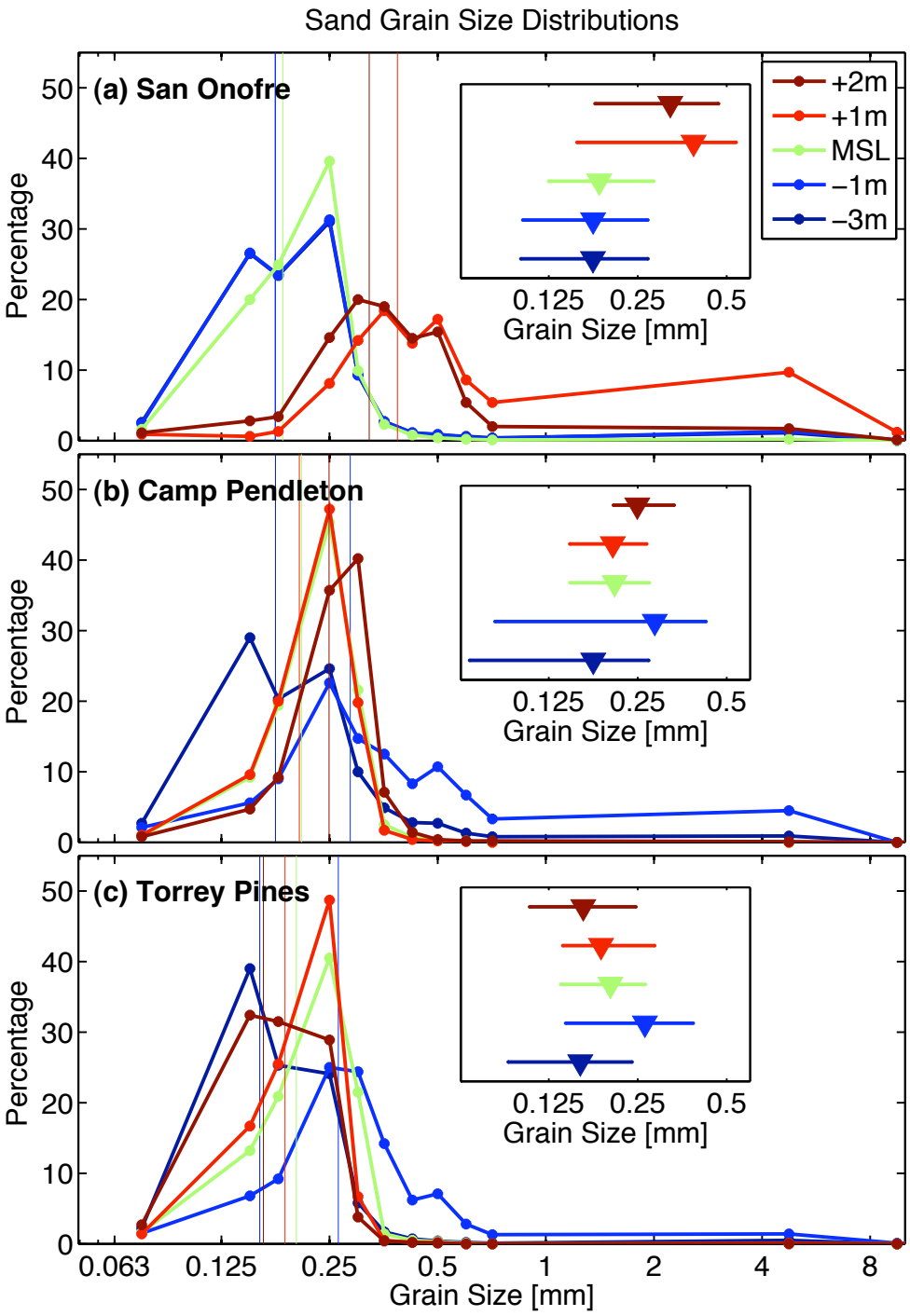

Figure 2.7: Sand grain size distributions and median sand grain size (D50) at the three focus sites: (a) San Onofre, (b) Camp Pendleton, and (c) Torrey Pines. The colors identify the elevation (-3 m, -1 m, MSL, +1 m, and +2 m) of the cross-shore samples (see legend), and the inset shows the median (triangle; D50) and spread (horizontal line; D16 to D84) of the grain size distributions.

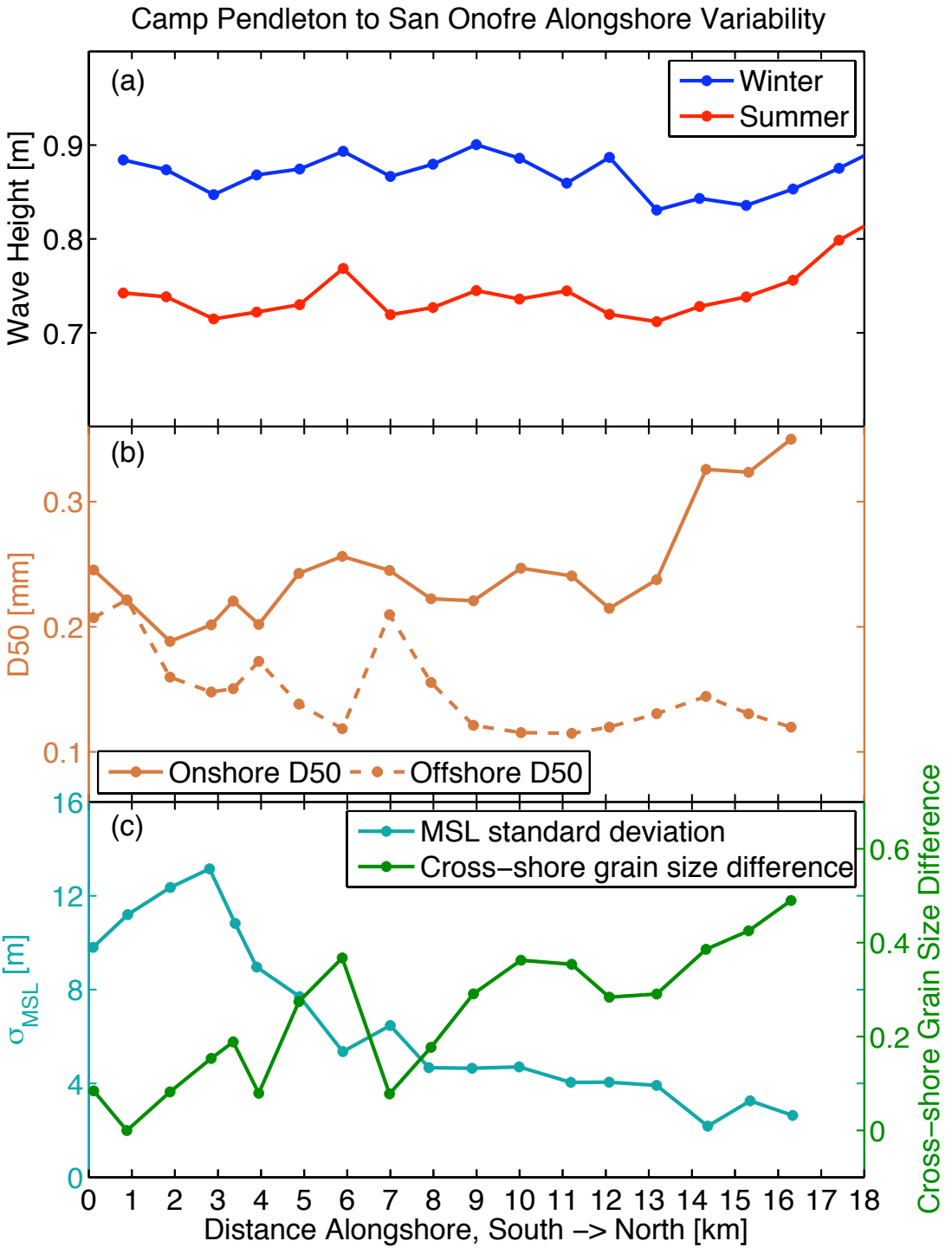

Figure 2.8: Alongshore variation between Camp Pendleton (0-2 km) and San Onofre (14-18 km) survey sites: (a) seasonal significant wave height, (b) onshore and offshore median sand grain size (D50), and (c) MSL standard deviation (light blue; σ_{MSL}) and cross-shore grain size difference [green; α, (2.1)].

istics. Alternatively, an unidentified mechanism, such as limited sand supply could also be important. The extent of the offshore sand supply may also limit the volume of sand available to be transported cross-shore to the beach face or between underwater contours. Unfortunately, sand grain size distributions, underlying geology, sand layer depth, cliff contributions, and even inner shelf bathymetry are often unknown over large spatial scales. The limited geological data, and limited understanding of the effect of geologic factors on beach processes, allows only qualitative discussion of the influence of cobbles, exposed bedrock, lagoons, and sand grain size variability.

2.7 Summary and future work

The well-known seasonal cycle of sand level changes on southern California beaches (Shepard, 1950) shows significant alongshore variability, which is not uniquely controlled by the alongshore variability in waves, suggesting that geological factors influence the seasonal cycle magnitude. Along a 17-km reach with little alongshore variability in waves, the difference between the onshore and offshore sand grain size is negatively correlated with the magnitude of shoreline change. For the same wave energy, shoreline change is less with large cross-shore variations in grain size, with relatively coarse sand at the shoreline. Additionally, exposed cobbles and bedrock, available sand supply, cliff sediment input, and lagoon mouths may have significant, but unquantified effects on seasonal changes in beach morphology. Future work includes quantifying the volume of sand available in the beach system to determine if sand availability plays an important role in limiting the magnitude of the seasonal cycle.

Acknowledgements

Lidar surveys were sponsored by the U.S. Army Corps of Engineers and collected by Dr. Roberto Gutierrez of the University of Texas. Wave information

was provided by the Coastal Data Information Program and funded by the California Department of Boating and Waterways and the U.S. Army Corps of Engineers. The in situ survey system was constructed and operated by Brian Woodward, Bill Boyd, Dennis Darnell, Kent Smith, and Ian Nagy. Marissa Yates was partially supported by an NDSEG Fellowship.

The text of Chapter 2 contains some material that has been reformatted from the paper "Overview of Seasonal Sand Level Changes on Southern California Beaches," *Shore & Beach*, **77**(1), 1-8, which was awarded the 2008 American Shore & Beach Preservation Association Educational Award. The dissertation author was the primary researcher and first author with guidance provided by R.T. Guza, W.C. O'Reilly, and R.J. Seymour.

3

Seasonal persistence of a small southern California beach fill

3.1 Abstract

Torrey Pines State Beach, a site with large seasonal fluctuations in sand levels, received a small shoreface beach fill (about 160,000 m^3) in April 2001. The 600-m long, flat-topped nourishment pad extended from a highway riprap revetment seaward about 60 m, terminating in a 2 m-tall vertical scarp. A 2.7 km alongshore span, centered on the nourishment region, was monitored prior to the nourishment and biweekly to monthly for the following two years. For the first seven months after the nourishment, through fall 2001, significant wave heights were small, and the elevated beach fill remained in place, with little change near and above Mean Sea Level (MSL). In contrast, the shoreline accreted on nearby control beaches following a seasonal pattern common in southern California, reducing the elevation difference between the nourished and adjacent beaches. During the first winter storm (3 m significant wave height), the shoreline retreated rapidly over the entire 2.7 km survey reach, forming an alongshore-oriented sandbar in -4 to -3 m water depth (Seymour et al., 2005). The current study shows that the winter sandbar, most pronounced offshore of the nourishment, moved back onto the beach face during summer 2002 (following the usual seasonal pattern) and formed a wider beach above MSL at the site of the original nourishment than on the control

beaches. Thus, the April 2001 shoreline nourishment was detectable until late fall 2002, persisting locally over a full seasonal cycle. In an extended seven-year time series, total sand volumes (summed between the back beach and -8 m water depth, over the entire 2.7 km reach) exhibit multi-year fluctuations of unknown origin that are twice as large as the nourishment volume.

3.2 Introduction

Beach nourishments can protect shoreline infrastructure and enhance beach recreational use without intrusive hard structures (e.g. seawalls and groins) that may have undesirable local, and even regional, impacts (Marine Board, 1995). Nourishment monitoring, including simultaneous monitoring of nourished sites and nearby unaltered beaches (Stive et al., 1991), helps improve coastal management practices both by directly observing the nourishment fate and by providing guidance and calibration for numerical models used to plan future nourishments (Marine Board, 1995; Dean, 2002).

In an effort to improve the predictability of nourishments, many monitoring programs track nourishment evolution over a few years, but surveys are usually completed on an annual to biannual basis, with no reports of monthly or seasonal variability. A large beach nourishment (approximately 7 million m^3) of Perdido Key near Pensacola Pass, FL, was surveyed once or twice yearly for eight years (Browder and Dean, 2000). Significant changes were caused by hurricanes, but the nourishment and adjacent regions remained relatively stable between these events (Work, 1993; Browder and Dean, 2000). Biannual surveys for two years recorded losses for a large nourishment at Hilton Head Island, SC (Bodge et al., 1993), showing no seasonal recovery. Monthly monitoring of Atlantic City, NJ (Sorensen et al., 1988) and Pinellas County, FL (Creaser et al., 1993) nourishments reported only end-of-winter or post-storm losses, also with no indication of recovery. Nearly quarterly monitoring of a two-phase nourishment at Ocean City, MD showed two

examples of post-storm recovery after a series of closely spaced storms (Stauble and Kraus, 1993). However, in all of these cases, the beach response was dominated by the nourishment profile shape equilibration and the long-term net loss of sediment, often attributed to alongshore transport. None of these observations concern the evolution of a nourishment at a site with a very strong cross-shore seasonal pattern, and very few reports utilized time as the independent variable.

Nourishments in Europe are often monitored frequently initially and then once or twice a year thereafter (Hanson et al., 2002). Dean (2002) recommends one-half year to two year survey intervals, unless unusual behavior is expected. The results of the current study suggest more frequent monitoring is needed on beaches with large seasonal cycles. At Terschelling, Netherlands, three to four times yearly surveys were completed as part of an extensive nourishment monitoring program, and a large volume of sand (2 million m^3) was added to the beach so that the nourishment trends would stand out above the seasonal and interannual variability (Hamm et al., 2002). Overall, there are few observations of nourishments on beaches with large seasonal cycles, and the predictability of nourishment evolution on these beaches is severely limited (Marine Board, 1995; Capobianco et al., 2002).

In southern California, seasonal fluctuations in wave energy, with moderate energy winter storms and low energy summer waves, drive strong seasonal fluctuations in sand levels. The seasonal cycle is characterized by offshore sand movement causing shoreline erosion and the formation of an offshore bar in winter, and onshore sand migration resulting in shoreline accretion in summer (Shepard, 1950; Winant et al., 1975; Aubrey, 1979). Cross-shore profiles located approximately 2 km south of the present study region showed vertical seasonal sand level fluctuations of about 2 m near the shoreline and the offshore bar (Winant et al., 1975).

In 2002, the San Diego Association of Governments (SANDAG) sponsored the Regional Beach Sand Project, nourishing San Diego County Beaches with 1.6

million cubic meters of sand, which was divided between twelve nourishment sites, with each site receiving between 77,000 and 320,000 m^3 of sand along 300 to 1300 m of coastline. The 600 m-long, 160,000 m^3 subaerial nourishment at Torrey Pines Beach eroded rapidly during a November 2001 storm (Seymour et al., 2005). As anticipated by Stive et al. (1991) and others, the subaerial beach nourishment spread across the entire cross-shore profile. On a beach with a large seasonal cycle, the effects of the nourishment sand may persist after the initial erosion from the subaerial beach because the nourishment sand may be stored in the offshore bar and returned to the beach face during the following summer.

Here, the evolution of nourished and adjacent beach profiles are quantified and compared over several seasonal cycles. In section 3.3, the observations are described, and the surveyed alongshore span is divided into nourishment, buffer, and control regions. In section 3.4, the evolution of cross-shore profiles in the nourishment is shown, and the horizontal displacement of depth and elevation contours (related to changes in the width of the subaerial beach available for recreation) is compared in these three alongshore spans. The effect of the nourishment on seasonal cross-shore fluxes of sand between the shoreline and the offshore sandbar are examined in section 3.5. In section 3.6, the evolution of total volumes (sum of shoreline and offshore bar volumes) in the three alongshore spans is contrasted. Results are discussed in section 3.7 and summarized in section 3.8.

3.3 Description of observations

Sand levels were surveyed with a GPS-equipped all terrain vehicle, hand-pushed cart, and personal watercraft with an acoustic depth sounder (Seymour et al., 2005). Locally shore-normal transects, extending from the backing cliffs or revetment seawards to about -8 m water depth, were surveyed every 20 m alongshore over a 700 m-long reach centered on the fill, and at 100 m alongshore intervals for 1000 m on adjacent up- and down-coast beaches, for a total of 56

transects (Figure 3.1b). One pre-nourishment survey was completed at the end of February 2001. Approximately biweekly surveys began following the fill construction in April 2001 (Figure 3.1b), continuing through a storm in November 2001, with less frequent surveys thereafter. Beginning with the November 2001 survey, twelve additional transects decreased the survey line spacing immediately south of the nourishment from 100 m to 25 m. Approximately seven years of observations, through the beginning of 2008, are considered in detail here. Of the forty-two

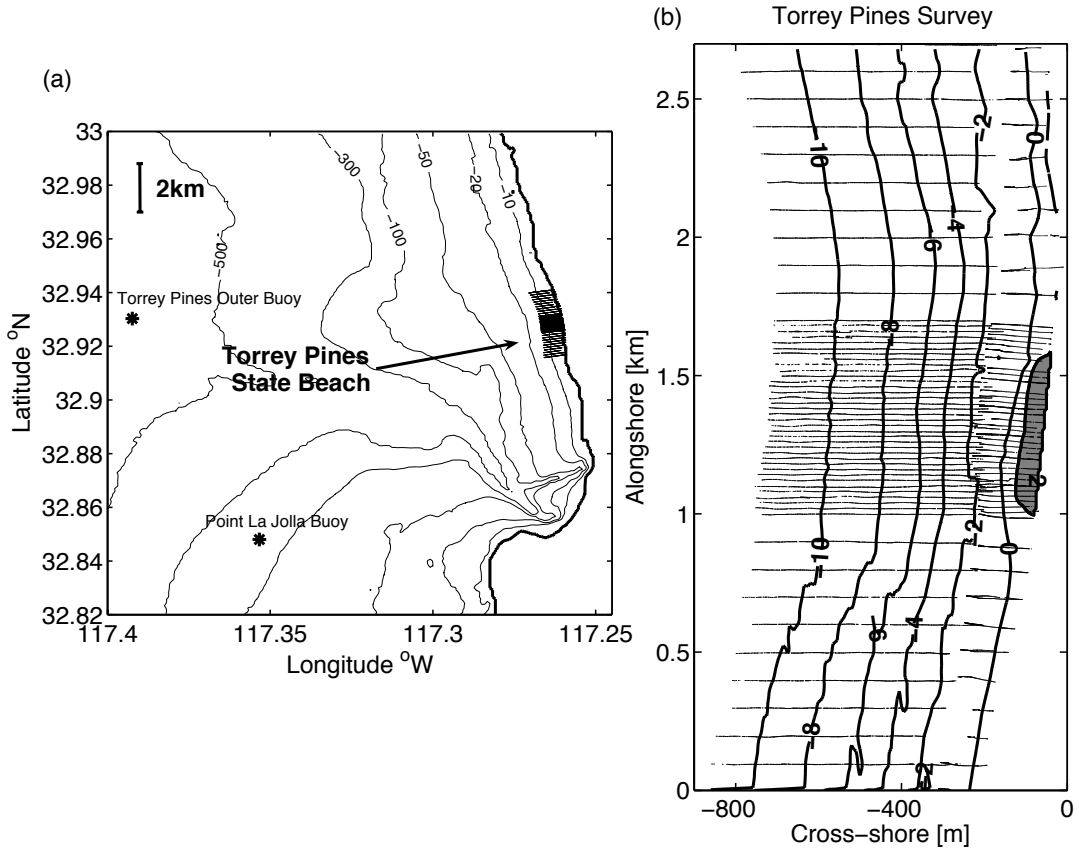

Figure 3.1: (a) Location of the Torrey Pines Beach fill surveys (arrow pointing to cross-shore transects) and nearby wave buoys (asterisks). Contours (thin curves) are depth in meters below MSL, and the Scripps Submarine Canyon is in the lower right corner. (b) Plan view of the 2.7 km alongshore span surveyed from the 27-29 April 2001, shortly after the nourishment was completed. Survey data (thin, nearly parallel lines) were collected along cross-shore transects, and estimated elevation contours (bold alongshore curves) are shown in meters above or below MSL. The 2-m high nourishment pad near the shoreline is shaded gray.

full bathymetry surveys collected, two were excluded owing to large gaps in the spatial coverage caused by energetic waves and the presence of surfers. Thirty-six additional surveys of the subaerial beach face, between the backbeach (the revetment) and the waterline (about MSL), were obtained with an all-terrain vehicle approximately monthly between February 2004 and January 2007.

Depth contours for a few km on either side of the nourishment are relatively straight and parallel, and waves in the survey area are not influenced by the Scripps Submarine Canyon (Figure 3.1a). Wave conditions were monitored with the Coastal Data Information Program wave network (nearby buoys are shown in

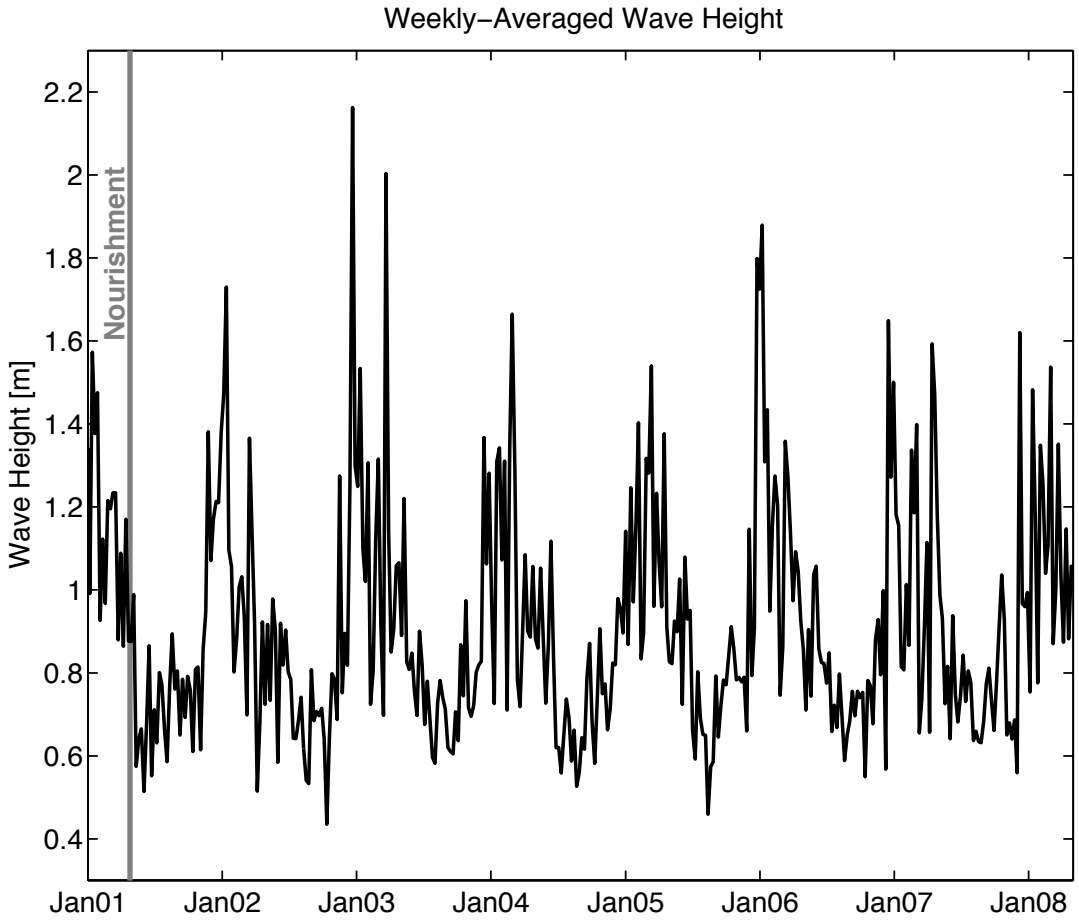

Figure 3.2: Weekly-averaged wave height at Torrey Pines along the 2.7 km survey span shows strong seasonal variation. The nourishment was completed on April 27-29, 2001 (vertical gray line).

Figure 3.1a). A spectral refraction wave model was combined with offshore buoy observations to estimate wave height on the 10 m depth contour, every 100 m alongshore. Wave height varies seasonally, with larger winter swell arriving from the northwest Pacific Ocean, and generally smaller summer swell arriving from the south Pacific Ocean (Figure 3.2). Tidal vertical ranges were about 1.0 m (neap) and 2.5 m (spring).

3.4 Displacement of elevation contours

Prior to the nourishment, in February 2001, the beach was in a typical winter state. The subaerial beach was narrow, and shoreline depth contours (e.g. MSL, +1 m) were located close to the backshore revetment or cliff (n_0, pre-nourishment survey, Figure 3.3b, +1 m contour shown). Immediately after the nourishment in late April 2001 (n_1, post-nourishment survey, Figure 3.3b), the shoreline contours bulged approximately 40 m seaward between alongshore coordinate 1.0 and 1.6 km. This 600-m alongshore span is hereafter referred to as the nourishment region (N). Buffer regions (B) defined adjacent to the nourishment (0.5-1.0 km and 1.6-2.2 km), and control regions (C) defined furthest from the nourishment (0-0.5 km and 2.2-2.7 km), showed little shoreline change during this two-month period (compare n_1 with n_0, Figure 3.3b). Additionally, there was little change in the location of the -4 m contour over the entire 2.7 km alongshore span (compare n_1 with n_0, Figure 3.3a).

In the seven months following the fill completion, the significant height of incident waves was low (typical for summer, Figure 3.2). Hourly-estimated significant wave heights were between 0.4 and 1.5 m, and were usually less than 1 m. Bathymetry changes in B and C, away from the fill region, were consistent with the usual seasonal cycle in southern California with summertime offshore erosion (about 1 m of vertical erosion between -5 and -2 m depth) and shoreline accretion (often >1 m) as the winter bar moved shoreward and merged with the

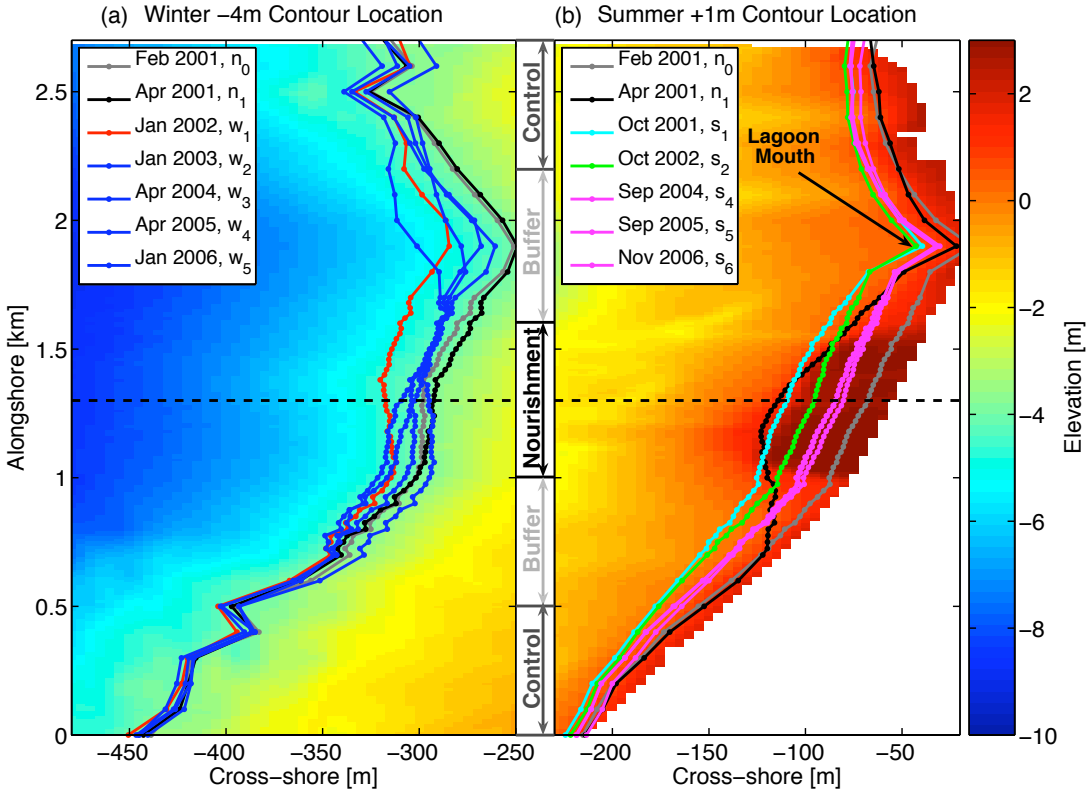

Figure 3.3: Plan view of the post-nourishment survey (April 27-29, 2001, color scale is to the right). The beach is backed by steep cliffs or a highway revetment [white area in (b)]. The curves indicate the location of the (a) 4 m depth contour in winter (w_{1-5}), when the offshore sandbar is most developed, and (b) +1 m elevation contour during summer (s_{1-6}), when the exposed beach is widest. Legends give survey times and a survey index number for cross-referencing to Figures 3.4 - 3.8. The pre-nourishment (n_0, gray line) and immediate post-nourishment (n_1, black line) surveys are shown in both panels for reference. The alongshore extents of the nourishment, buffer, and control regions are indicated between the panels.

shoreline. By October 2001, the +1 m contour in B and C moved seaward an average of 20 m (compare s_1 with n_1, Figure 3.3b), with about 1 m of vertical shoreline accretion (Seymour et al., 2005).

Time series of the horizontal location of shoreline elevation (average of the 0 m and +1 m contours) and offshore bar depth (average of the -5 m and -4 m contours), averaged over N, are shown in Figure 3.4, and the evolution of a representative cross-shore profile in N (location indicated with dashed line in

Figure 3.3) is shown in Figure 3.5. During summer 2001, waves reached the fill only once or twice, and shoreline contours moved offshore about 5 m (compare s_1 with n_1, Figure 3.4). In detail, the +1 m contour remained rather stationary in the southern fill end (1.0-1.4 km) and moved slightly offshore (accretion) in the northern fill end (1.4-1.6 km, compare s_1 with n_1, Figure 3.3b). The offshore bar contours in N were displaced landward (erosion) approximately 30 m (compare s_1 with n_1, Figures 3.4 and 3.5a), but this sand was largely blocked by the nourishment from reaching the shoreline. For example, the nourishment (n_1) and summer (s_1) cross-shore profiles remained nearly unchanged above approximately -1 m water depth, while the offshore sandbar eroded (Figure 3.5a). The fate of sand displaced from the bar and blocked from returning to the beach face, is unknown.

The first winter storm in November 2001, with significant wave height exceeding 2 m for about three days, eroded the shoreline over the entire surveyed span (Seymour et al., 2005). This storm and subsequent winter storms removed most of the fill from the shoreline, displacing shoreline contours landward (erosion) about 50 m (compare w_1 with s_1, shoreline, Figures 3.4 and 3.5b). The sand eroded from the shoreline formed an offshore bar, indicated by the 50 m seaward displacement (accretion) of the bar depth contours (compare w_1 with s_1, bar, Figure 3.4). The offshore bar volume was enhanced in N, pushing the depth contours farther offshore than observed in the subsequent four winters (compare w_1 with w_{2-5}, Figures 3.3a and 3.5b, and bar curve, Figure 3.4). The nourishment sand eroded from the beach face appears to have fed the offshore sand bar during the winter following the nourishment, when it was not yet too widely dispersed to be measured.

During the following summer (2002), the offshore winter bar remerged with the shoreline, again creating a detectable shoreline bulge in the nourishment region (s_2, Figures 3.3b and 3.5a). Offshore erosion moved bar contours landward more than 40 m (s_2, bar, Figure 3.4), and shoreline accretion displaced the shoreline seaward more than 30 m (s_2, shoreline, Figure 3.4). By the end of the summer,

the beach was wider in the nourishment region than observed in the subsequent three summers (compare s_2 with s_{4-6}, Figures 3.3b and 3.5a, and shoreline curve, Figure 3.4). The bulge of sand in the nourishment region was not detectable in the shoreline or offshore bar contour locations after the end of the second summer following the nourishment.

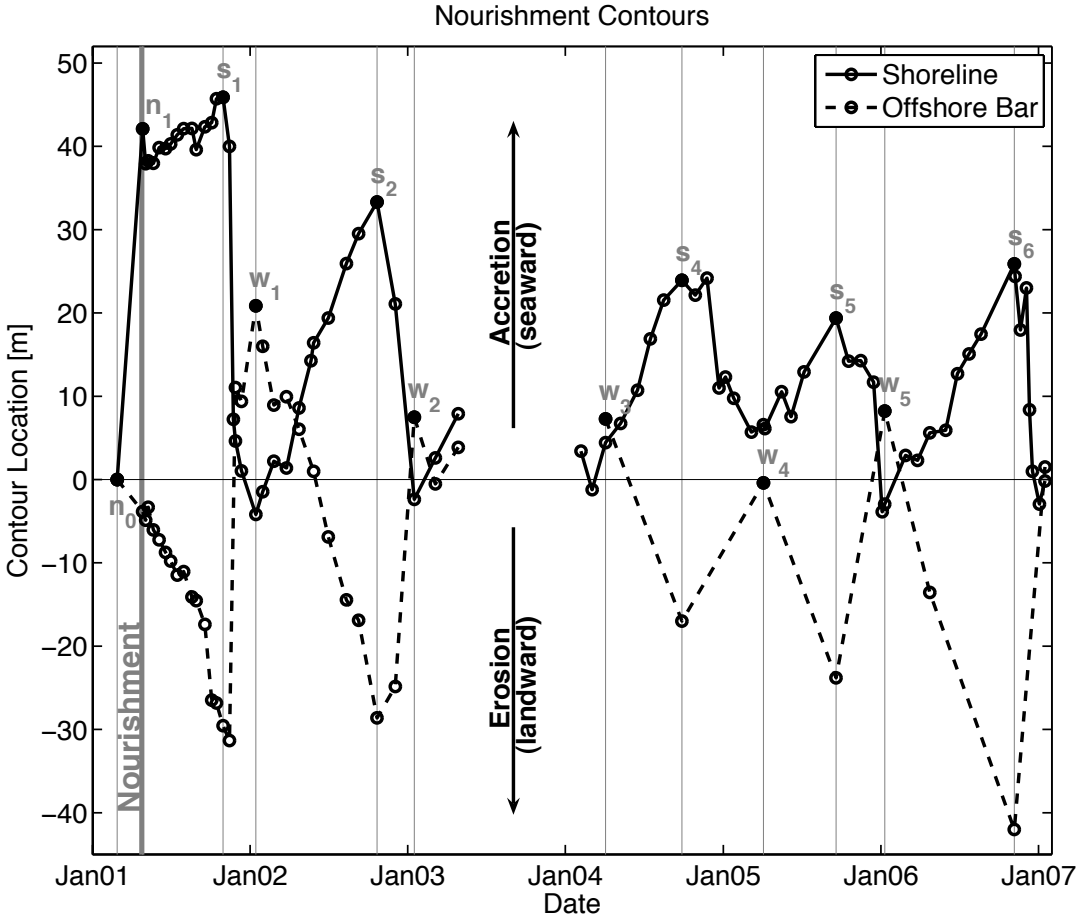

Figure 3.4: The elevation contour cross-shore location evolution is shown in the nourishment region (1.0-1.6 km alongshore, see Figure 3.3). The shoreline (solid) curve is the average of the 0 m and +1 m elevation contours, and the offshore bar (dashed) curve is the average of the -5 m and -4 m depth contours. Locations are relative to the pre-nourishment survey, with positive change indicating seaward movement (accretion). Observations (circles) were more frequent near the shoreline and show that the offshore surveys between 2004 and 2007 were obtained close to seasonal extrema in shoreline location. Filled circles and vertical lines correspond to surveys shown in Figure 3.3.

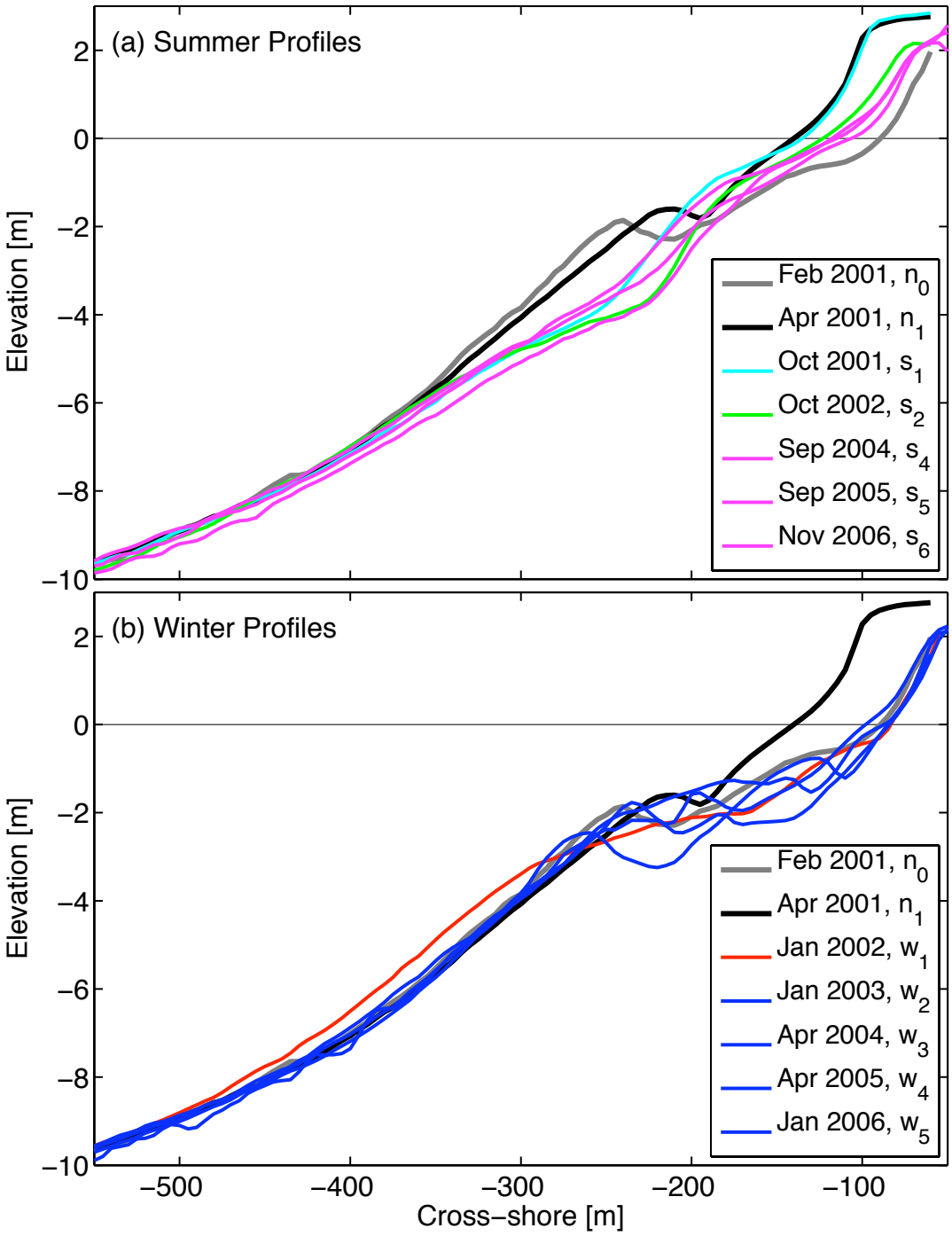

Figure 3.5: Cross-shore profiles at a representative transect in the nourishment region (location indicated with dashed line in Figure 3.3): (a) summer profiles (s_{1-6}) and (b) winter profiles (w_{1-5}), with the same legend as Figure 3.3. For reference, pre-nourishment (n_0, gray line) and post-nourishment profiles (n_1, black line) are shown in both panels.

3.5 Cross-shore fluxes between the offshore bar and the shoreline

To estimate cross-shore fluxes, time series of beach face and offshore bar volumes were calculated for N, B, and C using survey transects common to the forty selected surveys, extending from the backbeach to approximately -8 m depth. The -2 m depth contour (approximately the pivot point of seasonal sand level changes) was used to separate the beach face and offshore bar regions. Volumes were calculated relative to the pre-nourishment survey (Figure 3.6), and normalized volumes (m^3/m, or volume per unit alongshore length) are shown because the alongshore lengths of N, B, and C are different and somewhat arbitrary. Normalized volumes address the effect of the nourishment on local cross-shore transport processes, allowing comparisons between N, B, and C. Non-normalized volumes (m^3) are discussed in sections 3.6 and 3.7. The full bathymetry surveys necessary to estimate volumes were collected biweekly to monthly through mid-2003, then an average of about three times yearly from 2004 to 2007 (Figure 3.6). Monthly surveys of the subaerial beach show that the biannual to quarterly full bathymetry surveys were obtained close to seasonal extrema in shoreline location (Figure 3.4), as desired.

The nourishment was the largest shoreline accretion event (200 m^3/m volume increase, n_1, Figure 3.6a). Between the nourishment and the end of summer 2001, the beach face volume did not change significantly in N (compare n_1 with s_1, Figure 3.6a), while accretion occurred steadily throughout this period in B (+100 m^3/m) and C (+75 m^3/m). Alongshore leakage of sand from N to B may have increased the volume in B above C during the first two summers that the nourishment sand was detectable (s_1 and s_2, Figure 3.6a).

During the November 2001 storm and the remainder of the 2001 to 2002 winter, the beach face was severely eroded along the entire 2.7 km alongshore reach (losing between 80 and 250 m^3/m), resulting in similar shoreline volumes in each

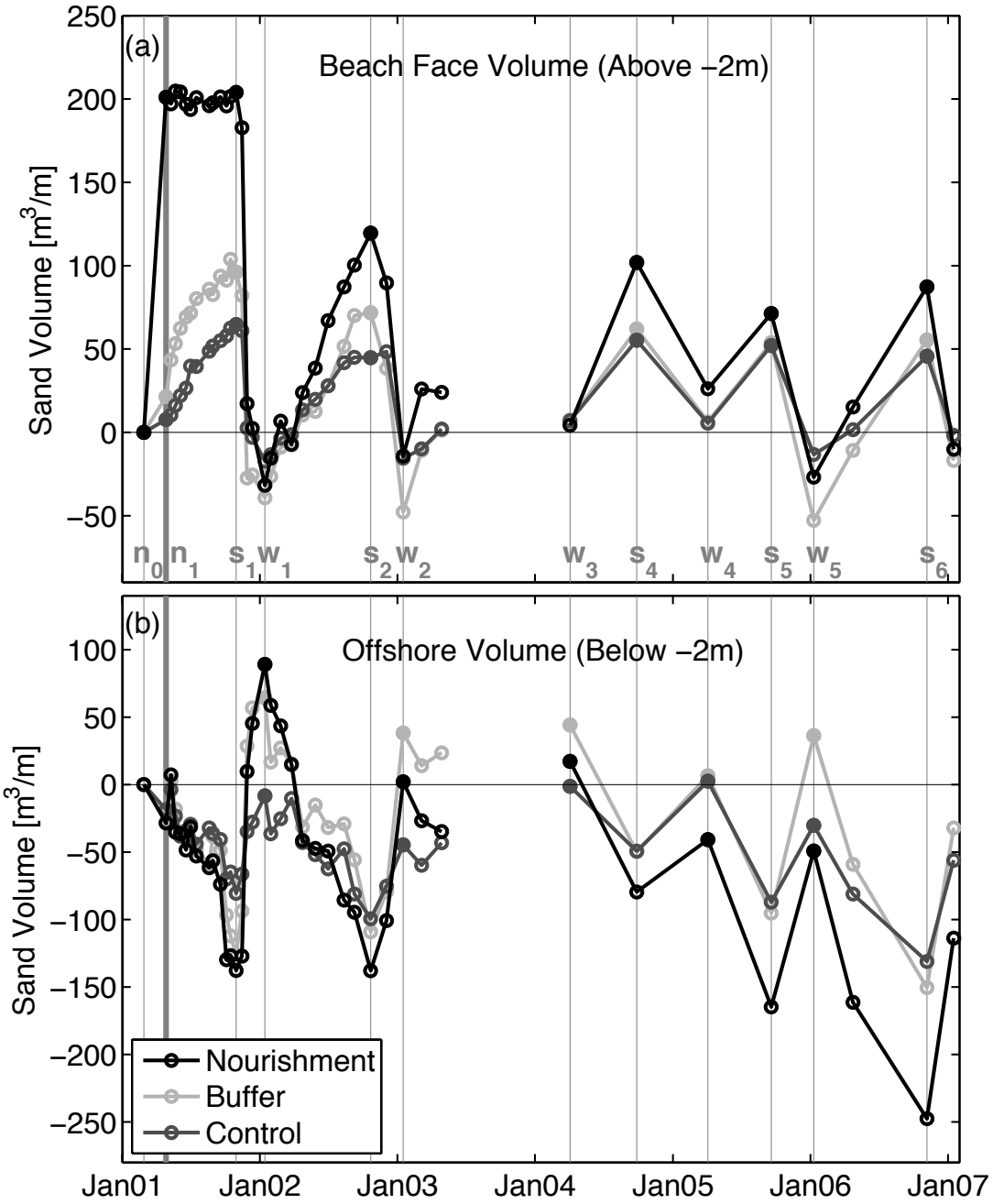

Figure 3.6: Normalized sand volume (m^3/m) versus time (a) near the shoreline (above the -2 m contour), and (b) near the offshore sand bar (below the -2 m contour). Volumes normalized by alongshore length of each section are shown for the nourishment, buffer, and control regions, relative to the pre-nourishment survey (n_0). Filled circles and vertical lines identify survey dates shown in Figure 3.3.

region (w_1, Figure 3.6a). That is, the nourishment was completely eroded from the beach face, as shown by Seymour et al. (2005). In the offshore, alongshore leakage of sand from N to B is apparent as B gained 200 m^3/m (difference between w_1 and s_1, Figure 3.6b), similar to the N (230 m^3/m), and significantly larger than C (70 m^3/m). The offshore bar volumes in N and B were elevated compared with both C (w_1, Figure 3.6b), and with future years in these regions (compare w_1 with w_{2-5}, Figure 3.6b).

In summer 2002, the offshore bar moved back onshore, and the beach face accreted preferentially in the nourishment region, with a slightly larger sand volume than in any following year (compare s_2 with s_{4-6}, Figure 3.6a). By the following winter, the nourishment sand eroded from the beach face was not clearly detectable in the offshore bar volumes: N was larger than C, but smaller than B (w_2, Figure 3.6b). Cross-shore fluxes of sand from the beach face to the offshore bar in N and B show the presence of an additional bulge of sand (in comparison to C) through a complete seasonal cycle until late fall 2002.

3.6 Cross-shore integrated volumes

The total volume in each region (sum of offshore bar and beach face, relative to the pre-nourishment survey) does not show large seasonal changes (Figure 3.7). Perhaps surprisingly, the total N volume decreased substantially during the first summer after the nourishment (compare s_1 with n_1, Figure 3.7). In survey s_1, prior to the November 2001 storm, the offshore bar volume decreased substantially in all regions (25-60 m^3/m, Figure 3.6b). However, in B and C there was some compensating shoreline accretion (20-30 m^3/m, Figure 3.6a), whereas in N there was not. Thus, low waves during summer 2001, coupled with the blocking of shoreline accretion by the nourishment, caused the loss from the entire cross-shore region of N of roughly two-thirds of the initial nourishment (compare s_1 with n_1, Figure 3.7). The first storm of winter moved large amounts of sand from the beach

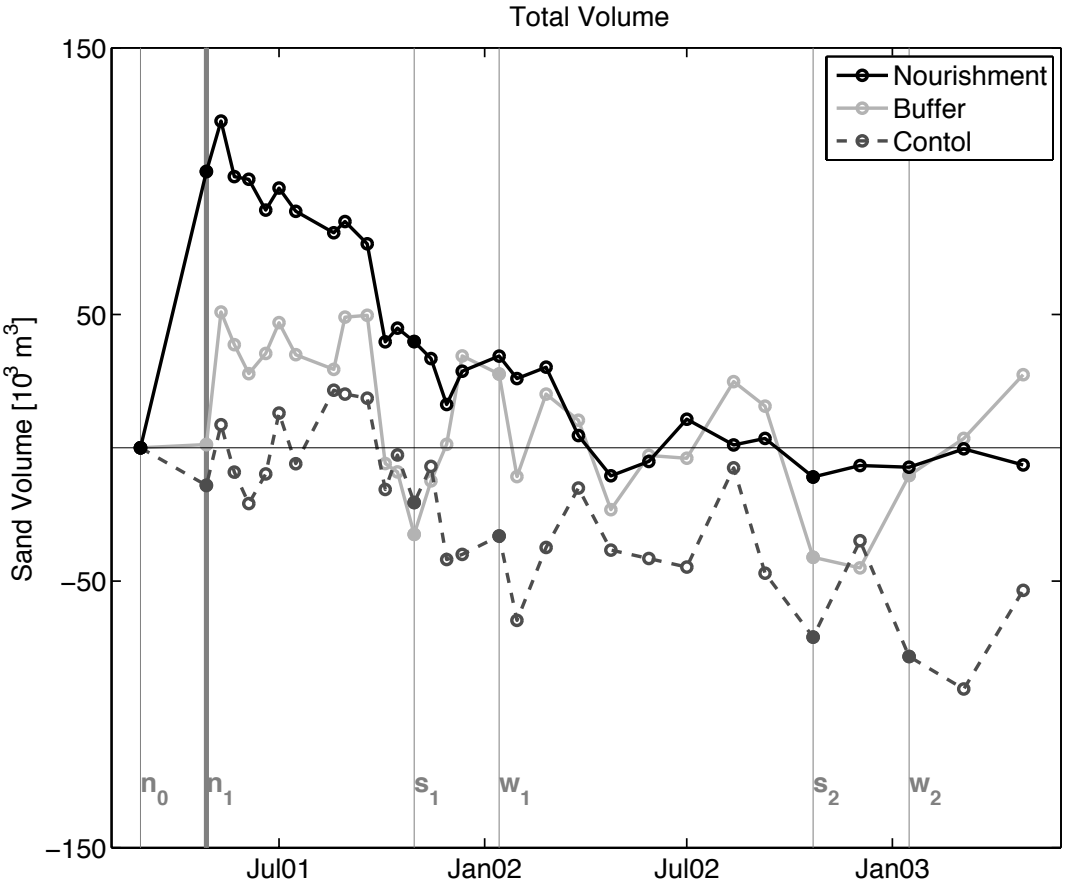

Figure 3.7: Total sand volume (m^3) versus time for the nourishment, buffer and control regions. Total volumes relative to the pre-nourishment survey (n_0) are the sum of shoreline and offshore bar volumes (similar to Figure 3.6, but here the volumes are not normalized). The first 2.5 years of surveys are shown.

face to the offshore bar, but the total sand volume (sum of beach face and offshore bar) did not vary greatly in any region. By the end of the winter, the total sand volume in B actually increased (compare w_1 with s_1, Figure 3.7). By mid-summer 2002 (between w_1 and s_2, Figure 3.7), the total N volume decreased and became indistinguishable from C. Thus, the nourishment sand was detectable through fall 2002 from a bulge in shoreline contours (s_2, Figures 3.3b, 3.4, and 3.5a) and elevated beach face volumes (s_2, Figure 3.6a), but not in the total nourishment region volume (Figure 3.7).

3.7 Discussion

Nourishment effects on the local 600 m-long nourishment beach were observed first as a shoreline bulge, then as an enhanced offshore bar, and finally as a reduced shoreline bulge. Total volumes, summed over the entire profile, suggest that sand was leaking from the nourishment region when the nourishment was completed, even though waves were low (Figure 3.7). After about two years, the nourishment could not be detected in either contour locations or cross-shore integrated volumes.

Volume fluctuations at longer temporal and spatial scales are apparent in sand volume observations extended to April 2008 (Figure 3.8). Similar patterns of temporal change in total N, B, and C between 2004 and 2008 indicate spatially coherent sand movement into or out of the survey region. In only two years between January 2005 and January 2007, the grand total volume (sum of the cross-shore volume for the entire 2.7 km reach) decreased by 350,000 m^3, about twice the volume of the 160,000 m^3 spring 2001 nourishment. Variations in the grand total volume between surveys in 2007 are also as large as the nourishment volume. Large amounts of sand were presumably transported across the survey boundaries, both alongshore and cross-shore. Unknown, but believed relatively small sand volumes fluxed through a small lagoon mouth (that was sometimes closed) into the buffer region (lagoon mouth identified in Figure 3.3b). Over the seven-year survey period, a total of 84,000 m^3 of sand was dredged from the lagoon (on eleven occasions) and placed adjacent to the lagoon mouth near the shoreline. An unknown amount of this sand was pushed into the lagoon mouth by alongshore transport and was thus returned to the beach through the dredging operations. The dredged sand volumes placed on the beach did not appear to cause any significant deviations in the seasonal sand volume changes and are not expected to have affected the observations of the nourishment response. The size of errors arising from the measurements and from the alongshore sampling (100 m spacing outside of the

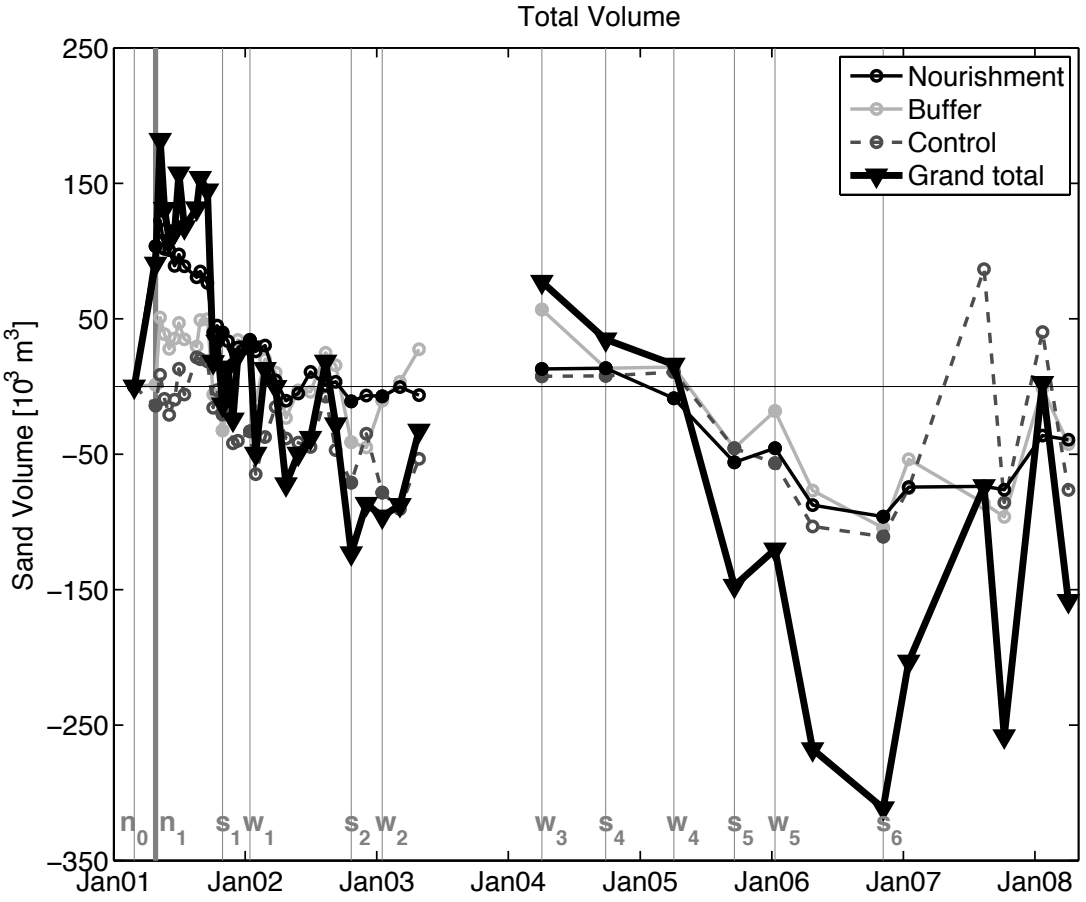

Figure 3.8: Total sand volumes (m^3) relative to the pre-nourishment survey (n_0) in the nourishment (N), buffer (B), and control (C) regions versus time (as in Figure 3.7, extended for over seven years). Grand total volume (bold) is the sum of the N, B, and C total volumes.

nourishment region), are poorly known.

The lack of shoreline accretion in the nourishment region during summer 2001, seen in both the shoreline contours (Figures 3.3b, 3.4, and 3.5a) and the beach face volume (Figure 3.6a), suggests that the nourishment timing may have impacted its persistence. The shoreline nourishment bulge appeared to effectively block sand that would naturally have returned to the shoreline during the summer, as part of the usual seasonal cycle. If the same nourishment volume had instead been placed on the seasonally accreted beach face in late summer 2001, bringing the maximum beach elevation up to +4 m (instead of +2 m), the nour-

ishment sand may have remained on the beach face longer, perhaps over several seasons. On the other hand, the benefit of having the widest subaerial beach during the summer months, immediately following the end-of-winter nourishment, is lost. The tradeoffs of completing nourishments at different times of the year on beaches with strong seasonal cycles are not well understood. Note however that the present nourishment only spanned 600 m, and the nourishment volume (per meter of beach) was smaller than the seasonal cross-shore exchange of sand between the shoreline and the offshore bar. This nourishment was likely too small, regardless of timing, to have had a significant, long-term impact on the beach.

3.8 Conclusions

The Torrey Pines Beach nourishment (160,000 m^3) was monitored bi-weekly to monthly for 2.5 years through several seasonal cycles. Although seasonal cross-shore volume fluxes exceeded the total nourishment volume, the nourishment was detectable for nearly twenty months. The nourishment sand formed bulges in both contour locations and volumes at the shoreline (in summer) and at the offshore bar (in winter) until the end of the second summer following the nourishment. An extended seven-year time series of monitoring showed large changes in the total beach volume, which were not associated with the seasonal cycle or the nourishment. The origin of these volume fluctuations is unknown. Future monitoring of nourished beaches with large seasonal cycles would benefit from extending the cross-shore profiles farther offshore to try to capture all cross-shore fluxes, and from having more observations, through at least one seasonal cycle prior to the nourishment, to establish a better baseline.

Acknowledgements

Financial support from the California Department of Boating and Waterways (California Resources Agency) and the U.S. Army Corps of Engineers is

gratefully acknowledged. The bathymetry measuring system was constructed and operated by Brian Woodward, Bill Boyd, Dennis Darnell, Kent Smith, and Ian Nagy. Marissa Yates was partially supported by an NDSEG Fellowship.

The text of Chapter 3, in full, is a reprint with minor modifications of the paper "Seasonal Persistence of a Small Southern California Beach Fill," *Coastal Engineering*, doi: 10.1016/j.coastaleng.2008.11.004 (in press). The dissertation author was the primary researcher and first author with guidance provided by R.T. Guza, W.C. O'Reilly, and R.J. Seymour.

4

Equilibrium shoreline response

4.1 Abstract

Shoreline location and incident wave energy, observed for almost five years at Torrey Pines beach, show seasonal fluctuations characteristic of southern California beaches. The shoreline location, defined as the cross-shore position of the mean sea level elevation contour, retreats by as much as 40 m in response to energetic winter waves and gradually widens again during low energy summer waves. The fluctuations in hourly incident wave energy and monthly or more frequent shoreline location are used to develop and calibrate an equilibrium model, where the change in shoreline location depends on both the magnitude of the wave energy E and the wave energy disequilibrium $\Delta E(S) = E - E_{eq}(S)$. The equilibrium energy $E_{eq}(S)$, which causes no change in shoreline location, is a function of the current shoreline location S. Using calibrated values of model free parameters, observed and modeled shoreline location are well correlated. The model also reproduces shoreline location observed at two additional survey sites, with optimal fit free parameter values similar to Torrey Pines. Correlations between observed and modeled shoreline location are above 0.6 for 16 subregions, each spanning a 500-m alongshore reach. However, the model fails when neglected geologic factors are important (e.g. underlying bedrock limits erosion, or sand availability limits accretion). The model free parameters can be estimated with as little as two years

of monthly shoreline observations or five years of ideally-timed, biannual shoreline observations. The model successfully reproduces shoreline location for withheld time periods not used in tuning and can be used to predict beach response to past or hypothetical future wave climates.

4.2 Introduction

Sandy beaches erode and accrete in response to changing wave conditions. Models for wave-driven change in beach sand levels span a wide range of complexity. Broadly, the more complex formulations are flux gradient models, and the simpler ones are bulk response models. Flux gradient models estimate changes in sand level using conservation of mass, with spatial gradients in time-averaged sediment flux balanced by erosion or accretion. At the complex end of the flux-gradient-model spectrum are wave-phase resolving, two-phase flow models that include both inter-granular interactions and turbulent suspension [e.g. Dong and Zhang (2002); Hsu et al. (2004)]. These computationally intensive models predict time-dependent fluid velocities and sediment fluxes in the wave boundary layer and require input time series of velocity (including wave orbital velocity) above the wave boundary layer at many grid points. Values of several model coefficients are often unknown because the many complex processes included are not well understood. Flux gradient models that parameterize wave-induced sediment transport using wave-averaged statistics are less detailed. Only wave-averaged, low-order moments (e.g., variance, skewness) are used, and empirical coefficients relate velocity and acceleration moments to the seabed stresses and resulting sediment transport. For example, skewness (or third-moment) of cross-shore velocity (Bailard, 1981) and cross-shore acceleration (Drake and Calantoni, 2001) time series have been used in morphologic change models [Roelvink and Stive (1989); Gallagher et al. (1998); Hoefel and Elgar (2003); and others]. Similar to the more complex two-phase models, spatial gradients in the estimated sediment flux are

balanced by erosion or accretion.

Bulk response models are essentially phenomenological: observations of waves and beach change are used to validate and calibrate simple heuristic rules for beach change. Equilibrium profile response models are one subset of these models, where the equilibrium beach profile is the shape that the beach attains when exposed to steady wave conditions until no further change occurs. Equilibrium shapes have been suggested, for example $h(x) = Ax^{2/3}$, where h is the water depth, x is the distance offshore, and A depends on the sediment grain size [Bruun (1954); Dean (1977); and others]. Alternative shapes for the equilibrium beach profile, with finite shoreline slope or the inclusion of offshore sandbars, have also been proposed [e.g. Inman et al. (1993); Özkan Haller and Brundidge (2007)]. Equilibrium beach response concepts have been used to model evolution of beach profiles (Larson and Kraus, 1989), beach nourishment projects (Dean, 1991), sea level rise (Dubois, 1990), storm surge (Kriebel and Dean, 1993), the interannual variation in the cross-shore location of the sandbar crest Plant et al. (1999), and shoreline change (Miller and Dean, 2004).

Wright and Short (1984) developed a set of equilibrium beach states, including straight and alongshore variable sandbars, which depend on the value of Dean's parameter, $\Omega = H_b/w_s T$ (Dean, 1973), where H_b is the breaking wave height, w_s is the grain-size dependent sediment fall velocity, and T is the wave period. Beach morphologies do not respond instantaneously to changes in the wave field, and correlations between instantaneous beach state and instantaneous Ω were weak in their observations. Wright et al. (1985) suggested that the present beach state is determined by a weighted Ω, which includes the previous beach state by averaging over a time period that depends on the local wave climate. Dalrymple (1992), Masselink and Short (1993), List and Farris (1999), Larson and Hanson (2000), Miller and Dean (2007b), and Quartel et al. (2008), among others, used instantaneous or averaged wave properties to define transitions between beach states. However, Morton et al. (1995), Lee et al. (1998), Anthony (1998), and

Jiménez et al. (2008) emphasize that the morphology of beaches dominated by storms, with intermittent and seasonal recovery periods, are not well correlated with instantaneous wave conditions because of the importance of the previous beach state. Recently, Miller and Dean (2007b) tried to include the effects of the antecedent beach in relationships between beach states and a variety of wave parameters with lagged correlations.

Sonu and James (1973) suggested that transitioning from erosion to accretion was dominated not by the instantaneous wave field but by the time derivatives, emphasizing the importance of the history of the beach. Wright et al. (1985) also observed that large changes in beach state occurred simultaneously with large changes in the wave field (with both H_s and Ω), although a direct correspondence was weak. Wright et al. (1985) further suggested that the beach adjustment rate toward equilibrium depends on the instantaneous disequilibrium of the wave field ($\Omega - \Omega_{eq}$) and the relative magnitude of the wave event (Ω or Ω^2), but they lacked sufficient measurements to demonstrate this concept. This study pursues the equilibrium concepts of Wright et al. (1985), using extensive sand level change observations and hourly estimates of the wave field to resolve even short-lived storms.

At Torrey Pines Beach in southern California, the site of the present study, quantitative descriptions of seasonal erosion and accretion patterns were made with empirical eigenfunctions of monthly cross-shore profiles (Winant et al., 1975; Aubrey, 1979). Aubrey et al. (1980) made statistical predictions of weekly profile eigenfunctions using a combination of the weekly-averaged wave energy and the previous profile eigenfunction values as predictors to include both the instantaneous forcing and the antecedent beach state, but they suggested that a longer data set and shorter sampling interval would decrease the forecast error.

Here, multiyear observations of shoreline position and incident waves at Torrey Pines Beach (described in section 4.3) are used qualitatively to illustrate equilibrium beach change concepts (section 4.4). A simple equilibrium shoreline

model is developed (section 4.5), which reproduces well the observed shoreline movement at Torrey Pines and two nearby survey sites (section 4.6). The effects of survey sampling frequency and duration on model performance, and the strong relationship between displacement of the shoreline and other depth contours, are discussed (section 4.7).

4.3 Observations

Sand levels and waves were monitored at four study sites within a 65-km alongshore reach in San Diego County, CA (Figure 4.1).

4.3.1 Study sites

The general survey site characteristics (e.g. beach slope, sand grain size) are summarized in Table 4.1. Torrey Pines (8 km) is a wide, sandy beach backed by a revetment in the northern section and approximately 100 m high cliffs in the southern section. Patches (10's of meters alongshore) of a single layer of cobbles may be exposed on the beach face during winter. Approximately 15 km to the

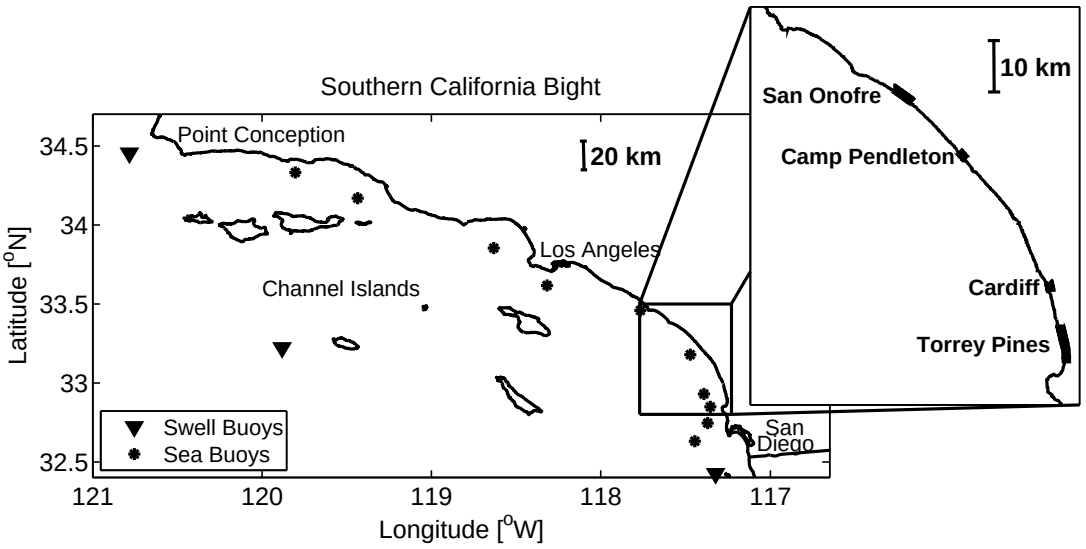

Figure 4.1: Map of the Southern California Bight identifying the wave buoy (see legend) and in situ survey (see inset) locations.

Table 4.1: Beach width (MSL to backbeach), beach slope at MSL, and median sand grain diameter (D50) at MSL and at approximately +1 to +2 m elevation for each survey site.

Survey site	**Beach width (m)**	**Beach slope**	**MSL D50 (mm)**	**+1 to +2 m D50 (mm)**
Torrey Pines	20 - 120	0.01 - 0.03	0.2	0.18
Cardiff	20 - 50	0.02 - 0.04	0.2	-
Camp Pendleton	50 - 130	0.02 - 0.04	0.2	0.23
San Onofre	20 - 70	0.03 - 0.05	0.3	0.35

north, Cardiff (2 km) is a narrow, sandy beach with regions (100's of meters alongshore) of exposed bedrock on the beach face and in the surf zone. The northern end of the beach is backed by a revetment, and the southern end is backed by cliffs (about 20 m high). Cobble layers (100's of meters alongshore) often cover portions of the exposed beach face during winter months. Farther to the north, Camp Pendleton (2.5 km) is a wide, sandy beach, similar to Torrey Pines. However, the beach is backed by vegetated dunes and remains sandy throughout the entire year. The northernmost survey site, San Onofre (4 km), is a narrow and steep beach. The upper portion of the beach face, which is exposed to wave action at high tide, is mostly covered in thick cobble cusps throughout the year. Shoreward of the cusps, a flat, silty and sandy region extends landward to the base of 40 m high cliffs. Neap and Spring tidal ranges are approximately 1.0 and 2.5 m, respectively.

4.3.2 Sand level observations

Weekly to monthly surveys above the low tide waterline, spanning the subaerial beach, were acquired with a GPS-equipped all terrain vehicle (ATV) driven on shore-parallel transects, separated by approximately 10 m in the cross-

Table 4.2: Alongshore survey length, survey date range, number of surveys, and approximate frequency of surveys for each survey site.

Survey site	Alongshore length (km)	Date range	Number of surveys	Alongshore survey frequency
Torrey Pines	8	Dec. 2002 - Jul. 2008	134	Weekly to monthly
Cardiff	2	May 2007 - Jul. 2008	32	Biweekly to monthly
Camp Pendleton	2.5	Dec. 2006 - Jul. 2008	26	Monthly
San Onofre	4	May 2005 - Mar. 2007	17	Monthly*

*sampled monthly until August 2006, with one additional survey in March 2007

shore direction (Figure 4.2b). Two to four times yearly full bathymetry surveys spanned from the backbeach (e.g. cliffs, revetment) to approximately -10 m water depth along pre-defined cross-shore transects (Figure 4.2a). At low tide the ATV and a hand-pushed cart surveyed to wading depths, and at high tide a personal watercraft with a GPS and a depth-sounder surveyed from -10 m depth to the breaker line. Root-mean-square (RMS) vertical errors are estimated to be less than 15 cm. See Table 4.2 for survey details.

4.3.3 Wave observations and estimates

In the Southern California Bight, the Channel Islands (Figure 4.1) shelter incoming wave energy creating wave shadows along the coastline (Pawka, 1983). A spectral refraction wave model (O'Reilly and Guza, 1998), which resolves the island shadows and refraction over offshore bathymetry, is used to estimate the hourly directional wave properties every 100 m along the -10 m depth contour. Swell waves (0.04 - 0.1 Hz) are initialized with buoys exposed to the open ocean,

located seaward of the Channel Islands within a 400 km radius of the prediction location (solid triangles, Figure 4.1), and sea waves (0.08 - 0.5 Hz) are initialized with buoys located within a 75 km radius of the prediction location (solid circles, Figure 4.1).

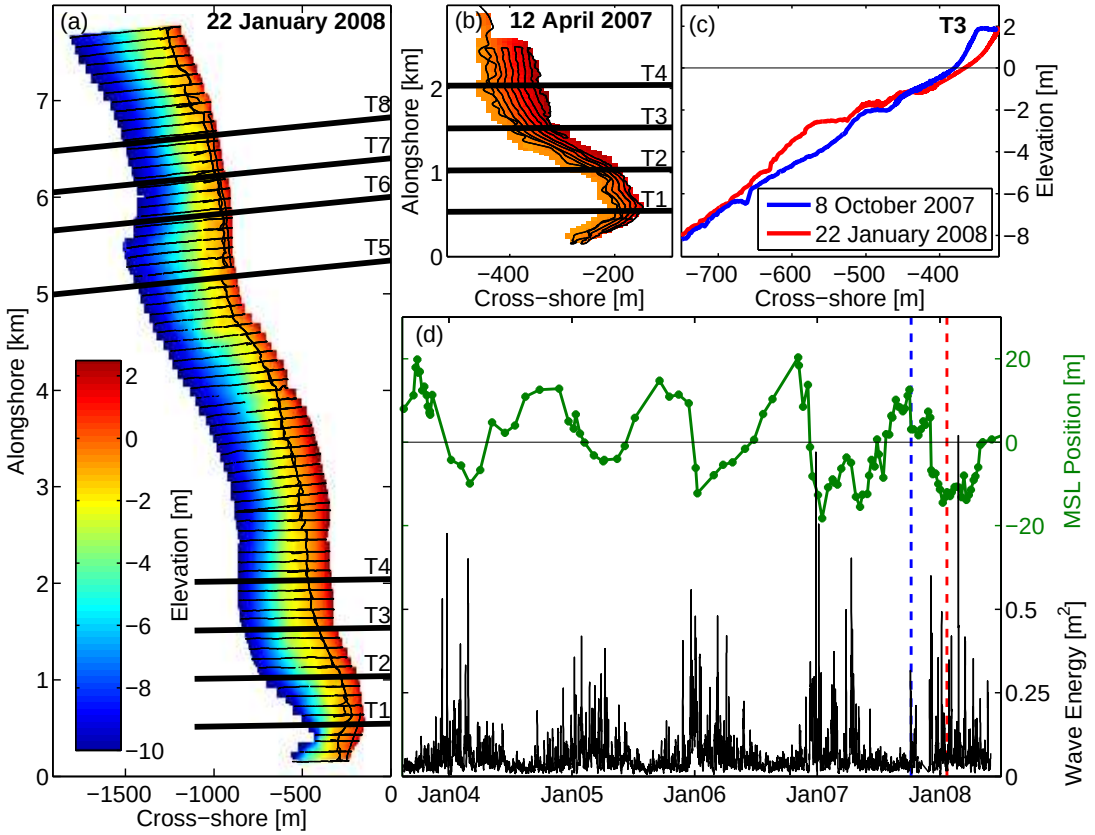

Figure 4.2: Torrey Pines bathymetry: (a) 22 January 2008 full bathymetry survey, with bold, black lines labeled T1-T8 (south to north) indicating the 500 m alongshore sections over which the MSL observations were averaged, (b) southern 2 km reach of 12 April 2007 subaerieal beach survey (approximately 0 to +2 m elevation), (c) depth versus cross-shore location for a typical accreted and eroded beach (section T3), and (d) MSL position, with the temporal mean removed (green), and hourly wave energy (black) versus time. In (a) and (b) the thin, black lines show the cross-shore and alongshore survey tracks, respectively, and the depth color scale is shown in (a). Dashed vertical lines indicate the survey dates of the cross-shore profiles shown in (c).

4.4 Equilibrium change observations

Beach sand level changes and waves are first related qualitatively using the extensive multiyear observations at Torrey Pines Beach. Monthly and more frequent subaerial surveys of two approximately 2-km reaches were separated into eight 500-m alongshore sections (T1-T8, south to north, Figure 4.2a). To facilitate integration with the cross-shore, full bathymetry surveys, Mean Sea Level (MSL) position was determined along cross-shore transects spaced approximately every 100 m alongshore. The mean beach width (beach width range shown in Table 4.1) was removed from the MSL position time series at each cross-shore transect. Then the MSL position time series were averaged within each 500-m section (MSL position, Figure 4.2d). Mean hourly wave energy was obtained by averaging spectral wave energy estimates, spaced every 100 m, over each 500-m alongshore section (wave energy, Figure 4.2d).

In all eight sections, MSL position and wave energy show large seasonal cycles. The wave energy is typically low during summer, with episodic large winter storms. At all alongshore locations, the beach is most accreted (positive MSL position) after low energy summer waves, and the beach is eroded (negative MSL position) after episodic, large winter storms. Statistics of MSL position and wave energy vary relatively little in the alongshore between most 500-m sections. Section T3 is representative and is shown in Figures 4.2d, 4.4, 4.5, 4.8, and 4.11.

Time series of MSL position S and average wave energy $\bar{E}$ (where the overbar denotes the average value between surveys) between successive surveys are only weakly correlated ($R^2 < 0.14$ at the eight alongshore sections). However, the average MSL change rate $\overline{dS/dt}$, based on successive surveys, does depend on $\bar{E}$ for a given initial S (Figure 4.3). Eroding and accreting waves are separated by the equilibrium energy $\bar{E}_{eq}$ that causes no MSL change for a particular MSL position (black line at blue-red boundary, Figure 4.3). The equilibrium energy is dependent on the initial MSL position; therefore, the shoreline response can vary

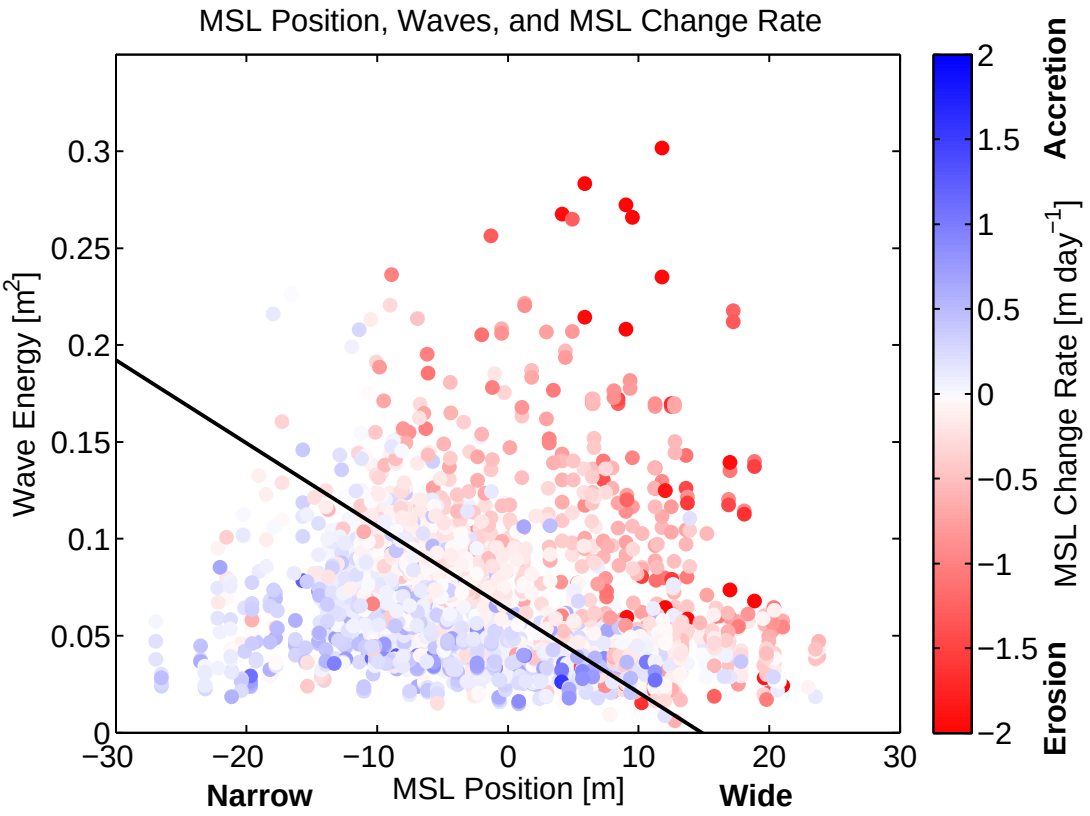

Figure 4.3: MSL change rate $\overline{dS/dT}$ between two consecutive surveys (weekly to monthly survey frequency) is shown in color for the initial MSL position S and the average wave energy between surveys $\bar{E}$, for all alongshore sections at Torrey Pines. The equilibrium wave energy $\bar{E}_{eq}$ (solid line) is the best fit line to the observed $\bar{E}$ causing no MSL position change.

for two events with the same wave energy but different initial MSL position. For example, a moderate wave energy of about 0.05 m^2 ($H_{sig} = 0.9m$), which erodes an accreted beach (positive MSL, right of the black equilibrium line, Figure 4.3) can accrete an eroded beach (negative MSL, left of the black equilibrium line, Figure 4.3). Larger wave energy events are required to continue eroding an already eroded beach. The MSL change rate (see color scale in Figure 4.3) appears to increase when the incident wave energy is farther from the equilibrium wave energy or in greater disequilibrium (e.g. as $\bar{E} - \bar{E}_{eq}$, the deviation from the solid line, increases).

4.5 Model

The beach response observations at Torrey Pines (Figure 4.3) suggest a simple equilibrium-type model. Following the concepts of Wright et al. (1985), the instantaneous MSL change rate is assumed proportional to both the instantaneous energy E and the instantaneous energy disequilibrium ΔE for the current MSL position,

$$\frac{dS}{dt} = C^{\pm} E^{1/2} \Delta E, \tag{4.1}$$

where $C^{\pm}$ are change rate coefficients for accretion (C^{+} for $\Delta E < 0$) and erosion (C^{-} for $\Delta E > 0$), and

$$\Delta E(S) = E - E_{eq}(S). \tag{4.2}$$

The equilibrium wave energy E_{eq} is dependent on the current MSL position, and the sign of the energy disequilibrium ΔE determines the sign of the MSL change rate dS/dt. The factor $E^{1/2}$ is arbitrary in form and prevents non-physical changes in MSL position when E is small (or zero). For simplicity, we let

$$E_{eq}(S) = aS + b, \tag{4.3}$$

where a and b are the slope and y-intercept (similar to the solid line $\bar{E}_{eq}$ in Figure 4.3). The expression states that for a given beach state, there is an equilibrium wave energy that will cause no further change. Conversely, the expression could be rewritten as a function of E to determine the equilibrium MSL position for a given wave energy:

$$S_{eq}(E) = \frac{E - b}{a}. \tag{4.4}$$

The model's behavior is illustrated in the simple case when the wave energy E is a step function, either increasing or decreasing to fixed level and remaining constant thereafter. In this case, the solution to (4.1)-(4.4) is

$$S(t) = (S_0 - S_{eq}) e^{-aC^{\pm}E^{1/2}t} + S_{eq}, \tag{4.5}$$

where S_0 is the initial MSL position, and S_{eq} is the equilibrium MSL position for the wave energy E, depending on a and b (4.4). If the constants C^+ and C^- are the same, the half-time scale $[aC^{\pm}E^{1/2}]^{-1}$ shows that adjustment to high energy waves is faster than the adjustment to low energy waves. Time scale estimates, based on the free parameters fit to the observations, are discussed below.

The model has four free parameters: two coefficients relating the equilibrium energy and the MSL position [a and b, (4.3)], and the accretion and erosion rate coefficients [$C^{\pm}$, (4.1)]. Initially, a and b were determined from the observations using $\bar{E}$ averaged over the period between successive surveys (solid line $\bar{E}_{eq}$ in Figure 4.3). The optimal $C^{\pm}$, yielding the minimum square error between modeled and observed S, were then found explicitly by solving (4.1)-(4.3) using the observed average $\bar{E}$ and $\overline{dS/dt}$ between surveys, and the initial S. However, weekly to monthly-averaged wave energy $\bar{E}$ unacceptably smoothed storm events and obscured the timing of storms within the averaging period (Appendix B). The model is therefore run on an hourly basis, and the E_{eq} line determined using one-hour time steps (using optimization, see below), which resolve individual storms, is steeper than the approximate $\bar{E}_{eq}$ line determined using $\bar{E}$ averaged over the period between observations (Appendix B).

Hourly E resolve even rapidly varying wave conditions, and after the free parameters are determined, allow hourly updates of shoreline location (4.1). However, the many hour time steps (about 44,000 in five years) complicate the numerics of finding the best fit parameters in this nonlinear system. Two derivative-free techniques were used to solve for the four free parameters that minimize the root-mean-square error (RMSE) between the model and observations: simulated annealing (Barth and Wunsch, 1990) and surrogate management framework (Booker et al., 1999; Marsden et al., 2004). Derivative-free methods are used because the present system has many local minima in the four-dimensional parameter space that can trap gradient methods. Simulated annealing and surrogate management framework (SMF) use different techniques to search the parameter space, but yield

similar results (see Appendix C). SMF required significantly fewer cost function evaluations to produce the best results in minimizing the RMSE; therefore, SMF results are presented below.

4.6 Results

4.6.1 Torrey Pines

Using optimal model parameters, the modeled and observed MSL both show strong seasonal variation, with slow accretion for long periods of low energy waves, and faster erosion during episodic, large energy wave events (Figure 4.4).

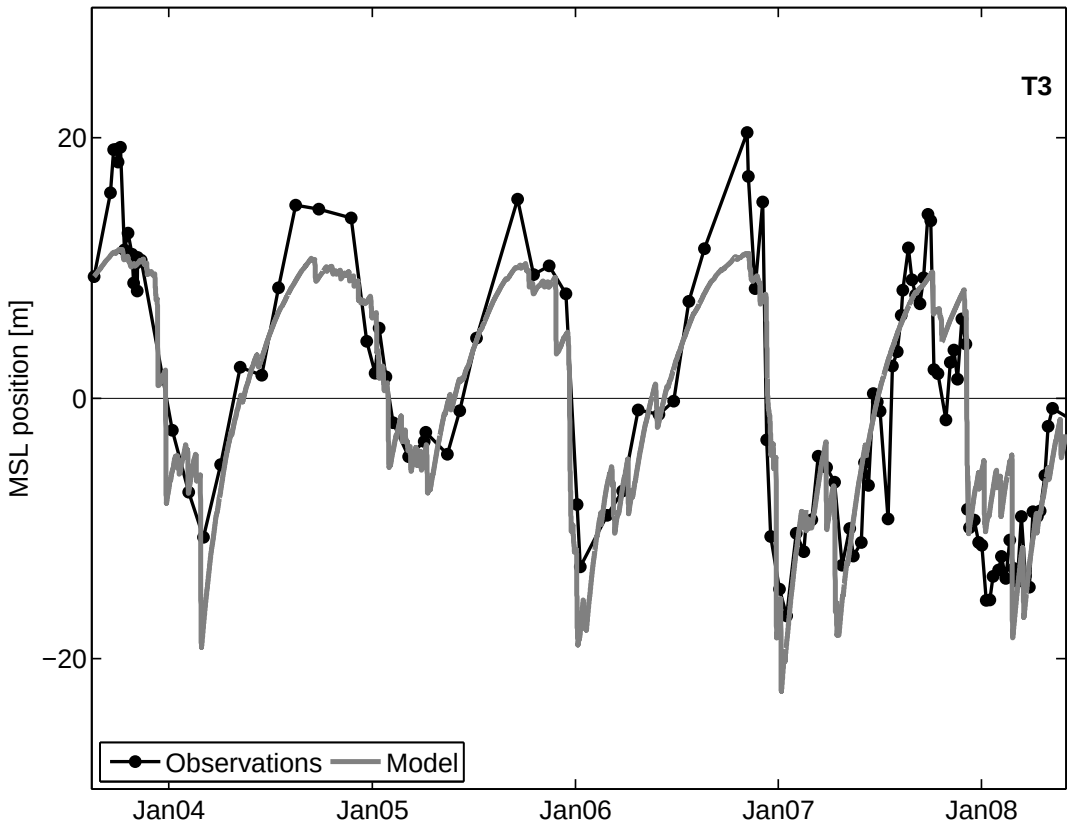

Figure 4.4: Weekly to monthly observations of MSL position (black), with the temporal mean removed, are compared to the hourly model results (gray) at Torrey Pines section T3 (RMSE = 4.0 m).

Erosion is particularly rapid when the first winter storm waves reach an accreted beach. Section T3 (Figure 4.4) is representative of all eight sections, which have RMSE ranging between 3.3 and 5.2 m.

The optimal erosion and accretion change rate coefficients ($C^{\pm}$) are of the same order of magnitude. The change potential $|E^{1/2}\Delta E|$, which is the product of the relative magnitude of the wave energy and the wave energy disequilibrium, accounts for much of the variability in the relative size of erosion and accretion events (4.1) within a section. The change potential is consistently small for accretion events, with larger, episodic spikes for erosion events (change potential, Figure 4.5c). The modeled shoreline accretes between 60-90% of the year, depending on the year and alongshore location.

Although E may be elevated often through the winter and early spring (wave energy, Figure 4.2d), accretion can begin in winter. On a severely eroded beach, even moderate E are smaller than the current E_{eq} (gray line, Figure 4.5b), and the beach will accrete until the next storm (e.g. January to April 2007, Figure 4.5a).

The half-time scale $[aC^{\pm}E^{1/2}]^{-1}$ from (4.5) calculated with the free parameters determined for Torrey Pines, ranges from approximately one to three weeks for strongly erosive events with high wave energy, to approximately one to three months for accretion events during lulls in wave energy. Shoreline location time series are much smoother than the corresponding wave energy series (Figure 4.5), consistent with response times much longer than storm durations. In the summer months, the beach slowly approaches its maximum width $-b/a$ but does not fully equilibrate with the low energy summer waves (E_{eq}, gray line, larger than E, black line, Figure 4.5b) because the time scale of equilibration is longer than the time period during which the low waves persist.

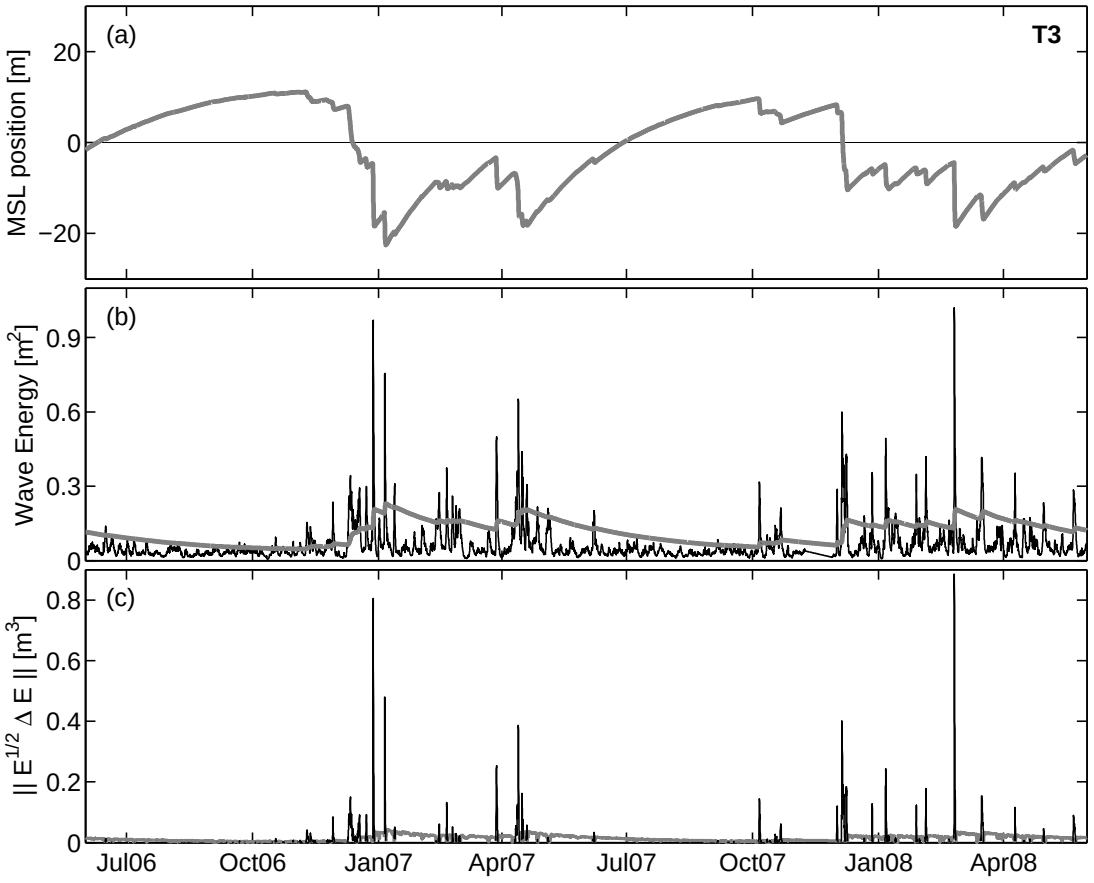

Figure 4.5: Model results for two years at Torrey Pines section T3 showing: (a) modeled MSL position, (b) wave energy E (black) and equilibrium energy E_{eq} (gray), and (c) change potential $|E^{1/2}\Delta E|$ for accretion (gray) and erosion (black), where $\Delta E = E - E_{eq}$.

4.6.2 Additional sites

The model was applied at three additional sites that were surveyed at least monthly for over one year. Similar to Torrey Pines, the beaches were divided into 500-m alongshore sections, yielding four sections at Cardiff, four sections at Camp Pendleton, and six sections at San Onofre.

At Camp Pendleton and Cardiff, the model reproduced the observations with RMSE similar to Torrey Pines. With approximately 1.5 years of monthly observations at Camp Pendleton, the RMSE for the four sections ranges from 3.5 to 5.4 m (e.g. section P1, Figure 4.6a). With slightly more than a year of

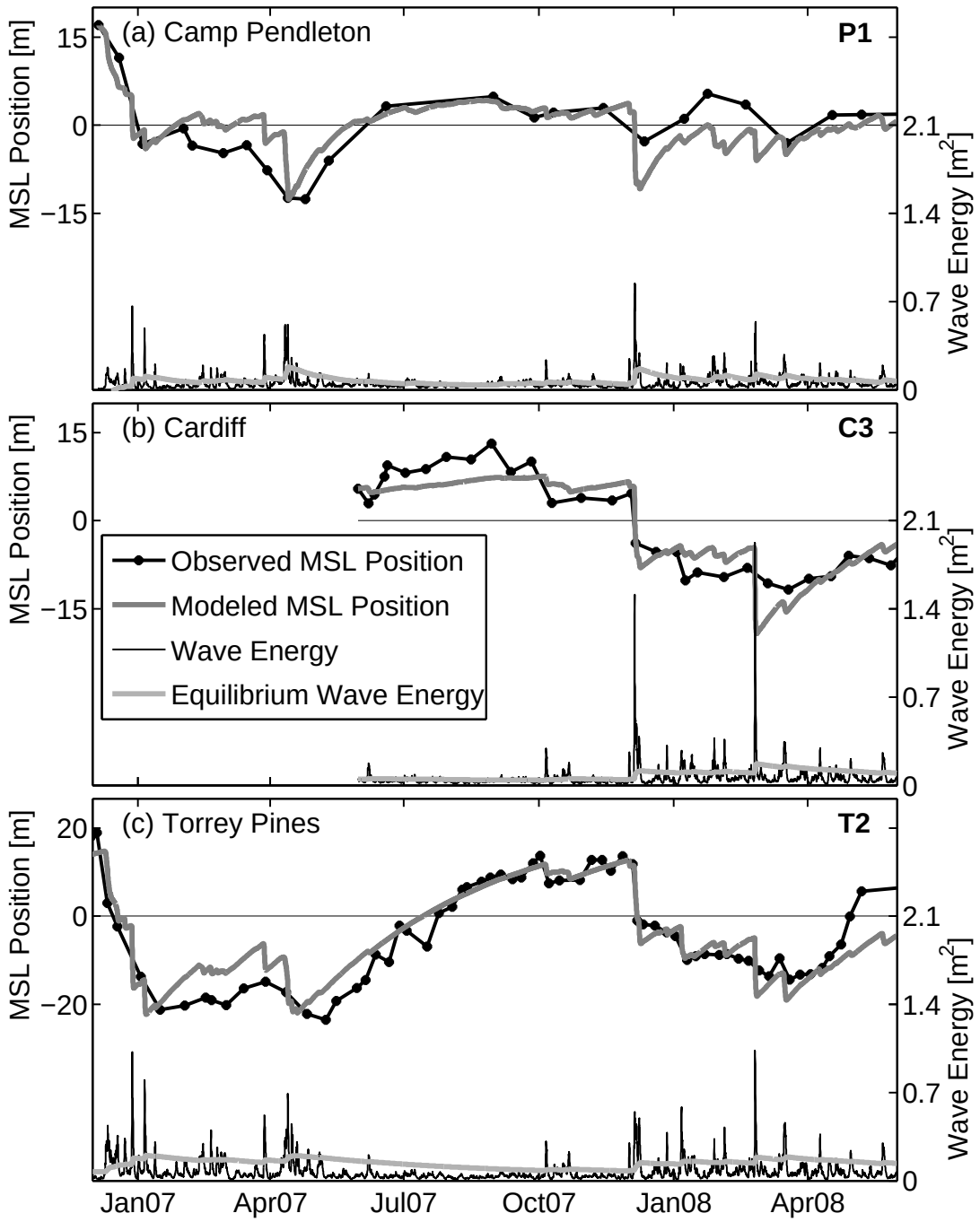

Figure 4.6: Observed and modeled MSL position (black and gray curves, respectively, top) and wave energy E and equilibrium wave energy E_{eq} (black and gray curves, respectively, bottom) for 500-m alongshore sections at: (a) Camp Pendleton, (b) Cardiff, and (c) Torrey Pines. Model errors (RMSE) are 3.5, 2.9, and 4.0 m, respectively.

biweekly observations at Cardiff, the RMSE for the four sections ranges from 2.7 to 5.3 m (e.g. section C3, Figure 4.6b). Monthly MSL position observations at San Onofre (not shown) exhibit a weak seasonal cycle even though the wave energy is seasonal and the storm event magnitudes are similar to Camp Pendleton (20 km to the south). Coarse-grained sand on the beach face or limited sand availability in the nearshore zone are hypothesized to cause shoreline stability at this location (Chapter 2). At San Onofre, the small MSL position changes (<5 m) were only slightly larger than the observation uncertainties, and the model did not perform well in reproducing the observations.

At the three sites where the model successfully reproduced the observations, the correlation (R^2) between observed and modeled shoreline location (using optimal parameter values for each section) is between 0.61 and 0.94 (Figure 4.7d). Most of the variance in the MSL time series can be explained by a equilibrium-type model driven with seasonal wave energy fluctuations resolving hourly waves.

The range of free parameter values for which the RMSE increases less than 10% was estimated for each alongshore section (Figure 4.7). The values of the free parameters a and $C^{\pm}$ are related and can have compensating effects. For example, an increase in the magnitude of the equilibrium slope a (with b constant) causes fewer erosion events because it takes a larger wave to initiate erosion, but it can be balanced by an increase in the erosion rate coefficient C^{-} to increase the impact of the remaining erosion events. The coupling between the free parameters creates broad minima in the free parameter space. The optimal free parameters show alongshore variability (Figure 4.7), but have similar free parameter ranges and demonstrate similar modeled MSL results (Figure 4.6). The equilibrium y-intercept b is not shown because it is dependent on the temporal mean removed from the MSL time series and is not comparable between different alongshore locations with variable temporal sampling.

The equilibrium slope a (4.3) is consistently larger at Camp Pendleton than at Cardiff and most of Torrey Pines (Figure 4.7 and Table 4.3), indicating that

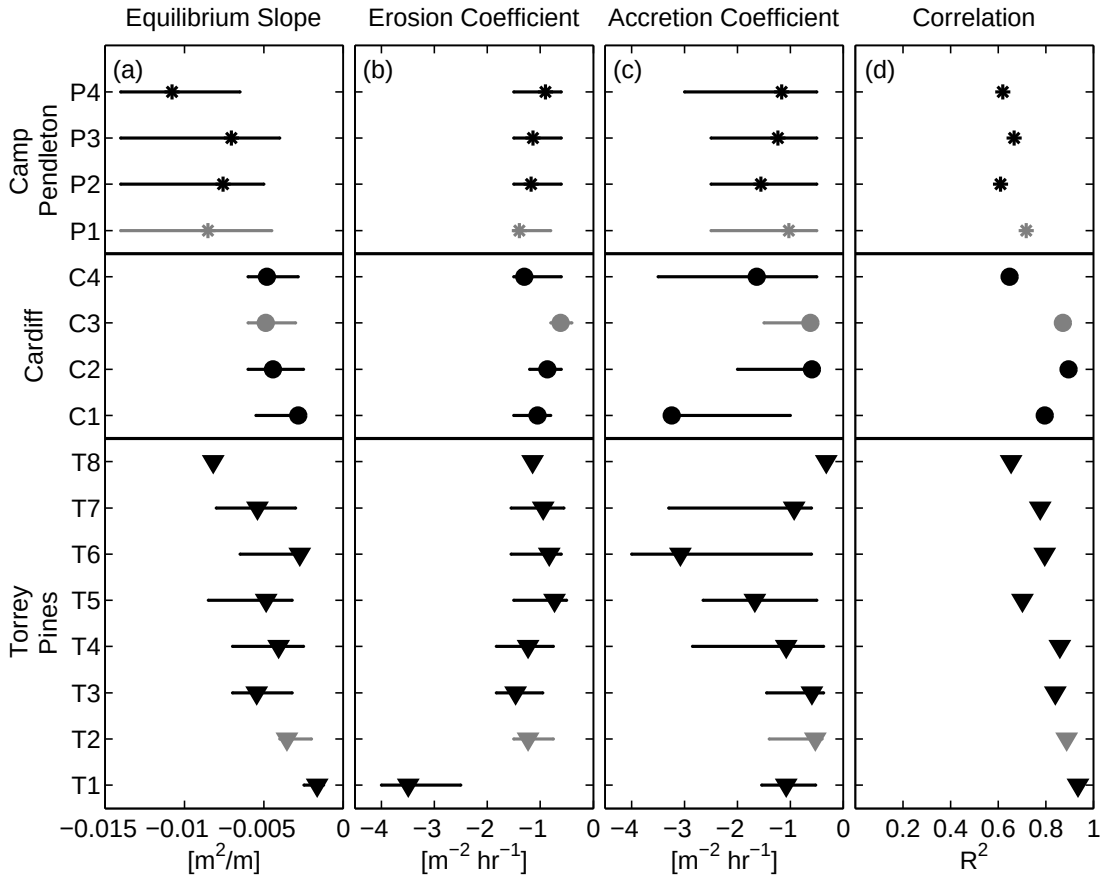

Figure 4.7: Optimal model free parameters at Torrey Pines, Cardiff, and Camp Pendleton: (a) equilibrium slope a (4.3), (b) erosion rate coefficient C^-, and (c) accretion rate coefficient C^+, and (d) squared correlation R^2 between modeled and observed MSL location. Scatter bars indicate range of free parameter values for which the RMSE increases by less than 10 % from the minimum. Gray symbols indicate the alongshore sections are shown in Figure 4.6.

a larger wave energy is required to initiate erosion and that the equilibrium MSL position has a smaller range of values for the same range of wave conditions (4.4). The magnitude and range of the optimal erosion rate coefficient C^- shows relatively little variation between alongshore sections and survey sites (Table 4.3), with the exception of T1 (Figure 4.7b). The lowest wave energy and largest alongshore gradients in energy (not shown) are at T1, suggesting that alongshore transport may be important.

The accretion rate coefficients C^+ show larger variability and ranges of

Table 4.3: Mean and standard deviation of the beach equilibrium slope a, erosion rate coefficient C^-, accretion rate coefficient C^+, and products of $aC^\pm$ for each site.

Survey site	$\boldsymbol{a}$ $\times \mathbf{10^{-3}}$ $(\mathbf{m^2/m})$	$\boldsymbol{C^-}$ $(\mathbf{ms^{-1}/m^3})$	$\boldsymbol{C^+}$ $(\mathbf{ms^{-1}/m^3})$	$\boldsymbol{aC^-}$ $\times\mathbf{10^{-3}}$ $(\mathbf{m^{-1}s^{-1}})$	$\boldsymbol{aC^+}$ $\times\mathbf{10^{-3}}$ $(\mathbf{m^{-1}s^{-1}})$
Torrey Pines	-4.5±2.0	-1.38±0.88	-1.16±0.88	5.4±2.3	4.4±2.6
Cardiff	-4.2±1.0	-0.96±0.29	-1.52±1.25	4.0±1.6	5.6±3.3
Camp Pendleton	-8.5±1.7	-1.15±0.20	-1.24±0.22	9.6±1.6	10±2.0

accepted values than the erosion coefficients C^-, both between and within sites (Figure 4.7c and Table 4.3). Accretion change potentials (gray curve, Figure 4.5c) are small and persistent, and a broad range of C^+ values will have a similar impact on MSL position change. Erosion change potentials (black curve, Figure 4.5c) are large and episodic, and C^- values are more constrained because a broad range of C^- values would significantly change the impact of erosion events. Additionally, changes in C^+ can be compensated for by small adjustments in the equilibrium slope a, which alters ΔE and has a more significant effect on the accretion change potentials than the erosion change potentials because of the relative magnitude of E during accretion and erosion events.

The half-time scale and (4.5) show that the rate of adjustment to equilibrium is dependent on the product $aC^\pm$ $[m^{-1}s^{-1}]$ and the magnitude of the wave event. Camp Pendleton has larger $aC^\pm$ values than the other two focus sites (Table 4.3), which is due to having an elevated equilibrium slope (with $C^\pm$ coefficients within the same range of variability at all three sites). Therefore, for the same magnitude wave event, the shoreline moves more quickly toward equilibrium at Camp Pendleton.

The model free parameters likely depend on sand grain size (Dean, 1977;

Wright et al., 1985), but the range of sand grain size between the three focus sites is too limited. Observations of shoreline location and hourly wave characteristics from beaches with different wave climates and sediment types would help establish the role of wave period and grain size (e.g. $\Omega = H_b/w_s T$, where w_s depends on grain size).

4.7 Discussion

4.7.1 Alternative model formulations

Model results are similar when E in (4.1) is replaced with H, E^2, Ω or Ω^2 (Wright et al., 1985), wave steepness, or the radiation stress component S_{xx}. Model RMSE are slightly reduced when the coefficient $C^{\pm}$ is allowed to vary with the shoreline location S, adding more than the present two adjustable values. In (4.1), the shoreline stops changing when $\Delta E = 0$ because the equilibrium wave condition was reached. With a linear equilibrium wave energy expression (4.3), the maximum MSL position occurs in the limiting case when $E = 0$ and the maximum accreted shoreline position $S_{max} = -b/a$ (4.4). Asymptotic forms (e.g. tanh) of the equilibrium wave energy (4.3) with an additional free coefficient allow ever slower accretion throughout the summer and no maximum MSL position. However, the data did not significantly constrain an exponential relationship between the equilibrium wave energy and MSL position.

4.7.2 Predicting change

Given free parameter values and the initial MSL position, the model can be used to estimate time series of MSL position given only a wave energy time series. Model free parameters determined by fitting three years of MSL position and wave energy observations at Torrey Pines (section T3) were used to predict 1.5 years of MSL position using only the observed wave energy. The model RSME, which was 3.6 m during the three-year tuning period, increased to only 4.2 m during

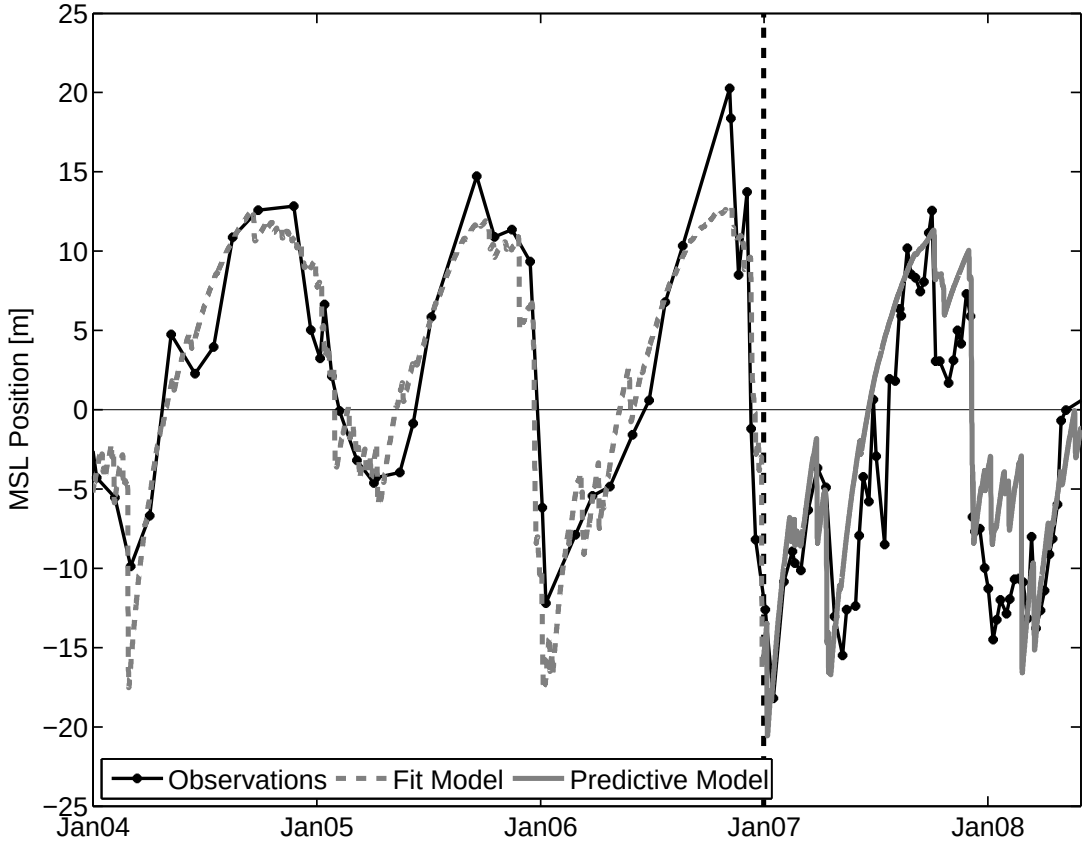

Figure 4.8: Three years of approximately monthly MSL observations (solid black curve prior to the vertical dashed line) at Torrey Pines section T3 were used to determine the model free parameters, with the best fit RMSE = 3.6 m. Using the tuned free parameter values and the observed wave energy, an additional 1.5 years of weekly MSL observations (solid black curve after the vertical dashed line) are predicted (solid gray curve) with RMSE = 4.2 m.

the 1.5-year prediction period (Figure 4.8). The model predicted the maximum and minimum MSL position within a few meters, but did not predict accurately the short time-scale (weekly to monthly) fluctuations in either the tuning or prediction periods.

4.7.3 Sensitivity to observation duration

The model performance was investigated with different durations of observations used for determining the free parameters in the model. The baseline

for comparison is the best fit using all of the weekly to monthly observations for almost five years at each of the eight alongshore sections at Torrey Pines (e.g. section T3 shown in Figure 4.4).

The observations were subsampled to monthly to remove effects associated with weekly sampling, and the four-year period from 2004 to 2008 was divided into consecutive one, two, three, and four-year periods (for a total of 4 one-year periods, 3 two-year periods, 2 three-year periods, and 1 four-year period at each alongshore section). Thus, for one-year tests, the model free parameters were determined with one year of data, and the RSME was estimated for the entire nearly

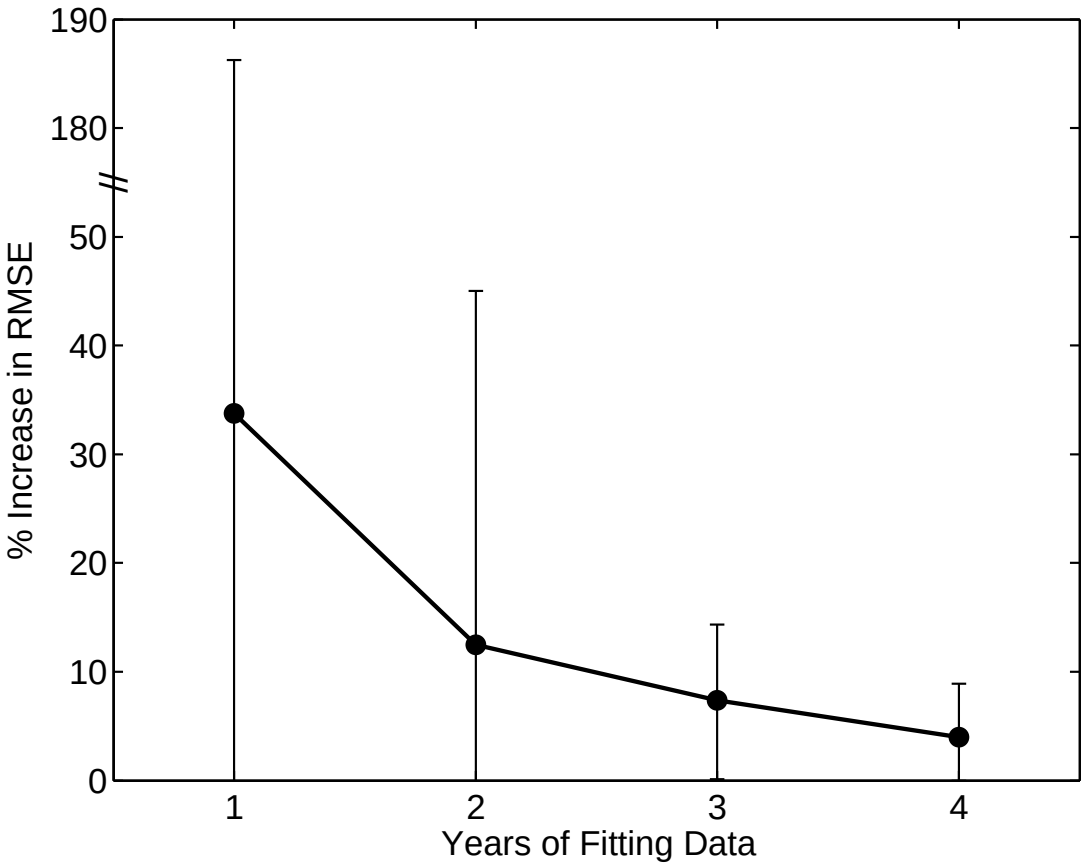

Figure 4.9: Percent increase in the model RMSE (above the baseline case) versus the number of years of monthly data used to tune the model free parameters (note the vertical scale break). Scatter bars show the range of values obtained, including variability from both the different test periods and alongshore sections (32 one-year tests, 24 two-year tests, 16 three-year tests, and 8 four-year tests).

five-year period. Each year was used for tuning at each of the eight alongshore sections, yielding 32 estimates of one-year model tuning. Using only one year of data to fit the model, the RMSE increases only 30% on average (Figure 4.9). No single year was the best or worst year for tuning in every alongshore section. An unexplained anomaly was noted at alongshore sections T5 to T7 when the year 2006 was used for tuning: the RMSE increases were nearly a factor of 3 larger than all other tests. When two years of monthly observations were used for tuning, the mean increase in RMSE dropped to less than 15% (Figure 4.9). Further increases in observation duration decrease the RMSE only slightly, suggesting that two years of monthly surveys are optimal for determining the model free parameters.

4.7.4 Sensitivity to observation frequency

Monthly versus weekly observations

From May 2007 to May 2008, Torrey Pines beach was surveyed weekly to resolve storm erosion events and subsequent beach recovery (Figure 4.4). The weekly observations were subsampled to monthly, and the weekly and monthly time series of the same year were used to determine the best fit model free parameters for that year (not shown). Using those parameter values, RMSE for the entire five years of observations at the eight alongshore sections differed by only 1%. Weekly observations did not improve significantly the model performance.

Biannual observations

Model performance was tested with biannual observations over an approximately four-year period, simulating seasonal surveys. The observations at each alongshore section were subsampled twice a year, starting with different months of the year and resulting in six biannual sets of observations (e.g. January and July, or February and August, etc.). Optimal free parameters were determined for each set of biannual observations, and the RMSE was calculated over the entire five-year observation period (Figure 4.10). The mean RMSE (over eight along-

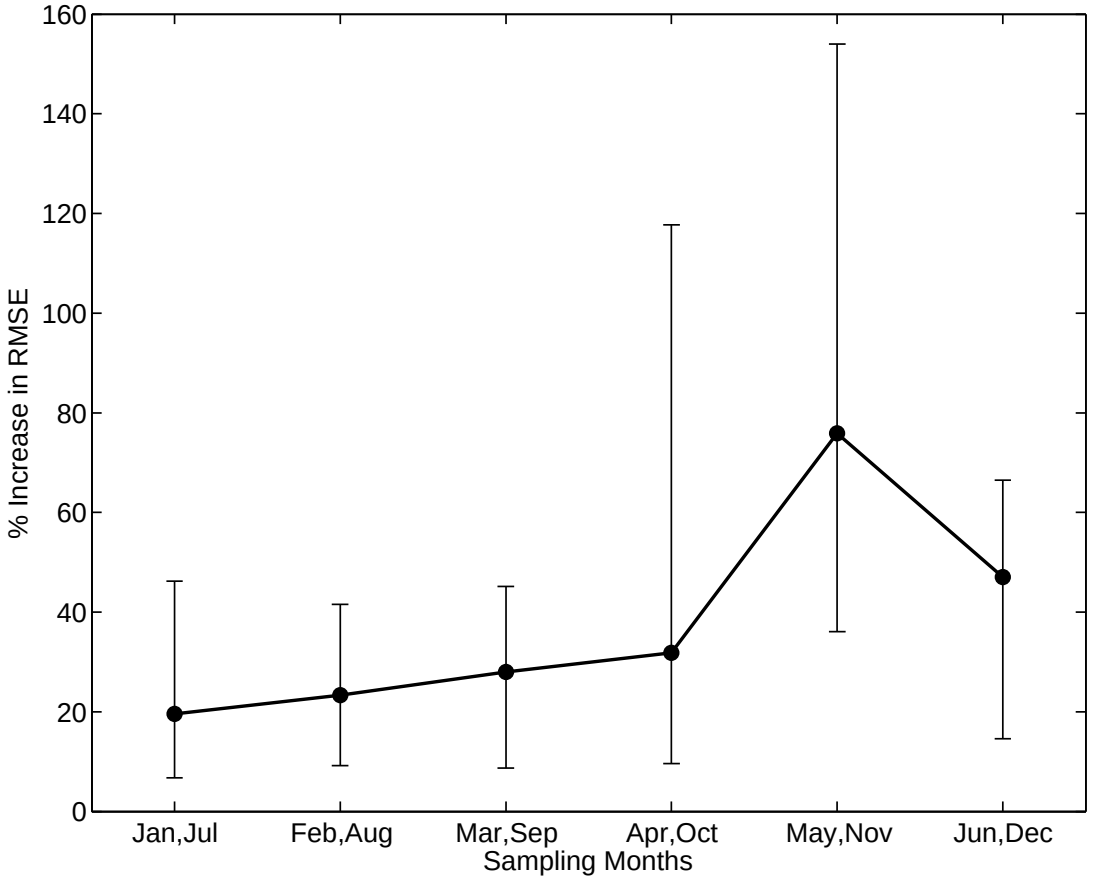

Figure 4.10: Percent increase in model RMSE (above the baseline case) versus the two survey months (separated by six months) of biannual surveys used to tune the model free parameters. Scatter bars indicate the range values for the eight alongshore sections at Torrey Pines.

shore sections) is only $\sim 25\%$ above the baseline for biannual surveys completed in January and July (similar to February and August, March and September, Figure 4.10). RMSE increases are larger for the remaining sets of biannual observations (April and October, May and November, June and December, Figure 4.10).

The model results vary using different sets of biannual observations because of the temporal sampling of the seasonal cycle. Biannual sampling in February and August (Figure 4.11a, similar to January and July, or March and September) approximately captures the MSL extrema. The model, constrained to fit the observations near the extremes, has RMSE only about 25% higher than using the

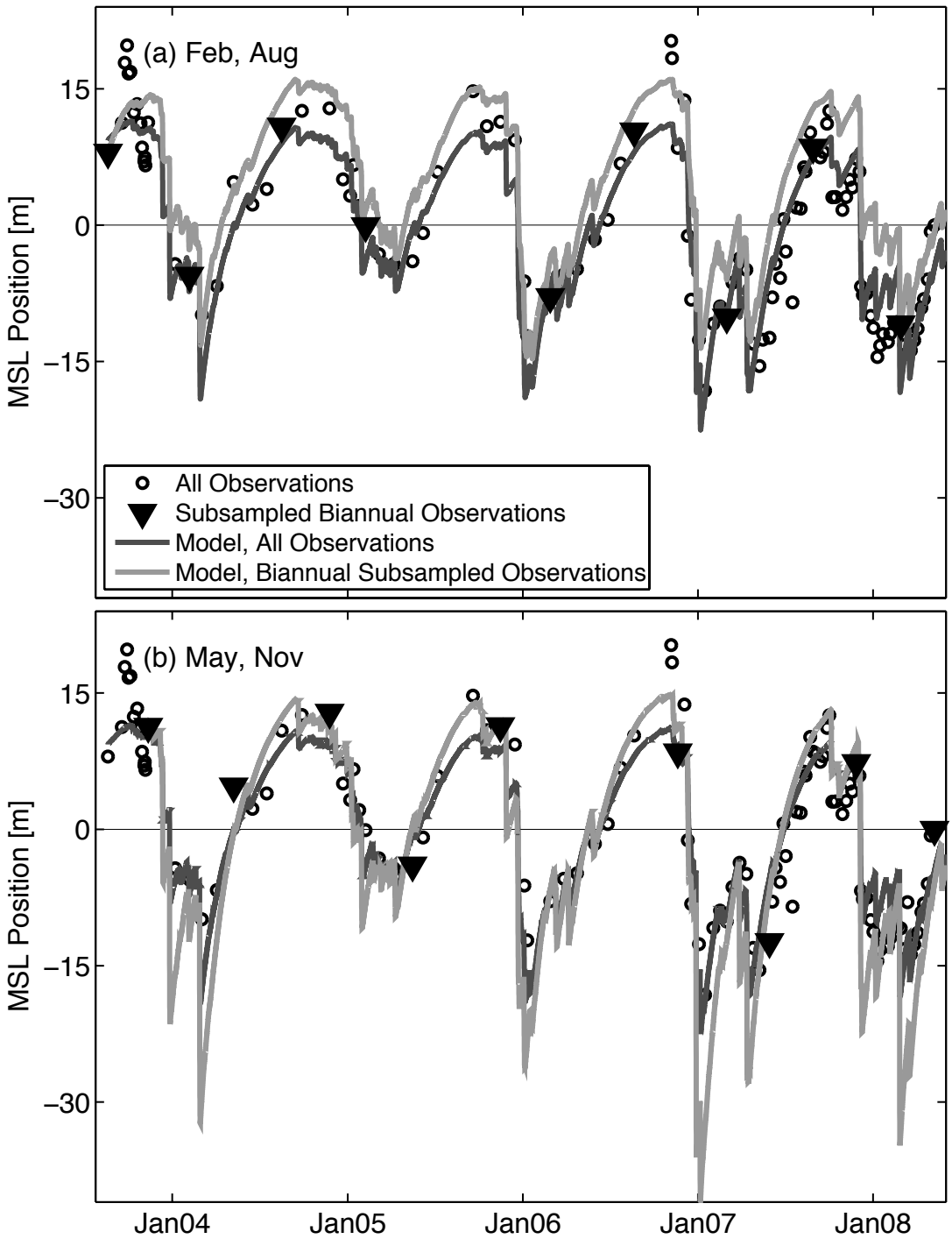

Figure 4.11: MSL position at Torrey Pines section T3 (with temporal mean removed) versus time. Symbols are observations, with biannual subsamples indicated with bold triangles. Models are tuned using all observations (RMSE = 4.0 m, dark gray curve) and subsampled observations (light gray curve) for: (a) February and August subsampling, RMSE = 4.6 m, and (b) May and November sampling, RMSE = 6.5 m.

entire weekly to monthly set of observations over the same time period. The May and November observations (e.g. Figure 4.11b, similar to April and October, or June and December) do not constrain well the minima in MSL position because the November survey is often too early in the winter to capture the large erosion events, and the MSL position has already begun to recover back to summer levels by the May survey. Summertime accretion is reproduced, but winter erosion is significantly over-predicted when the seasonal cycle extrema are not captured in the observations. However, several years of appropriately-timed biannual surveys (only 9 observations) can produce similar model results (RMSE increases of 25%) to several years of weekly to monthly surveys (over 100 observations).

4.7.5 Extension to include shallow depth contours

In addition to over 100 surveys of the subaerial beach used for MSL studies, 16 bathymetry surveys covered all eight alongshore sections at Torrey Pines, spanning from the backbeach to approximately -9 m water depth (Figure 2a). The beach profiles show a large seasonal cycle (Figure 4.2c), consistent with the observations of Winant et al. (1975).

The bathymetry changes are summarized with empirical orthogonal functions (EOFs) of contour locations. Time series of contour positions (-9 m to +2 m elevation, relative to MSL) were estimated for each 500-m alongshore section. The temporal mean of each contour position was removed before computing the contour position EOF for each alongshore section. The seasonal, mode-1 EOF temporal amplitudes are similar to time series of MSL position (Figure 4.12a) because MSL and other contour motions are correlated. The mode-1 EOF spatial amplitudes (Figure 4.12b) describe the magnitude of the spatially coherent motion of each contour and show that the offshore bar (-6 to -3 m elevation contours) and shoreline (-2 to +2 m elevation contours) are out of phase. Thus, in summer, when MSL is accreted, the bar contours are eroded, and the cycle reverses in winter.

The mode-1 EOF of contour position explains more of the fluctuations at

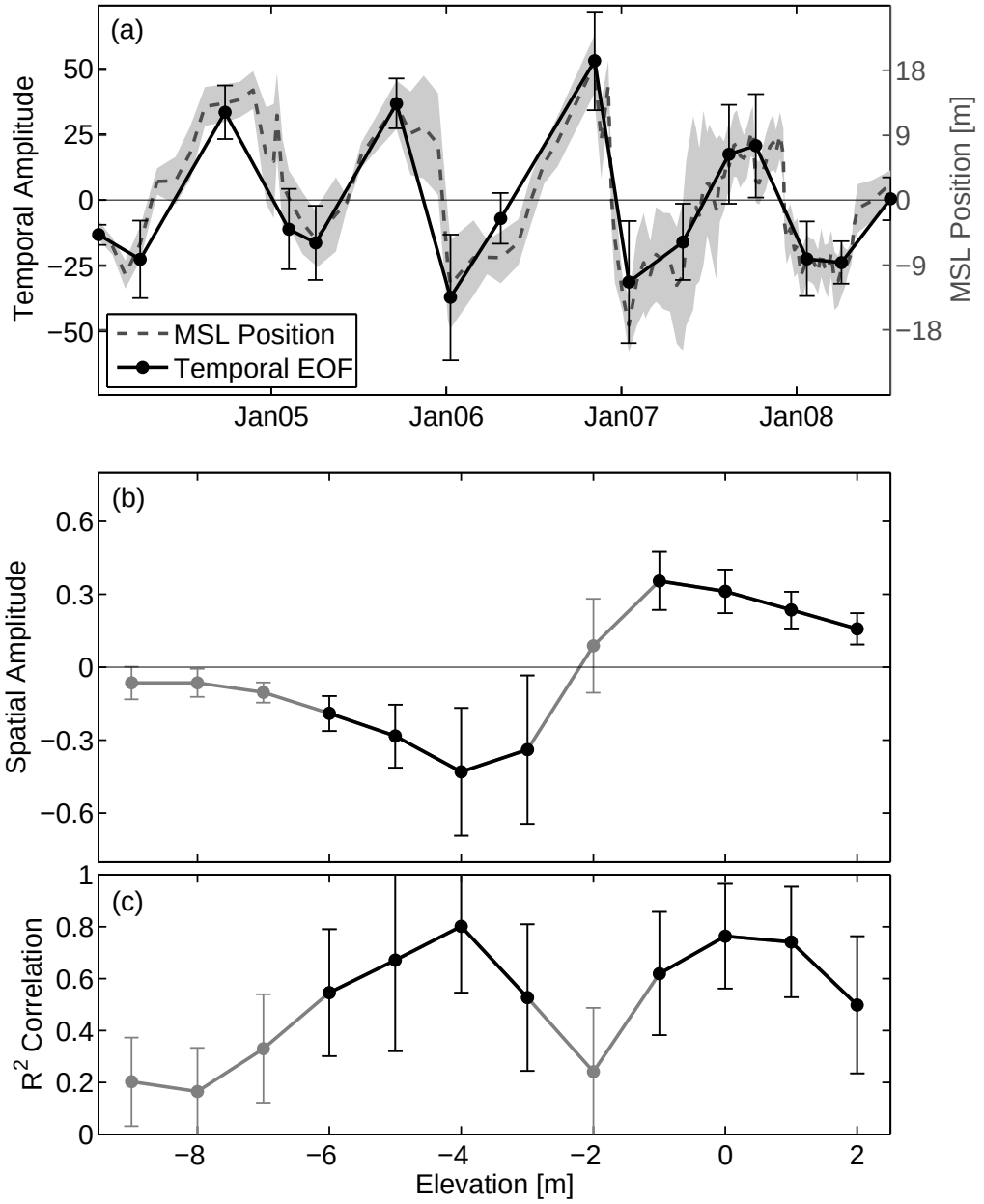

Figure 4.12: The mode-1 EOF of contour positions shows coherent changes in the location of depth contours at Torrey Pines section T3: (a) average mode-1 EOF temporal amplitude (black, explaining 48 to 82 % of the total variance in sections T1 to T8) is similar to the average MSL position time series (dashed gray), (b) average mode-1 EOF contour position spatial amplitude, and (c) average correlation R^2 between the mode-1 EOF temporal amplitude and the time series of each contour position. Averages are taken over the eight alongshore sections, and scatter bars and shading indicate the standard deviation between alongshore sections. In (b) and (c), black indicates $R^2 > 0.5$.

some contours than others (Figure 4.12c). The fraction of contour displacement variance (R^2) explained by the mode-1 EOF is highest (>60%) for the contours with the most change (e.g. largest spatial amplitudes, near the bar and shoreline, Figure 4.12b). The temporal EOF amplitude and the MSL position time series (Figure 4.12a) are similar, suggesting that the equilibrium formalism used to model MSL change can be extended to the entire profile through EOFs.

4.8 Conclusions

Shoreline location and wave energy observed for almost five years at Torrey Pines Beach demonstrate the applicability of equilibrium beach change concepts. The cross-shore MSL displacement rate depends on both the initial MSL position and the wave energy. A simple equilibrium shoreline response model with four tuned, free parameters reproduces the MSL observations with relatively low RMSE ($\leq$ 5 m). The model performs similarly, with comparable free parameter values, at two nearby survey sites, each with about a year of observations. There was relatively little alongshore variability in the optimal free parameters within each survey site, and a single set of free parameters could reproduce the observations at most alongshore locations within each site with a $\sim$ 10% increase in RMSE.

Using pre-determined free parameter values for a site, the model can predict MSL evolution given only the initial MSL location and the wave energy time series. Free parameters can be roughly approximated with about two years of monthly observations, or several years of biannual observations, which are timed to sample the approximate annual extremes in MSL position. The model will be less reliable when extrapolated beyond the range of values used to determine the free parameters, and will fail entirely if neglected geologic factors become important (e.g. underlying bedrock limit erosions, or sand availability limits accretion). Additional observations during atypical years and at sites with different wave cli-

mates are needed to extend the model to include more effects (e.g. sand grain size, wave period, and direction).

Acknowledgments

In situ surveys and wave data collection were supported by the United States Army Corps of Engineers and the California Department of Boating and Waterways, respectively. Brian Woodward, Kent Smith, Dennis Darnell, Bill Boyd, and Ian Nagy collected the bathymetry data. Marissa Yates was partially supported by a National Defense Science and Engineering Graduate Fellowship.

The text of Chapter 4, in full, is a reprint with minor modifications of the paper "Equilibrium Shoreline Response: Observations and Modeling," to be submitted for publication to the *Journal of Geophysical Research*. The dissertation author was the primary researcher and first author with guidance provided by R.T. Guza and W.C. O'Reilly.

5

Conclusions and future work

In conclusion, this dissertation utilizes unique sand level and wave observations to study the spatial and temporal variability of seasonal sand level changes in southern California. The seasonal wave field forces seasonal shoreline and bathymetry changes along most of the coastline, and the geologic characteristics of individual beaches strongly influence the seasonal beach change magnitude. Lagoons, cobbles, and bedrock have a significant impact on the seasonal cycle magnitude, but more observations are needed to quantify the impacts of these features. On a primarily sandy 20-km section of the coastline, sand grain size and the cross-shore sand grain size difference are hypothesized to cause the observed seasonal shoreline change to vary by more than a factor of four. Ongoing work includes exploring the influence of cliff material and offshore sediment availability on controlling shoreline and bathymetry change.

Monthly and more frequent shoreline measurements at four focus sites verified the seasonal behavior observed with the biannual lidar observations, and nearly quarterly bathymetry surveys demonstrated the formation of an offshore winter bar and the seasonal recovery of the beach face when the bar remerges with the beach face in the summer months. Even with a large seasonal beach change cycle, a small beach nourishment at Torrey Pines was tracked through nearly two seasonal cycles

Finally, the shoreline observations and wave estimates demonstrated an

equilibrium beach response at Torrey Pines, and these observations motivated the creation of a simple equilibrium response model. With four tuned, free parameters, the model accurately reproduces the shoreline change observations. Tests of the length and frequency of data required to determine the model free parameters demonstrated its ability to be applied at additional survey sites with multiple years of appropriately-timed biannual observations or at least two years of monthly observations. The model can then be used as a predictive tool given only the wave field.

The model can potentially be applied at any location with adequate data to determine the model free parameters. Tests indicate that the existing six-year biannual lidar data set is sufficient to be used to determine the model free parameters at Torrey Pines. In the future, the equilibrium model, coupled with high resolution wave estimates, can be applied along the 80-km surveyed reach between Point La Jolla and Dana Point. The relationship between the magnitude of the tuned free parameters and geologic factors can be explored within this reach. The equilibrium model formulation can also be extended to include bathymetry changes to -8 m water depth using EOFs. Although relatively few bathymetry observations are available at sites other than Torrey Pines, ongoing in situ surveys will provide additional observations at the other focus sites.

Appendix A

Eliminating water returns from lidar beach elevation surveys

A.1 Abstract

Airborne LIght Detecting and Ranging (lidar) systems can survey hundreds of kilometers of shoreline with high spatial resolution (several elevation estimates per m^2). Sequential surveys yield spatial change maps of beach and dune sand levels. However, lidar data include elevations of the exposed, subaerial beach and, seaward of the waterline, the ocean surface. Here, a simple method is developed to find the waterline and eliminate returns from the ocean surface. A vertical elevation cutoff is used, with the waterline elevation (W) above the known tide level due to the superelevation from wave setup and runup. During each lidar pass, the elevation cutoff (W) is assumed proportional (C) to the offshore significant wave height H_s. Comparison of in situ and lidar surveys on a moderately sloped, dissipative California beach yields $C \approx 0.4$, which is qualitatively consistent with existing observations of runup and setup. The calibrated method rejects ocean surface data, while retaining subaerial beach points more than 70m seaward of the mean high water line, which is often used as a conservative default waterline.

A.2 Introduction

Beach survey methods have evolved rapidly with the use of kinematic Global Positioning System (GPS) techniques (Morton et al., 1993). Airborne LIght Detecting and Ranging (lidar) systems (Brock et al., 2002) survey hundreds of kilometers of shoreline with high spatial resolution in a few days. With swath widths of a few hundred meters, coastal lidar surveys map the offshore ocean surface, the subaerial beach face, and the backbeach (e.g. cliffs, seawalls, landward development). Lidar surveys spanning long coastal reaches are a unique resource for studying variability across the entire exposed beach system. Repeated surveys can be used to monitor changes in shorelines (Stockdon et al., 2002), beaches and dunes (Saye et al., 2005; Woolard and Colby, 2002), and seacliffs (Sallenger et al., 2002; Young and Ashford, 2006). Additionally, lidar surveys have been used to quantify beach changes after a beach nourishment (Gares et al., 2006), after hurricanes (Zhang et al., 2005; Robertson et al., 2007), and during an El Niño event (Revell et al., 2002). Based on concurrent airborne lidar and ground-based beach surveys, root mean square (RMS) vertical lidar errors are about 15 cm (Sallenger et al., 2003), and RMS horizontal errors in the cross-shore location of the mean high water (MHW) vertical datum are about 2.5m on a moderately sloped beach (Stockdon et al., 2002).

Lidar data include elevations of the subaerial beach and, seaward of the waterline, the ocean surface. The waterline location depends on the local bathymetry and the tide and wave conditions. For small alongshore reaches at specific study sites, the exposed beach points have been identified manually (Woolard and Colby, 2002; Shrestha et al., 2005). However, for surveys of large alongshore distances, automated methods are needed to remove ocean surface data. Stockdon et al. (2002) used differences between multiple lidar passes to locate the shoreline. When all passes over a given area yielded similar elevations, the area was assumed to be subaerial beach. When independent passes yielded significantly

different elevations, the differences were ascribed to the variation between passes of the location of wave crests and troughs, and the area was classified as water. The method requires more than one pass and is less effective when wave heights are low and their effect is difficult to detect near the waterline.

Here, nearly concurrent lidar and in situ surveys (described in section A.3) are used to calibrate and test a simple method (section A.4) that, using lidar data and independently known tides and waves, estimates the seaward limit of subaerial beach lidar data points (e.g. the waterline location) in each pass. The tuned algorithm excludes ocean surface data while retaining most subaerial beach data (section A.5). The results are discussed in section A.6, and summarized in section A.7.

A.3 Observations

Five nearly concurrent in situ and lidar surveys were collected at Torrey Pines State Beach, CA between September 2002 and April 2005 (Figure A.1, Table A.1). The in situ surveys measured the elevation of the beach face shoreward of the waterline and the elevation of the seabed seaward of the waterline, whereas the lidar surveys measured the elevation of the ocean surface seaward of the waterline (Figures A.1c-d, A.3c, A.4c, and A.6c). For each lidar pass, the in situ and lidar surveys diverge seaward of the waterline. These divergence waterlines, based on in situ and lidar surveys, are used to calibrate the method that uses tides and wave heights to locate the waterline position in lidar surveys.

A.3.1 Study site

Torrey Pines State Beach (32.9° N, 117.26° W) is a relatively wide, sandy beach backed by high cliffs in most locations. The distance from the backbeach (e.g. seawall or cliff) to mean sea level (MSL) varied from about 20 to 150 m, with slopes near MSL between about 0.01 and 0.04 (Figures A.1c, A.3c, A.4c, and

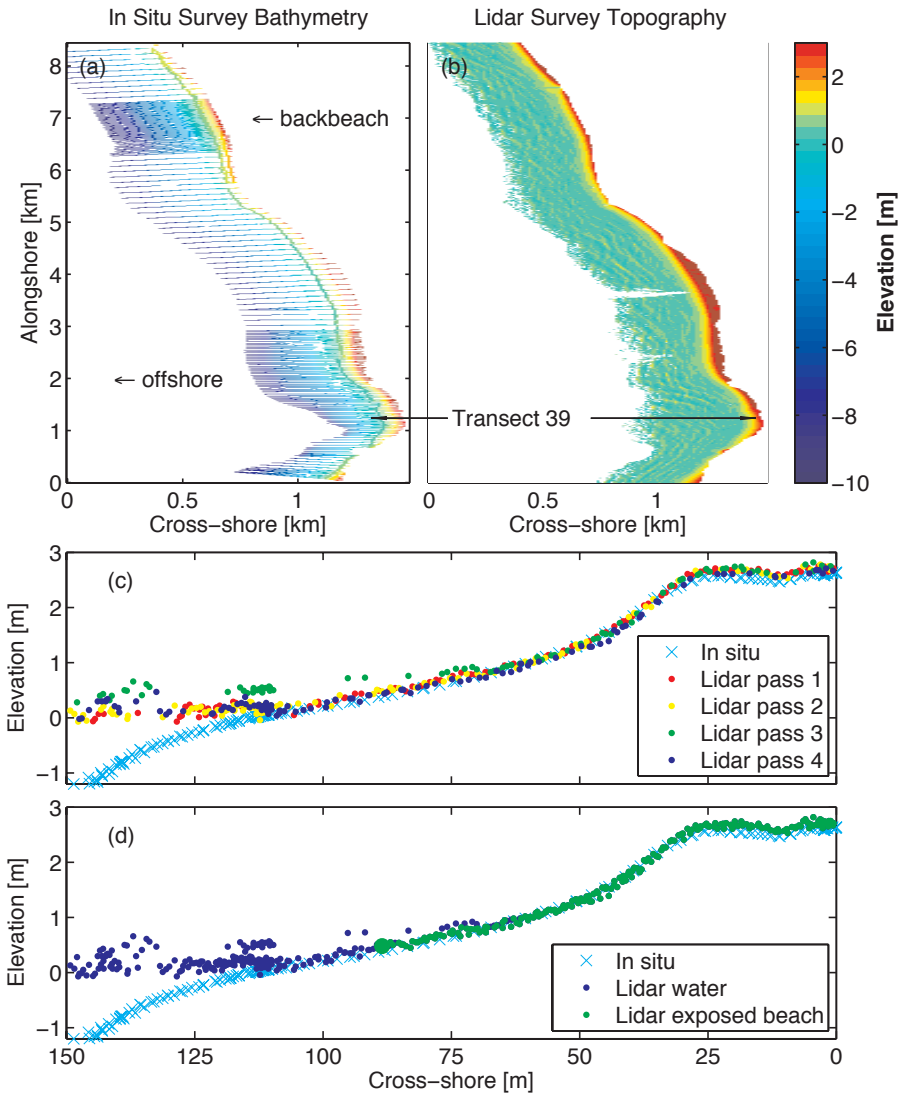

Figure A.1: Surveys of September 2004: (a) in situ bathymetry, 199 cross-shore oriented transects, extending from 10m depth offshore to the backbeach, and (b) lidar topography, one pass shown with wave crests visible in the offshore region and the subaerial beach a narrow, red strip. Color scale is to the right. (c) Elevation versus cross-shore location on survey transect 39: in situ (blue x) and four lidar passes (colored circles, see legend). The location of the ocean surface varies between passes due to surface waves and changing tide levels. The first two passes were completed at lower low tide on 28 September 2004, and the next two passes were completed about 24 hours later. (d) Elevation versus cross-shore location on transect 39: in situ (blue x) and lidar, all passes combined, separated using $C = 0.4$ in (A.1) into lidar water (dark blue) and subaerial beach (green). The large green circle is the most seaward lidar subaerial beach point. For clarity, every other data point is shown in (c) and (d).

A.6c). The sandy beach face, with median grain diameter of 0.2 mm (Seymour et al., 2005), sometimes contained a few cobbles.

The tide level was measured every six minutes at the Scripps Institution of Oceanography (SIO) pier (National Oceanic and Atmospheric Administration (NOAA) station 9410230, located less then one kilometer South of the survey region). The significant wave height was measured at the Torrey Pines Outer Buoy, operated by the Coastal Data Information Program (CDIP). The buoy was located in 550m water depth, about 10 km offshore of Torrey Pines State Beach, and wave heights were reported every 30 minutes. The nearest in time wave height and tide level were used, and the conditions during each survey are shown in Table A.1.

A.3.2 Lidar surveys

Each lidar survey included the 80 km stretch of coastline from Point La Jolla (South) to Dana Point (North). The in situ survey site, Torrey Pines State Beach, is located approximately five kilometers North of Point La Jolla. The Optech, Inc. Airborne Laser Terrain Mapper (ALTM) 1225 was used in conjunction with geodetic quality GPS airborne and ground-based receivers. For the September and December 2002 surveys, the ALTM 1225 was installed in a single engine Cessna 206. The later surveys (April and September 2004, and April 2005) used a twin engine Partenavia P-68 Observer.

The laser pulses at 25 kHz and scans at 26 Hz, with a scanning angle of +/-20 degrees. The near infrared laser has a wavelength of 1024 nm, which is unable to penetrate more than a few centimeters below the ocean surface (Mobley, 1994), effectively mapping the exposed beach and ocean surface, whereas green lasers are able to penetrate the water column (Guenther et al., 2000). The swath width was a few hundred meters and was determined by the altitude of the aircraft, which ranged from 320 m (when flying under low clouds) to 1150 m. The ground speed ranged from about 80 to 130 kts (40 to 70 ms^{-1}).

The instrument platform orientation was obtained with an Inertial Measurement Unit (IMU) containing three accelerometers and gyroscopes to measure the aircraft pitch, roll, and yaw. The aircraft position was determined using GPS trajectories and IMU outputs to calculate an aided-Inertial Navigation System solution. Elevation data were determined using the laser ranges and scan angles, the platform position and orientation, and calibration data and mounting parameters (Wehr and Lohr, 1999). The elevation processing and quality control, including eliminating reflections from birds, beach goers and other extraneous targets, were completed at the University of Texas at Austin Center for Space Research (and formerly in the Bureau of Economic Geology).

Each pass of the scanning lidar mapped a few hundred meter wide swath along the coastline. Multiple, overlapping passes ensured complete coverage of the subaerial beach. Each Torrey Pines lidar survey included between three and five passes (Table A.1), collected during one or two successive lower low tides (Figure A.1c). Aerial photography helped identify and exclude cliffs, revetments, piers, and seawalls from the lidar data. The retained lidar data included both the subaerial sandy beach and the wavy ocean surface (Figure A.1b).

A.3.3 In situ surveys

In situ surveys were completed on approximately cross-shore-oriented survey transects, separated by 20 to 100m in the alongshore, at Torrey Pines State Beach (Figure A.1a). At low tide, a GPS-equipped all-terrain vehicle and a hand-pushed dolly surveyed the beach to wading depths. During high tide, a GPS and sonar-equipped personal watercraft surveyed each transect from 10m water depth to as far onshore as the sonar could locate the seafloor in breaking waves. Nearly all of the in situ data used here were collected with the all-terrain vehicle and the dolly, which are more accurate than the personal watercraft system.

The first two surveys contained 65 cross-shore transect lines spanning two kilometers of coastline, and the remaining surveys were extended to 199 lines

Table A.1: For each survey, lidar survey dates and number of passes, in situ survey dates and number of cross-shore transects, net vertical offset, tide level range [relative to North Atlantic Vertical Datum of 1988 (NAVD88)], and significant wave height range are shown.

Lidar survey dates	Passes	In situ surveys	Number of transects	Vertical offset (cm)	Tide level (m)	Wave height (m)
9 Sep 2002	3	9-12 Sep 2002	65	11.8	0.09 to 0.19	1.2-1.3
3-4 Dec 2002	3	3-4 Dec 2002	65	15.8	-0.29 to 0.40	0.5-0.6
2 Apr 2004	4	3-6 Apr 2004	199	3.5	-0.11 to 0.14	1.2-1.3
28-29 Sep 2004	5	27-30 Sep 2004	199	1.7	0.1 to 0.68	0.9-1.0
4 Apr 2005	4	4-7 Apr 2005	199	1.0	-0.32 to -0.02	1.2-1.4

spanning eight kilometers (Table A.1). In situ surveys with 199 transects (Figure A.1a) took three to four days to complete, sampling during successive lower low (exposed beach) and higher high (offshore bathymetry) tides. Lidar and in situ surveys often overlap for at least one low tide and have a maximum offset of a few days (Table A.1).

In situ and lidar data were compared along cross-shore profiles constructed using the in situ data points within 10m alongshore of predefined survey transects. Alongshore offsets are due to human sampling error in the in situ surveys. Corresponding lidar points were defined as those within one meter of each in situ point (Figures A.1c-d, A.3c, A.4c, A.6c, and A.7b-d).

A.4 Finding the waterline in lidar data

A.4.1 Using tides and waves

The vertical elevation of the waterline (Figure A.2) was determined by tides, wave setup (a steady superelevation resulting from breaking waves), and wave runup (oscillations about the mean waterline due to individual waves and wave groups). There are many formulations for the dependence of setup and runup on incident wave conditions and beach morphology. Accurate, dynamically-based predictions of setup and runup at the shoreline require bathymetry across the entire surf zone, but this information is rarely if ever available for the long coastal reaches surveyed with lidar systems. A simple relationship for the maximum vertical waterline elevation (W) above the tide level, not dependent on bathymetry or details of the wave field is (Ruggiero et al., 2001):

$$W = \text{setup} + \text{runup} = CH_s, \tag{A.1}$$

where H_s is the offshore significant wave height. W is the sum of the magnitude of the wave setup (steady) and runup (unsteady), each of which has been suggested to depend on H_s. The cross-shore location of the W-defined, uprush waterline is X. The objective is to define C conservatively, so that spurious water points are rejected, but not so conservatively that larger than necessary swaths of subaerial beach are rejected. To account for the variations between passes (e.g. Figure A.1c), W was estimated for each lidar pass.

To find the waterline, lidar elevations were estimated at two meter cross-shore and alongshore intervals along East-West cross-shore transects, with smoothing over a five meter radius to reduce noise. On each cross-shore transect and for each pass and value of C, the lidar waterline was defined as the most shoreward point with a vertical elevation less than or equal to W. All raw lidar data points shoreward of the waterline cross-shore location X were selected as subaerial, exposed beach data. The passes were combined, yielding a set of beach face points

and a set of ocean surface points. For the combined passes, the lidar shoreline was defined as the location of the most seaward beach data point (e.g. large green circle in Figure A.1d is for the optimal $C = 0.4$). Waterlines were found with C ranging from 0 to 0.6, in intervals of 0.1.

A.4.2 Using in situ surveys

Lidar and in situ vertical elevation data contained the mean (bias) and scatter errors inherent to GPS measurements. A net mean vertical offset was removed from the lidar data, where the offset was calculated as the mean elevation difference between lidar (all passes) and in situ (spanning a few days) data above the Mean Higher High Water vertical datum, which was always well shoreward of the waterline. Offsets could have resulted from vertical GPS drift, or from changes in bathymetry during the completion time of the lidar and in situ surveys. The in situ data suggested that the bathymetry was not changing rapidly during the surveys. The largest offset was 15 cm, and in three of the five cases it was less than 4 cm (Table 1).

Based on repeat lidar and in situ surveys of piers, parking lots, United

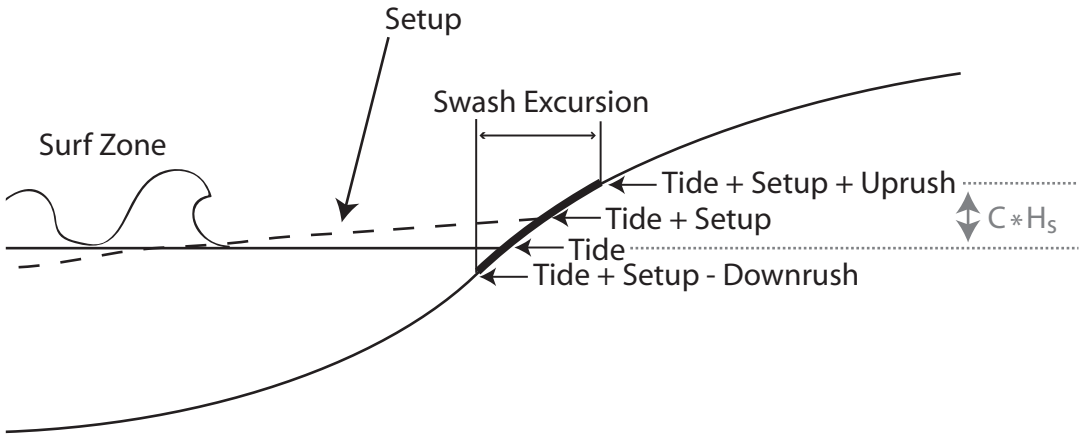

Figure A.2: Setup (dashed curve) elevates the mean water level above the local tide level (solid horizontal line). The swash excursion and vertical elevation reached by uprushes (CH_s above the tide level) and downrushes are also indicated.

States Geological Survey (USGS) benchmarks, and other fixed targets, and using the same one meter horizontal averaging cell size used here, expected RMS vertical differences between in situ and lidar surveys were about 21 cm. In situ and lidar surveys agree within the 21 cm error threshold on the subaerial beach and diverge seaward of the waterline, where the lidar survey does not measure the seafloor bathymetry (Figures A.1c-d, A.3c, A.4c, and A.6c). Using a smaller error threshold would include extraneous divergence points on the beach face instead of at the waterline, so this functional threshold was used.

The "true" waterline elevation, W_{true}, and cross-shore location, X_{true}, were defined for each pass as the elevation and cross-shore location where the in situ and lidar data diverge (black triangle in Figures A.3c, A.4c, and A.6c). The divergence point was defined as the cross-shore location where the vertical difference between the two data sets was larger than the noise expected from sampling errors, rather than the actual wet-dry beach separation point. When the bathymetry is known, the divergence waterline location, W_{true} and X_{true}, would be the lidar elevation and cross-shore location selected to identify subaerial beach data, whereas when the bathymetry is unknown, (A.1) is used to find W and X. Shoreward of X_{true}, even if the lidar is measuring the elevation of a thin tongue of water, the in situ and lidar elevation measurements are not distinguishable within the noise. The cross-shore location of the divergence waterline (X_{true}) is expected to vary alongshore, by about a swash excursion, as uprush and downrush are alternately sampled (Figure A.2).

A.5 Results

Two simple difference measures, horizontal and vertical, were used to select a single value of C that rejects lidar water returns from all passes, by comparing the divergence waterline (X_{true}, W_{true}) to the lidar waterlines (X, W for each value of C) for each pass.

The horizontal or cross-shore difference for each pass is $X_{true} - X$, the distance between the cross-shore location of the divergence waterline (X_{true}) and the most seaward point identified as subaerial beach waterline (X) using tides and waves (A.1). Negative cross-shore differences are undesirable because they indicate that the lidar waterline is seaward of the divergence waterline, and water elevations are erroneously classified as subaerial beach (e.g. $C = 0$, magenta symbols in Figures A.4a and A.6a). Large, positive cross-shore differences indicate that the lidar waterline is located far shoreward of the divergence waterline, and many subaerial beach elevations are eliminated because they are classified as water (e.g. $C = 0.6$, dark blue symbols, lidar waterlines are about 40 m shorewards of X_{true} in Figures A.3a, A.4a, and A.6a). Alongshore variability of W_{true} and X_{true} within a pass is due to alongshore variation in the runup phase (e.g. uprushes and downrushes), and possibly alongshore variation in the runup amplitude. Beach slope and divergence waterline elevation (W_{true}) were not correlated (at the 5% significance level), suggesting that beach slope variations, which were small (0.01-0.04), did not significantly contribute to the alongshore variations in runup amplitude. A single deep water value of H_s was used to estimate W, and alongshore variation of H_s was neglected.

The vertical or elevation difference for each pass is W minus the in situ elevation at the cross-shore location of the lidar waterline (X). When the lidar waterline (X) is erroneously located seaward of the divergence waterline (X_{true}), the elevation difference is positive and potentially large ($C = 0$, magenta symbols in Figures A.4b,c and A.6b,c). When the lidar waterline is located at or shoreward of the divergence waterline, both in situ and lidar surveys are measuring sand level, or the lidar survey measures only a thin tongue of water, and their differences will be distributed around zero, with scatter due to noise in both the lidar and in situ surveys, as seen for C values greater than zero in Figure A.3b.

Significant wave heights during lidar surveys ranged between 0.5 and 1.4m. During the survey with the smallest wave height, wave setup and swash

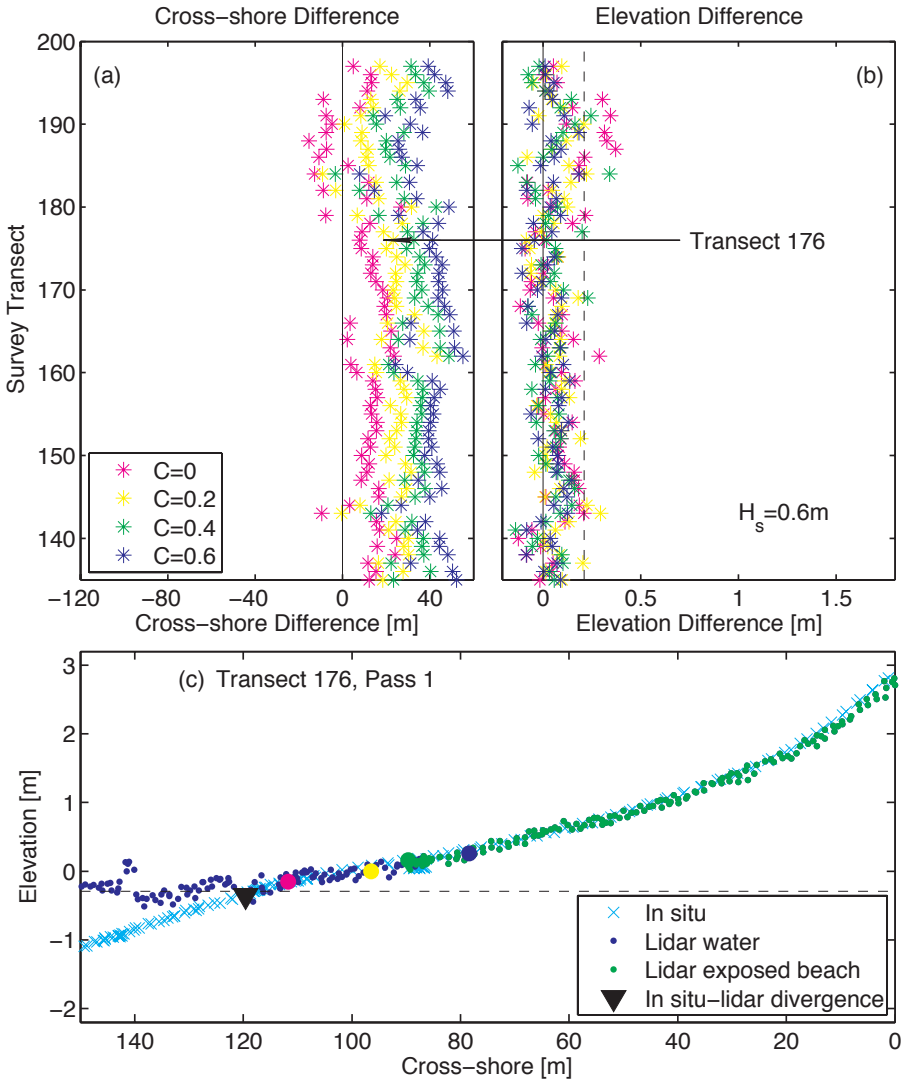

Figure A.3: Results for pass one in December 2002 along 65 in situ cross-shore survey transect lines. Wave heights were relatively low ($H_s = 0.6$m). (a) Cross-shore (horizontal) difference ($X_{true} - X$) between the divergence waterline (X_{true}, black triangle in (c)), and the lidar waterline (X, large circles in (c)) estimated using tide and wave data (A.1). The colors correspond to C values ranging from 0 to 0.6 (for clarity, not all C are shown). (b) Elevation (vertical) difference between the lidar waterline (W) and in situ data at the cross-shore location (X) of the lidar waterline for different C. The vertical dashed line indicates the 21 cm elevation error threshold. (c) Elevation versus cross-shore location on transect line 176: in situ (blue x), lidar water (dark blue), and lidar subaerial beach (green), defined with $C = 0.4$ (A.1). For clarity, every other data point is shown. The dashed horizontal line is the tide level measured at the end of a nearby pier. Also shown are the divergence waterline (X_{true}, black triangle) and the lidar waterlines (X, large circles for different C values, same legend as (a)).

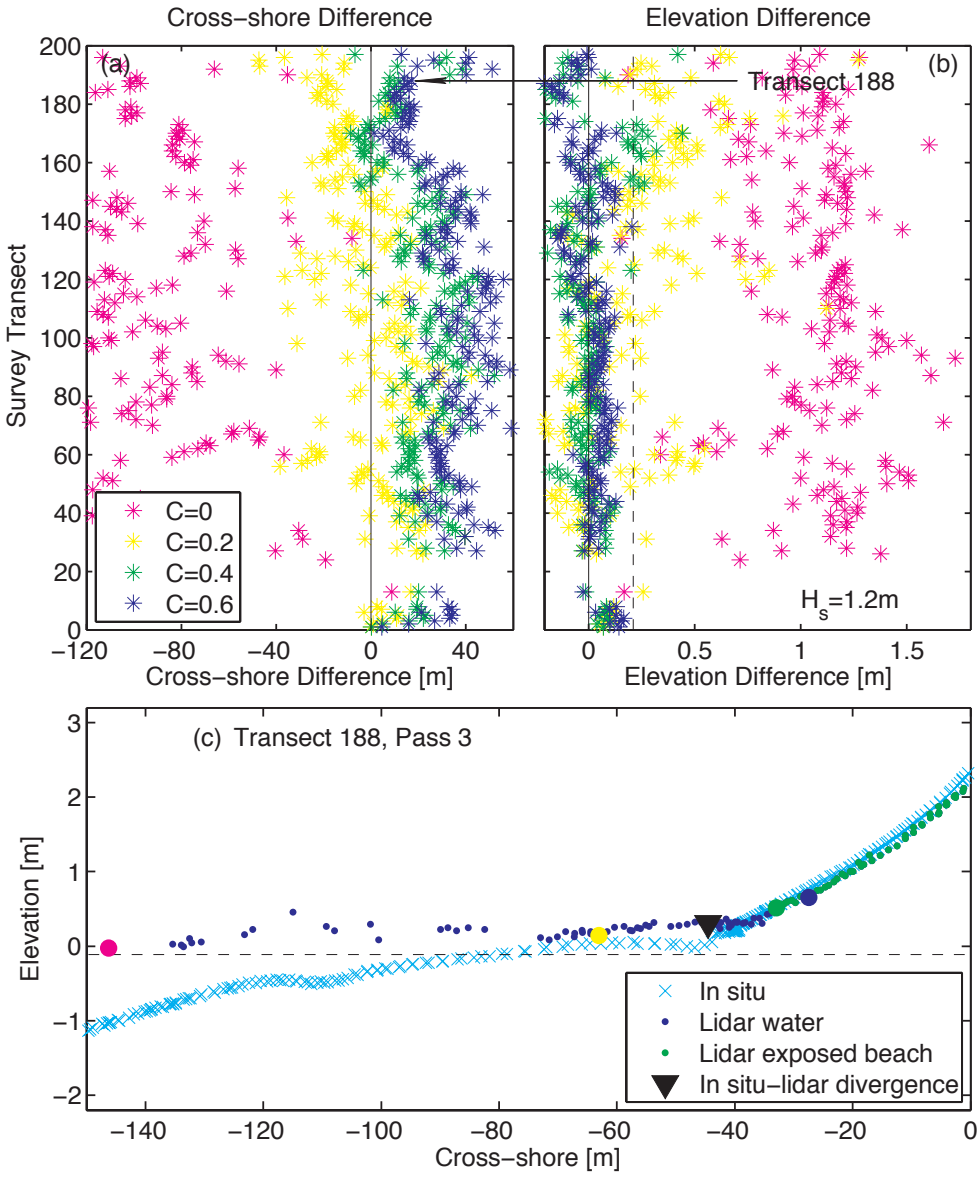

Figure A.4: Results for pass 4 in April 2004 on 199 cross-shore survey transect lines. Waves heights were relatively large (H_s = 1.2m). Same format as Figure A.3.

effects on the lidar waterline location were small (December 2002, H_s=0.5-0.6m, pass 1 shown in Figure A.3). Using $C = 0$ included only a few lidar water returns with negative values in Figure A.3a and elevation differences larger than 21cm in Figure A.3b. For larger C, lidar waterline locations are shoreward of the divergence waterline (vertical solid line in Figure A.3a), and nearly all elevation differences are less than the 21cm estimated noise threshold (vertical dashed line in Figure A.3b).

With large waves (April 2004, H_s=1.2-1.3m, Figures A.4 and A.6), wave setup and runup significantly affected the waterline location. With waves neglected ($C = 0$), points located more than 100m seaward of the true waterline are misidentified as subaerial beach, and elevation errors are as large as 1.5m (magenta symbols in Figure A.4a,b, respectively). Increasing C to 0.4 eliminates the lidar water returns, with vertical differences within the estimated noise threshold. Further increasing C excludes beach face data.

To select an overall C value, RMS cross-shore and elevation differences were calculated for each survey and C value (solid lines, Figure A.5). For small C and the largest wave heights (April 2004 and April 2005), the lidar waterline is seaward of the divergence waterline yielding large RMS cross-shore differences, and many water returns are erroneously classified as subaerial beach. For the largest C, the large RMS cross-shore differences indicate the lidar waterline is located far landward of the divergence waterline, eliminating subaerial beach points. For intermediate C values, RMS cross-shore differences may be relatively small when the lidar waterline is slightly seaward or slightly shoreward of the divergence waterline. To distinguish between these two cases, the fraction of points shoreward of the divergence waterline was calculated for each survey and C value (dashed lines in Figure A.5a).

Elevation differences are large for small C when lidar water returns are included, and decrease with larger C to less than the 21cm error threshold (within the shaded grey area in Figure A.5b). The percentage of lidar waterlines with

elevation differences less than the error threshold also increases as C increases (dashed lines in Figure A.5b).

The optimal C value was selected for each survey as the smallest C with 90% of the retained lidar waterlines shoreward of the divergence waterline (X_{true}), and with 90% of the RMS elevation differences less than 21cm. Optimal C ranged between 0 in December 2002, the day with the smallest waves, to 0.4 in April 2004, when waves were larger. The optimal C also varied within surveys. For example, in the April 2004 survey, the optimal value for pass 3 was $C = 0.4$ (Figure A.4), while for pass 2 it was $C = 0.2$ (Figure A.6).

A value of C=0.4 removed water points from all surveys, while retaining most of the subaerial beach. With C=0.4, the strip between X_{true} and X, rejected as water by the present algorithm, is between 26 and 36m wide (Table 2). Reducing C would narrow this strip, but would increase the number of water data points that are included.

Table A.2: For each lidar survey (including between three and five passes), the range of elevation cutoffs (W), RMS horizontal difference between the cross-shore location of the $C = 0.4$ lidar waterline and the divergence waterline, and the RMS horizontal distance gained using the lidar waterline instead of the MHW contour are shown.

Survey	***W* range (m)**	**Cross-shore difference (m)**	**Distance to MHW (m)**
Sep 2002	0.60-0.66	26	47
Dec 2002	-0.13-0.63	29	68
Apr 2004	0.37-0.68	26	52
Sep 2004	0.49-1.05	29	57
Apr 2005	0.15-0.54	36	77

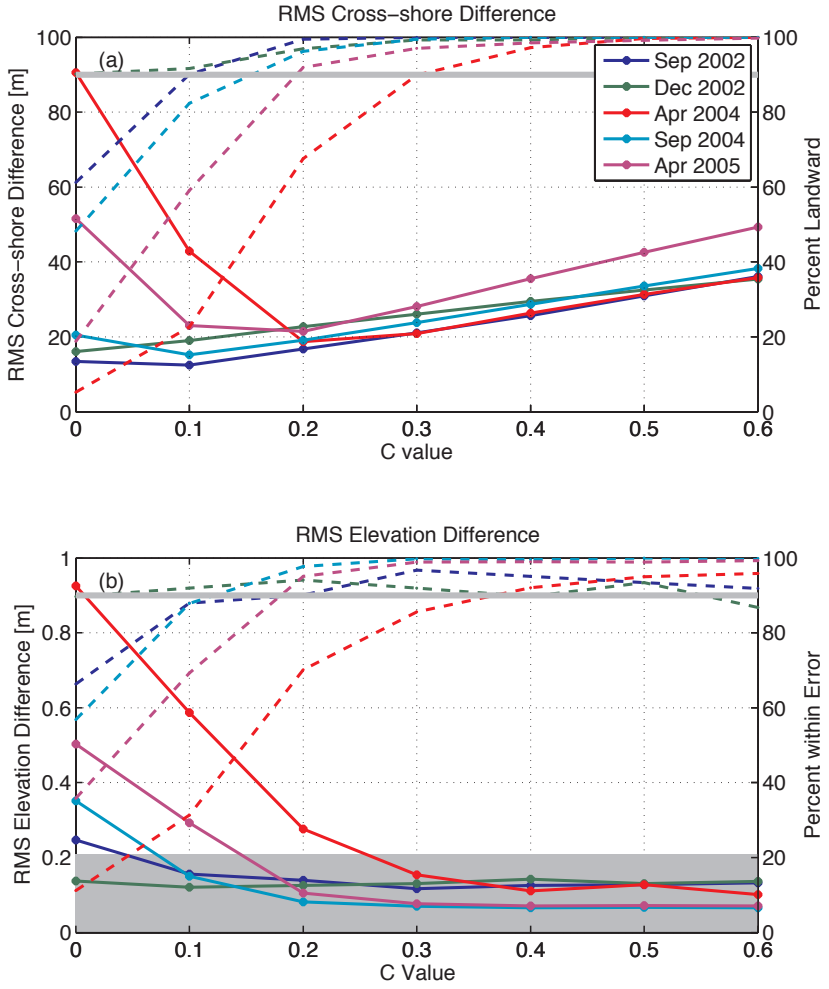

Figure A.5: In situ-lidar differences used to select C. (a) RMS cross-shore differences between divergence (X_{true}) and lidar (X) waterline locations (solid lines, left axis), and percentage of lidar waterlines shoreward of the divergence waterline (dashed lines, right axis). (b) RMS elevation differences between the lidar waterline (W) and in situ data at the cross-shore location (X) of the lidar waterline (solid lines, left axis), and percentage of lidar waterlines within the 21cm error threshold (dashed lines, right axis). The grey shaded area corresponds to elevation differences less than 21cm. The grey horizontal lines in (a) and (b) indicate 90%.

A.6 Discussion

A.6.1 Lidar return intensity and density

The intensity or strength of returns is increased by bubbles and foam (Mobley, 1994), and individual breaking waves create bands of high intensity and

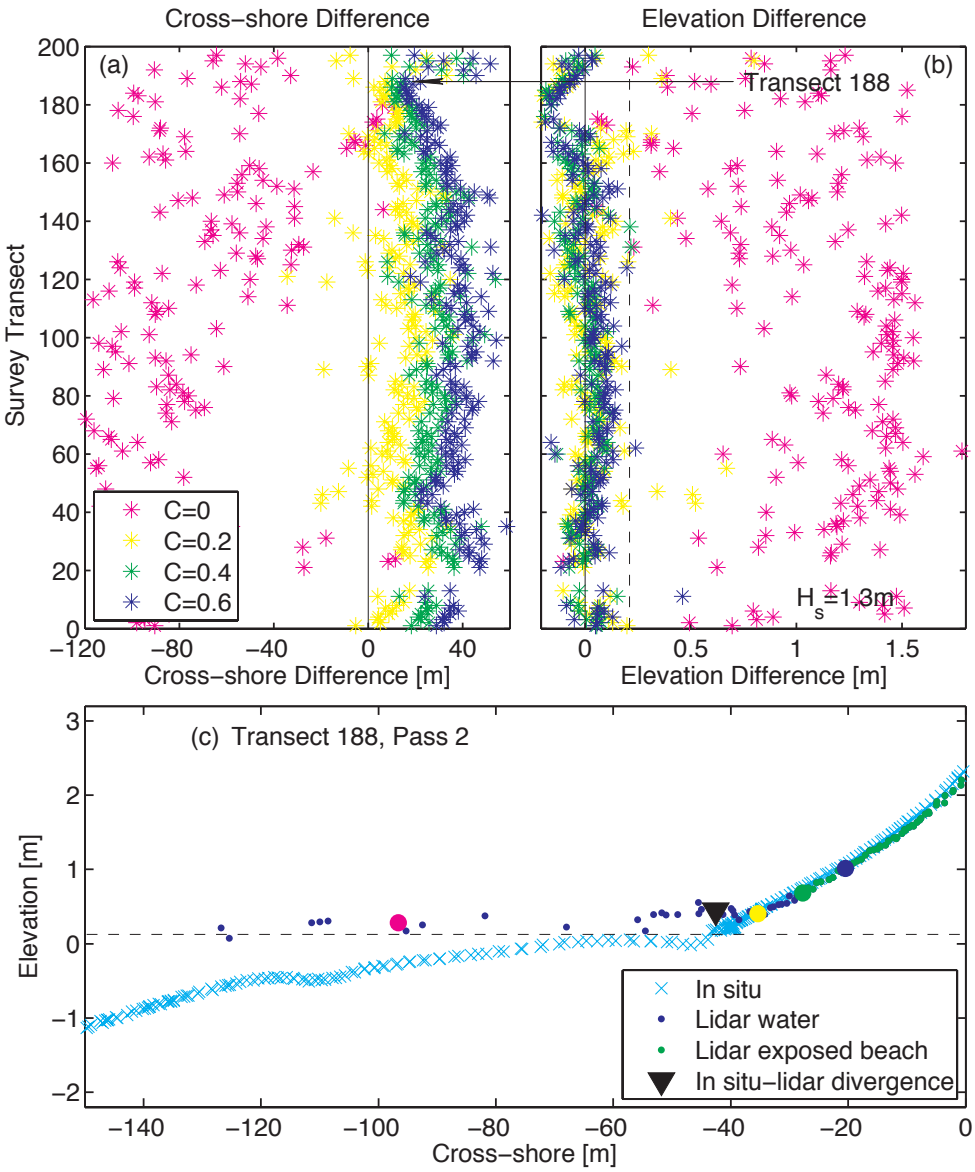

Figure A.6: Results for pass 2 in April 2004 on 199 cross-shore survey transect lines. Wave heights were relatively large (H_s=1.3), but C =0.2 is the optimal value, compared with $C = 0.4$ for pass 3 of the same survey (Figure A.4).

high intensity gradients (not shown). However, the intensity also depends on scanning angle, decreasing with increasing angle (Mobley, 1994). Simple methods based on intensity gradients approximately located the waterline along on some transects (not shown), but the results based on wave height and tide level (Table A.2) were not improved by including intensity.

Similarly, on many cross-shore transects, the return density or points per m^2, decreased seaward of the waterline (Figure A.6c). However, on some transects there was little or no decrease in point density near the waterline (Figure A.3c), and on other transects the variation in return density occurred farther offshore than the waterline (Figure A.4c), sometimes in the mid-surf zone (not shown). Previous studies suggest that the return density depends on the beam angle, as well as wind and wave conditions (Guenther et al., 2000; Krabill et al., 2000). The variation of return density across the surf zone and runup is not understood sufficiently to use for routine waterline identification.

A.6.2 Runup and setup parameterizations

Equating W with $W_{2\%}$, the vertical level exceeded by 2% of wave runups, the corresponding $C_{2\%}$ is between roughly 0.4 and 0.5 (Ruggiero et al., 2001) on Oregon beaches with Iribarren number (or surf similarity number) similar to Torrey Pines (between about 0.2 and 0.7). The Iribarren number, $\xi = \beta L_0^{\frac{1}{2}} H_0^{-\frac{1}{2}}$, where H_0 and L_0 are the deep water wave height and wave length, and β is a representative beach slope (Battjes, 1974), is widely used to characterize beaches. Small Iribarren numbers (less than about 1) denote dissipative beaches with spilling waves, and larger values correspond to reflective beaches with plunging or collapsing waves. Extensive field observations of the 2% exceedence runup suggest that $C_{2\%}$ depends on ξ (Holman, 1986; Ruggiero et al., 2001; Stockdon et al., 2006), reaching values as high as three on steep beaches with low energy swell waves ($\xi \approx 3$). Alternative empirical formulations that relate $C_{2\%}$ to H_0/L_0 (without a β dependence) also suggest higher values of $C_{2\%}$ for low energy swell (Ruggiero et al., 2001). In this

study, with small ranges of wave height (0.5-1.4 m) and beach slope (0.01-0.04), the Iribarren number remained in the dissipative range, varying between 0.2 and 0.7. The Iribarren number or H_0/L_0, calculated for each pass, and the optimal C value were weakly correlated (squared coefficients of 0.4 and 0.3, respectively) at the 5% significance level. However, these correlations were determined with very few (19) data points with significant scatter, and would likely not be valid over a larger parameter range. To avoid retaining water points, increased values of C are recommended for application of (A.1) to lidar obtained on beaches with significantly different waves and bathymetry than Torrey Pines. For example,

$$W_{2\%} = (0.83\xi + 0.2)H_s \tag{A.2}$$

(Holman, 1986) overpredicts W at Torrey Pines, but is valid at large ξ.

Setup and runup depend on wave transformation across the surf zone. As the tide level changes and incident wave conditions remain relatively stable, the effective surf zone bathymetry and wave transformation change. For example, a sandbar that causes wave breaking at low tide can be too deep to induce breaking at high tide (Raubenheimer et al., 2001). Infragravity wave energy levels, which can dominate swash (runup) on dissipative beaches, also depend on the tide level and the associated variations in the effective surf zone bathymetry (Thomson et al., 2006). Simple parameterizations of setup and runup used to estimate $W_{2\%}$, for example (2), are therefore necessarily of limited accuracy. Nevertheless, empirical formulations for $W_{2\%}$ provide useful estimates of W for a wide range of beach and wave conditions.

A.7 Summary

Coastal lidar data include elevations of the exposed, subaerial beach and, seaward of the waterline, the ocean surface. Here, a simple method was developed to remove water returns. A vertical elevation cutoff was used, with the waterline elevation (W) above the known tide level during each lidar pass, due to the

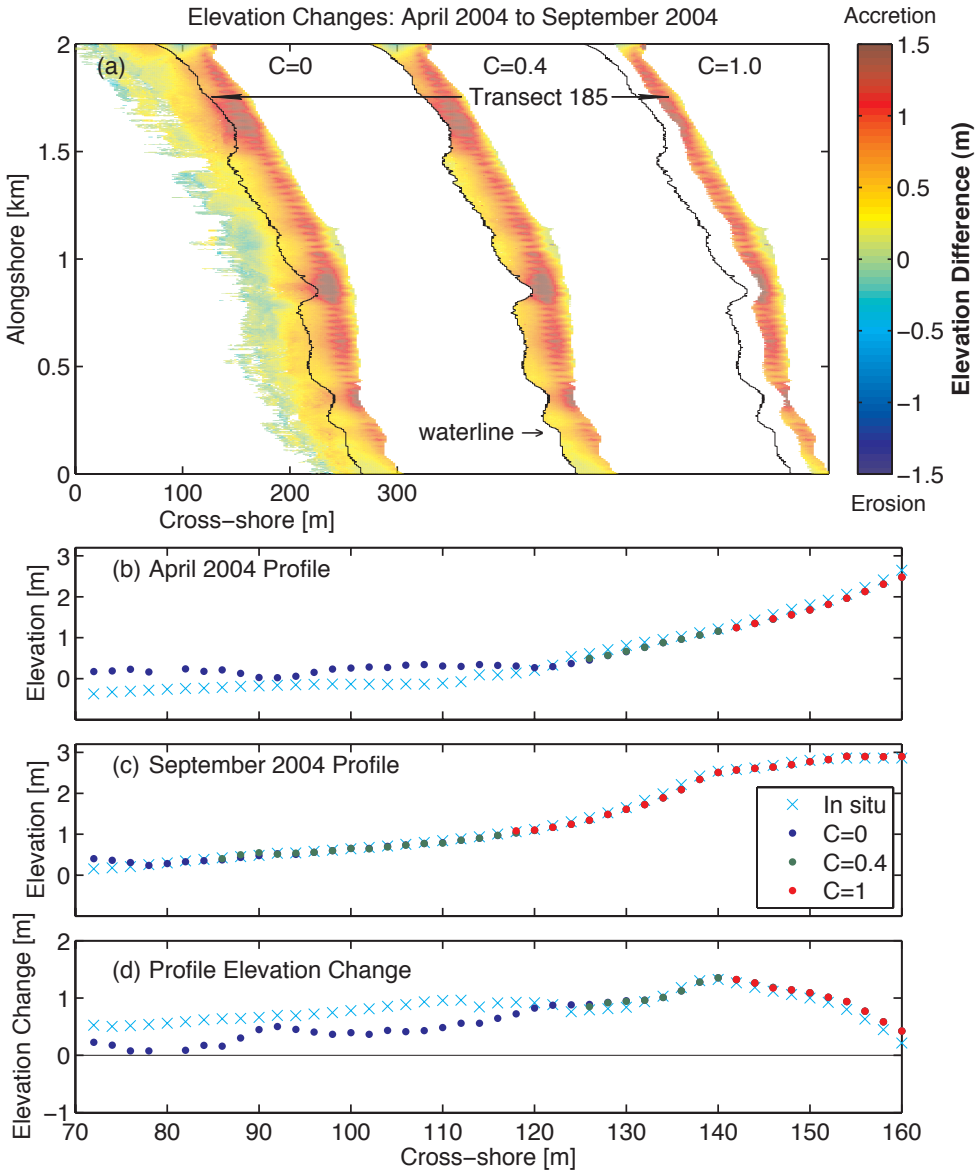

Figure A.7: (a) Plan view of beach sand level changes along 2 km of Torrey Pines State Beach from April 2004 to September 2004, estimated with lidar waterlines calculated using $C = 0$, 0.4, and 1.0 (left to right). Color scale is to the right. Each strip shows change between the cliffs bordering the backbeach (to the right) and the estimated waterline (to the left). The thin black curve superimposed on each change map corresponds to the lidar waterline with $C = 0.4$. Elevation versus cross-shore location for transect 185 (location indicated in (a)) for the (b) April 2004 and (c) September 2004 surveys. Elevations are binned every 2m. (d) Elevation change between April and September 2004, with in situ data (blue x) and lidar data (color indicates the C values, legend in (c)).

superelevation from wave setup and runup, assumed proportional to the offshore significant wave height H_s ($W = CH_s$). Spatial change maps using $C = 0$, 0.4, and 1 to estimate the lidar waterline are shown in Figure A.7a. An overly conservative estimate of setup and runup at Torrey Pines ($C = 1$) excludes many subaerial beach points, while $C = 0$ includes many water points (Figure A.7b) and yields spurious beach changes (dark blue points in Figure A.7d). Using $C = 0.4$ shows the desired result of excluding water points while retaining most subaerial beach points (green points in Figure A.7b-d).

The pass-by-pass processing, with lidar waterlines estimated for each pass, effectively combines surveys acquired at different tide levels and wave conditions (Figure A.1c,d). Even though each survey spanned only two days and was centered around low tide, there was as much as 0.7m vertical difference in the lidar waterline elevation (W) and 34m horizontal difference in the lidar waterline cross-shore location (X) between passes (Table A.2). Using $C = 0.4$ rather than MHW (sometimes used as a conservative default shoreline level, well above the waterline) added between (RMS) 47 and 77m to the width of the subaerial beach (Table A.2). The range of wave and beach conditions at Torrey Pines was limited. For application at beaches with waves or slopes very different than Torrey Pines, existing empirical formulas for C based on observations of setup and runup spanning a wide range of conditions [e.g. (A.2)] are recommended.

Acknowledgements

Lidar and in situ surveys were supported by the United States Army Corps of Engineers. Wave data collection was supported by the California Department of Boating and Waterways. Brian Woodward, Kent Smith, Dennis Darnell, and Bill Boyd collected the in situ bathymetry data. Marissa Yates was supported by a National Defense Science and Engineering Graduate Fellowship. A reviewer provided helpful suggestions.

The text of Appendix A, in full, is a reprint with minor modifications of the paper "A Technique for Eliminating Water Returns from Lidar Beach Elevation Surveys," *Journal of Atmospheric and Oceanic Technology*, **25** (9), 1671-1682, doi: 10.1175/2008JTECHO561.1 (Copyright of the American Meteorological Society 2008). The dissertation author was the primary researcher and first author with guidance provided by R.T. Guza, R. Gutierrez, and R.J. Seymour.

Appendix B

Wave averaging

The effects of wave averaging are to remove the significance of the magnitude and timing of individual wave events, which are important in understanding beach change (Morton et al., 1995; Lee et al., 1998). In a simple example from Torrey Pines alongshore section T3, two wave energy time series $E(t)$ with the same average wave energy $\bar{E}$ and approximately the same initial MSL position S, had significantly different wave time series and net MSL position change rates $\overline{dS/dt}$ (Figure B.1). In Figure B.1a, larger than average wave energy events occurred near the end of the two-week period, resulting in -2.3 m of net MSL position erosion, while in Figure B.1b, a large wave energy event at the beginning of the two-week period was followed by low waves, resulting in +2.1 m of net MSL position accretion. The magnitude and sign of MSL change is dependent on the magnitude and sequence of wave energy events. Thus averaging wave fields between surveys to relate to beach changes introduces errors.

In this paper, the approximate equilibrium wave energy $\bar{E}_{eq}$ was originally calculated using the observations (Figure 4.3) of the average wave energy $\bar{E}$ and net MSL change rate $\overline{dS/dt}$ between two surveys. However, the averaging creates a bias, and the hourly equilibrium energy E_{eq} determined by optimization (Figure B.2c, solid line) is steeper (the magnitude of a is larger) than the equilibrium energy $\bar{E}_{eq}$ calculated with averaged observations (Figure B.2c, dashed line).

A synthetic, hourly MSL position time series was created using model

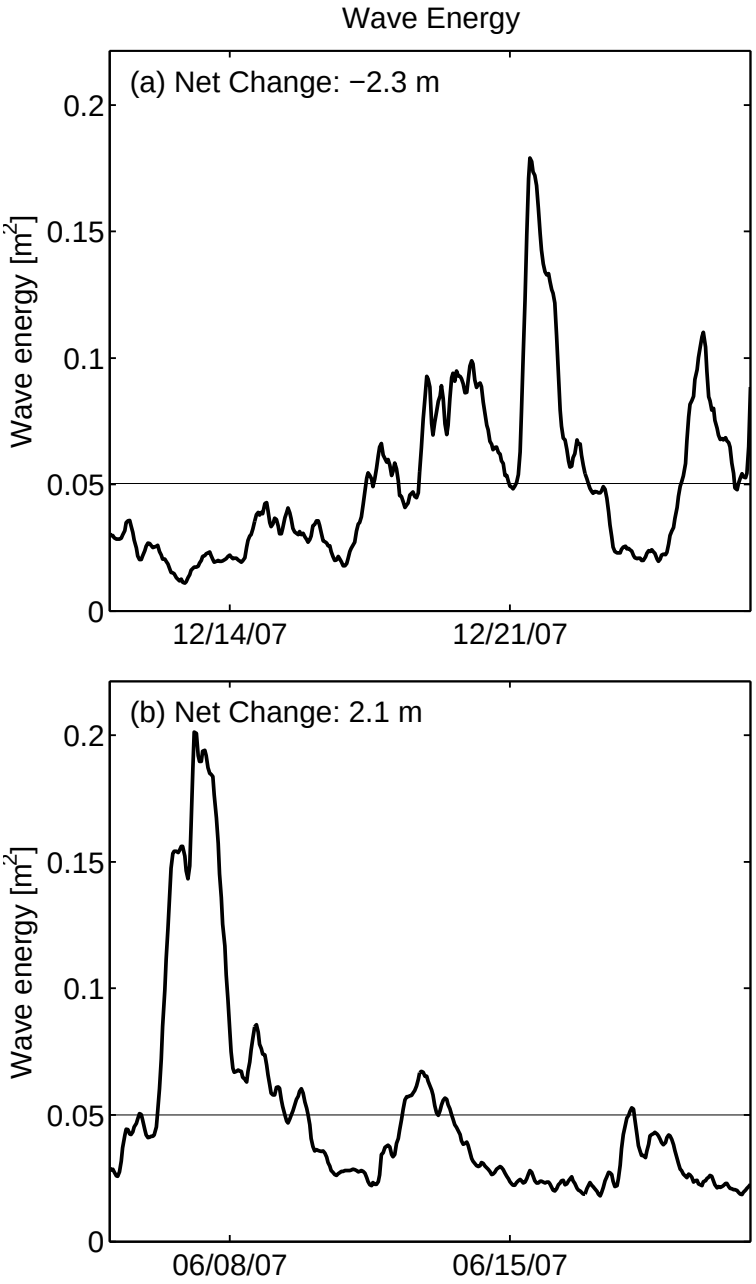

Figure B.1: Wave energy versus time for about two weeks in (a) December 2007 with net erosion -2.3 m, and (b) June 2007 with net accretion +2.1 m. These time periods have approximately the same initial MSL position and wave average $\bar{E}$, yet produce MSL changes of opposite sign.

output from the optimal free parameters and the energy time series at section T3. Figure B.2a shows the hourly synthetic data and the hourly equilibrium wave energy. The hourly wave energy events reach significantly higher values, and the erosion rates are significantly larger than in the averaged observations (compare Figure B.2a to Figure B.2b-c).

The hourly synthetic data was subsampled, calculating the average wave energy and net MSL change rate for time periods with the same spacing as the true observations. The averaging smooths the instantaneous large wave energy events and MSL change rates, increasing the data scatter and demonstrating that the hourly equilibrium energy is steeper than would be expected if only averaged observations were used (Figure B.2b).

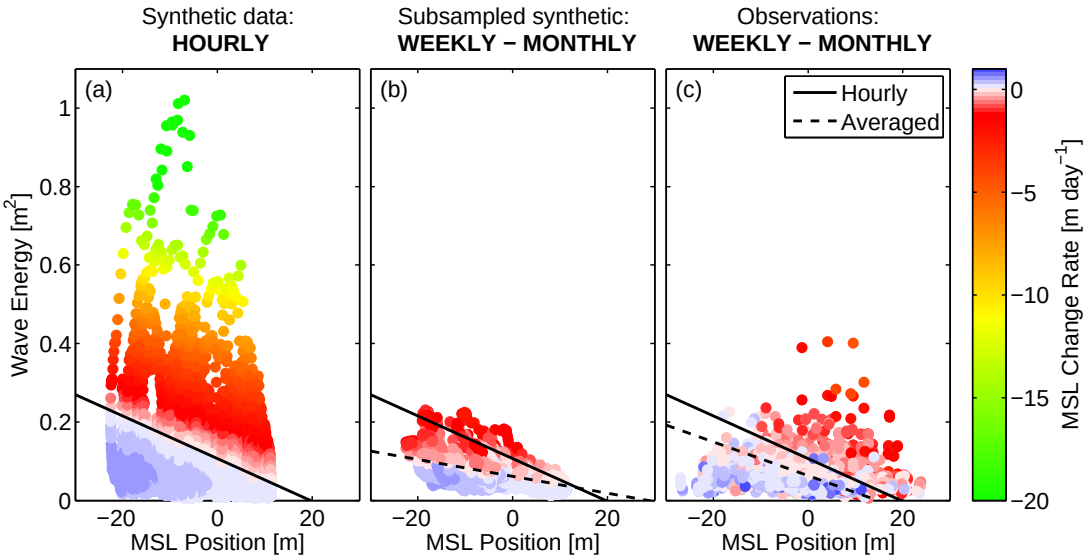

Figure B.2: The effects of using hourly and averaged observations to determine the equilibrium wave condition are shown: (a) hourly synthetic observations, (b) weekly to monthly averaged synthetic observations, and (c) weekly to monthly averaged true observations at Torrey Pines. The 'true' equilibrium wave energy E_{eq} was determined with modeled hourly data (solid line in all 3 panels). Dashed lines in (b) and (c) indicate the erroneous $\bar{E}_{eq}$ resulting when averaged $\bar{E}$ are used.

Appendix C

Optimization techniques

Two derivative-free optimization techniques were tested to define the free parameters in the model's multivariable nonlinear function (4.1) - (4.3): simulated annealing and surrogate management framework (SMF). The cost function, which quantitatively measures how well the model and the observations agree, was defined as the root-mean-square (RMS) difference between the model and the observations:

$$\mathscr{L} = \sqrt{\frac{1}{n_{obs}} \sum_{i=1}^{n_{obs}} [S_i - S_i^*(a, b, C^+, C^-)]^2}, \tag{C.1}$$

where S is the observed MSL position time series, S^* is the hourly modeled MSL position time series (which is a function of the model free parameters, a, b, C^+, and C^-), subsampled at the time of the observations, and n_{obs} is the total number of observations. With four model free parameters [a and b define the relationship between the equilibrium wave energy and the MSL position (4.3), and $C^{\pm}$ are the accretion and erosion change rate coefficients (explained in section 4.5)], the two optimization techniques search a four-dimensional parameter space to minimize the cost function (C.1). It is computationally expensive to evaluate the cost function at a large number of locations in the parameter space, and the optimization techniques limit the number of cost function evaluations by searching efficiently. The cost function is not sufficiently smooth to use gradient-based optimization techniques such as steepest descent; therefore, derivative-free techniques were tested.

The two optimization algorithms tested in this analysis use different meth-

Table C.1: Rescaling ranges for the four model free parameters.

	$\boldsymbol{a}$ (m^2/m)	$\boldsymbol{b}$ (m^2)	$\boldsymbol{C^+}$ ($m^{-1}s^{-1}$)	$\boldsymbol{C^-}$ ($m^{-1}s^{-1}$)
Minimum [p_{min}]	-0.01	0.05	-8	-8
Maximum [p_{max}]	-0.0005	0.15	0	0

ods to search the free parameter space, but the model results (and RMSE) are similar. Each of the four free parameters p (with $p = a, b, C^+$, or C^-) are rescaled to create an isotropic four-dimensional parameter space, with a defined range from $0 \leq \tilde{p} \leq 100$ (with $\tilde{p} = \tilde{a}, \tilde{b}, \tilde{C}^+$, or $\tilde{C}^-$). The range over which the parameters were rescaled was determined by evaluating the expected range of free parameter values that produce physical model results. The model free parameters p are calculated as:

$$p = \frac{(p_{max} - p_{min})\tilde{p}}{100} + p_{min}, \tag{C.2}$$

where p_{min} and p_{max} are the minimum and maximum values of the searchable free parameter space, as defined in Table C.1. By mapping the variables p to the rescaled variables $\tilde{p}$, the optimization techniques are able to search in a isotropic four-dimensional parameter space. The following two sections describe the optimization techniques and illustrate the procedures with an example at Torrey Pines Beach alongshore section T2. Finally, section C.3 describes the benefits of using SMF to determine the model free parameters in this analysis.

C.1 Simulated annealing

Simulated annealing was developed by Kirkpatrick et al. (1983) by applying a theory from statistical mechanics about the annealing or cooling process of a melt as it forms a crystal. If the melt cools too quickly, it does not form a regular crystal, and the crystal does not achieve the lowest possible energy state. At each step in the cooling process, the Boltzmann distribution determines the likelihood of a given energy state, and the Metropolis algorithm determines the probability

that one energy state is achieved over another (Metropolis et al., 1953):

$$P(En_2 - En_1) = \mathrm{e}^{-(En_2 - En_1)/k_b T}, \tag{C.3}$$

where En_1 and En_2 are energy states, k_b is Boltzmann's constant, and T is temperature. In this analysis, the two energy states En are two evaluations of the cost function $\mathscr{L}$ (C.1), and $k_b T$ is a cooling parameter D, which controls the shape of the probability distribution function. The probability of accepting one evaluation of the cost function as a step toward minimization is then:

$$P(\mathscr{L}_2 - \mathscr{L}_1) = \mathrm{e}^{-(\mathscr{L}_2 - \mathscr{L}_1)/D}, \tag{C.4}$$

such that the evaluation of the cost function is always accepted when $\mathscr{L}_2$ is less than $\mathscr{L}_1$ (i.e. the problem is minimized), and the evaluation of the cost function is accepted with a probability P when $\mathscr{L}_2$ is greater than $\mathscr{L}_1$ (Metropolis et al., 1953). The Metropolis algorithm accepts values that cause increases in the cost function in order to prevent the optimization from getting trapped in a local minimum.

As a crystal forms, the temperature T slowly decreases, which causes a decrease in the probability of accepting an energy state that increases the energy of the crystal. Similarly, as the cost function approaches a minimum value, the cooling parameter D decreases following an annealing schedule, which decreases the probability of accepting an increase of the cost function. As in Barth and Wunsch (1990), a simple annealing schedule is defined as a linear decrease in D with each iteration:

$$D^{(k+1)} = \Delta_d D^{(k)}, \tag{C.5}$$

where Δ_d is the factor by which D decreases.

Within each iteration k (while D is constant), a number (n_i) of cost function evaluations are made at random locations in the free parameter space. The random free parameter values are determined by jumping from the initial location to the new location by randomly changing one of the free parameter values, for example:

$$a^{(i+1)} = d_{jump} r + a^{(i)}, \tag{C.6}$$

where d_{jump} scales by how much each free parameter can change, and r is a random value from a normal distribution with a mean of zero and a standard deviation of one. The acceptance of the new location is tested in (C.4) until the maximum number (n_{max}) of accepted locations is reached for the given iteration k (still with D constant). From one iteration to the next, the distance jumped in the free parameter space also decreases:

$$d_{jump}^{(k+1)} = \Delta_d d_{jump}^{(k)}, \tag{C.7}$$

following the same linear decrease in D (C.5). The number of iterations or the number of steps in decreasing the searching radius is defined by setting a minimum jumping distance d_{min}, which prevents searching for infinitely smaller changes to the free parameter values. The simulated annealing algorithm stops when the minimum jumping distance is reached.

The values of D, Δ_d, d_{jump}, d_{min}, n_i, and n_{max} are all problem-specific. In the optimization problem applied to the equilibrium model, the first simulated annealing runs had large values for the width of the probability distribution function D, the initial searching radius d_{jump}, and the number of cost function evaluations n_i, accepted cost function evaluations n_{max}, and "cooling" steps or times that the searching radius was decreased (controlled by a small d_{min}). Initially, the rate Δ_d at which the probability distribution function changed and the searching radius decreased was nearly one, and the minimum jump d_{min} of a free parameter was very small relative to the size of the free parameter. The parameters were adapted to find the appropriate range (economizing speed, accuracy, and convergence), and the final values used in the analysis are: $D = 0.5$, $\Delta_d = 0.8$, $d_{jump} = 5$, $d_{min} = d_{jump}/500$, $n_i = 500$, and $n_{max} = 100$, for the isotropically defined four-dimensional free parameter space. An additional constraint was added to the rate change coefficients $C^{\pm}$, forcing them to be negative, such that wave energy higher than the equilibrium wave energy will cause erosion ($dS/dt < 0$ for $\Delta E > 0$) and wave energy less than the equilibrium wave energy will cause accretion ($dS/dt > 0$

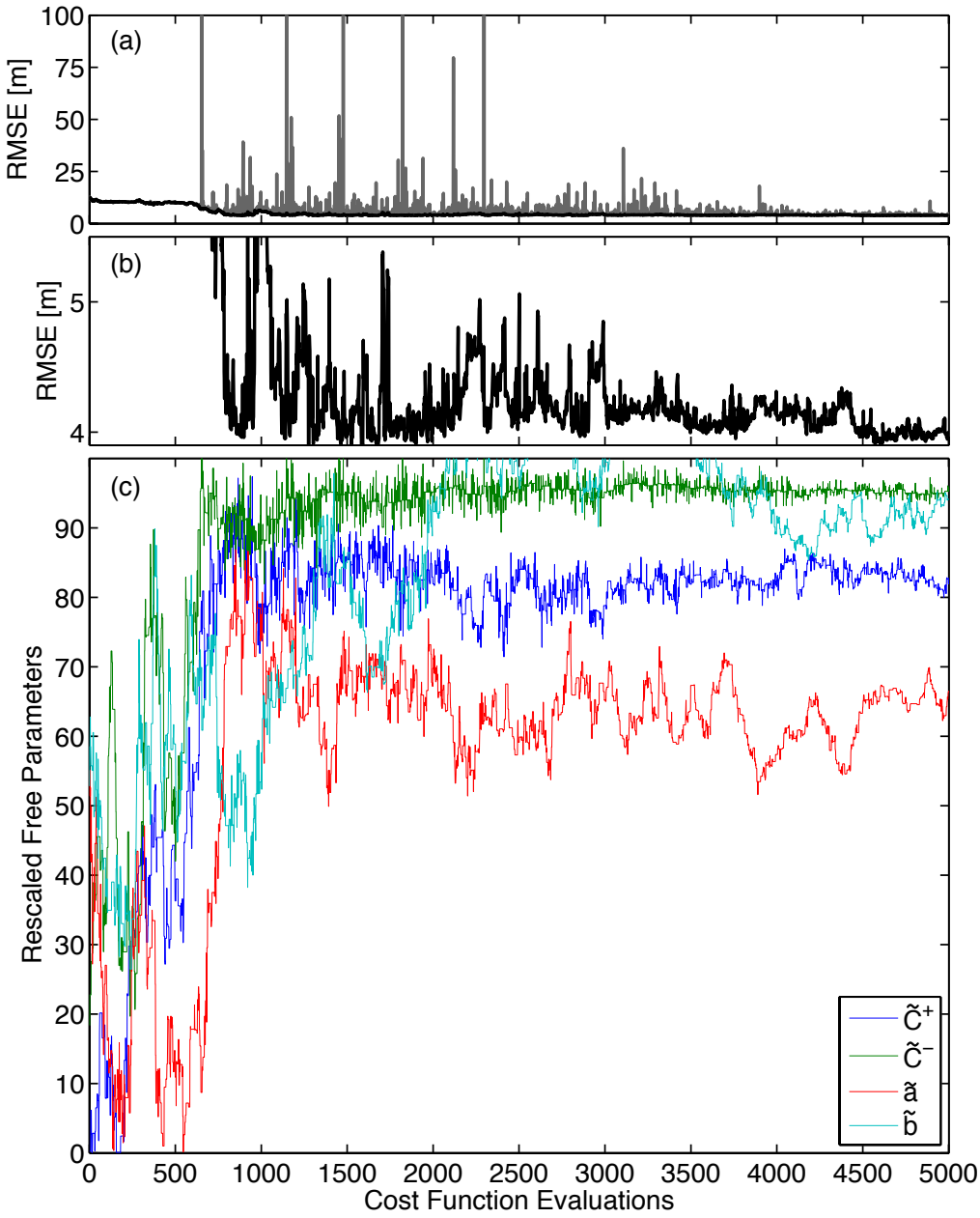

Figure C.1: Simulated annealing optimization: (a) progression of cost function (gray) being minimized, highlighting the accepted cost function evaluations (black), (b) closer view of the progression of accepted cost function values (black), and (c) progression of the free parameters (rescaled values) during the minimization.

for $\Delta E < 0$), as physically expected.

In this analysis, the simulated annealing algorithm performs a random walk through the free parameter space, evaluating the cost function (C.1) at each new location. The progression of the optimization code is shown at alongshore section T2 in Figure C.1. In Figure C.1a, each cost function evaluation is shown, with the accepted cost function evaluations (C.4) highlighted in black (Figure C.1b shows a closer view of the accepted evaluations only). The simulated annealing process began at a random location within the problem-specific boundaries of the four-dimensional free parameter space, evaluated the cost function at each random walk location, and decided whether to accept the new location by using the Metropolis algorithm (C.4). The Metropolis algorithm accepted all decreases in the cost function as steps toward the minimum value, and also accepted some increases in the cost function to insure that the minimization did not get trapped in a local minimum (e.g. increases in Figure C.1b). The random walk began with a large search radius (d_{jump}), which decreased with each iteration, as shown by the decreasing size of jumps in the parameter values in Figure C.1c. As a random walk process, the optimization technique made many (thousands of) cost function evaluations, slowly approaching the cost function's minimum value. The best fit free parameters were the final location accepted when the simulated annealing algorithm reached the minimum precision (d_{min}), and the cost function was minimized (e.g. Table C.3, simulated annealing for T2).

C.2 Surrogate management framework

Surrogate management framework (SMF), which is another derivative-free algorithm that is used to optimize multivariable nonlinear functions, was developed by Serafini (1998) and Booker et al. (1999). SMF takes advantage of two strategies commonly used in highly efficient derivative-free optimization problems: approximation modeling and pattern search methods. Approximation modeling

uses surrogate functions (i.e. polynomials, splines, and kriging functions) to approximate the cost function by interpolating between known values, and pattern search methods look for a minimum within the defined mesh, which is subsequently refined, rather than using derivatives of the function. SMF is an iterative process, alternating between the two methods.

In this analysis, SMF is used to minimize the cost function (C.1), following the method outlined by Booker et al. (1999) and Marsden et al. (2004). A uniform mesh was created with rescaled parameter values ranging from $0 \leq \tilde{p} \leq 100$ and equidistant point spacing [grid spacing is $100/(spc - 1)$, where $spc = 5$, initially] in all four-dimensions. A well-distributed set ($n_{pts} = 400$) of mesh points were selected using Latin hypercube sampling (McKay et al., 1979), and the cost function was evaluated (C.1) at each of the n_{pts} locations (e.g. gray shaded region in Figure C.2). The initial set of cost function evaluations were interpolated onto a surface using kriging via the Design and Analysis of Computer Experiments (DACE) Matlab toolbox (Lophaven et al., 2002). The kriging function interpolates between the selected mesh points to create a surface from which likely minima are identified. Due to the nature of this problem with many local minima, the search routine determines a number ($n_{sm} = 5$) of local minima in the kriging surface, which are mapped to the nearest mesh points, and the cost function is evaluated at these locations. If a new minimum is located, the kriging and searching processes are repeated until no new minima are located on the current surface.

When the search routine fails to find a new minimum, the poll routine begins by defining the poll point as the current minimum value in the mesh. The polling routine then evaluates the cost function at the closest mesh points that positively span the neighborhood surrounding the poll point. [Positively spanning vectors are a set of vectors that span the free parameter space with only positive linear combinations, with a minimum of $n + 1$ positively spanning vectors in an n-dimensional space (Marsden et al., 2004).] If a new minimum point is discovered in the polling routine, the kriging and searching process is repeated, including the

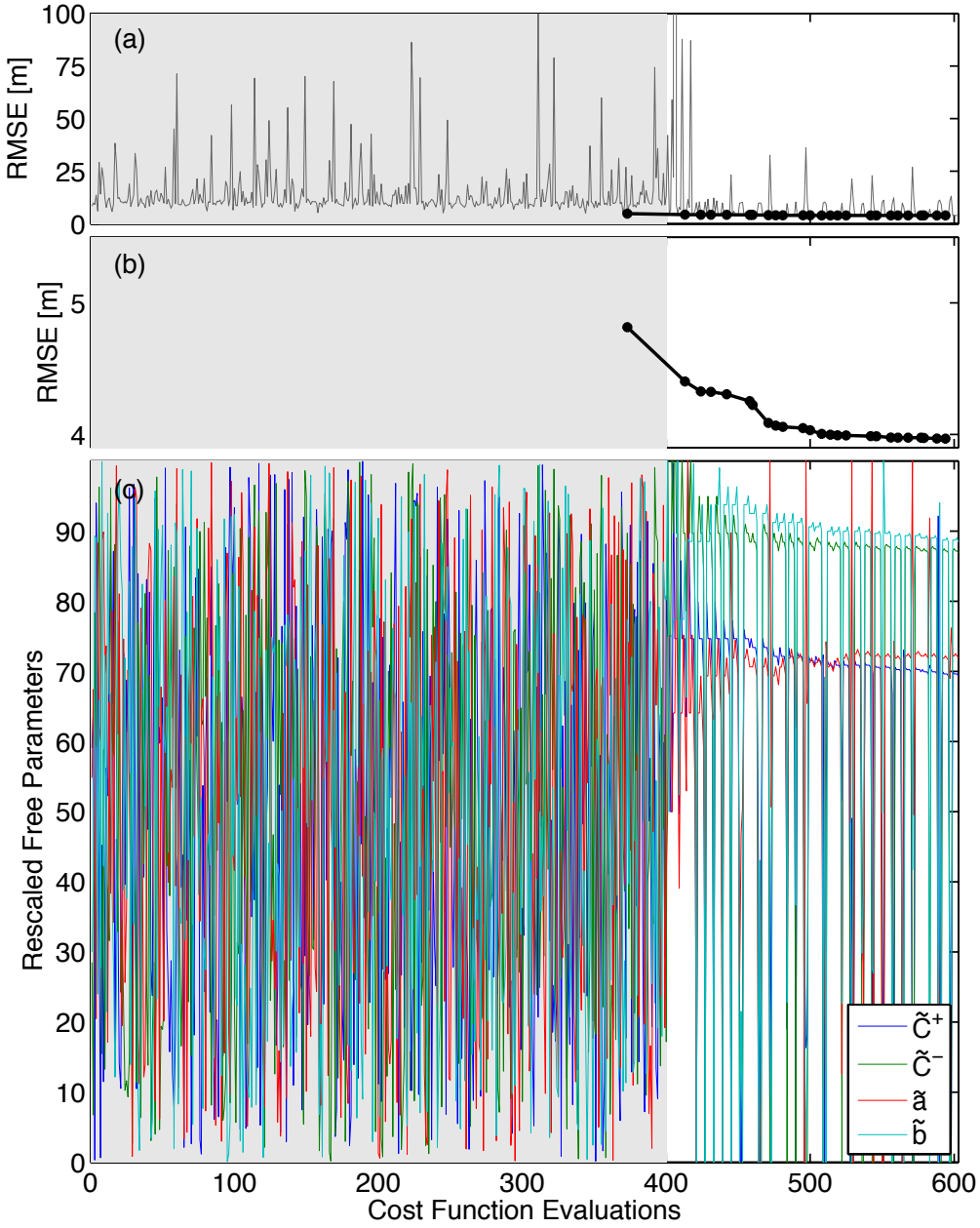

Figure C.2: Surrogate management framework (SMF) optimization: (a) progression of the cost function (gray) being minimized, highlighting the accepted cost function evaluations (black), (b) closer view of the progression of accepted cost function values (black), and (c) progression of the free parameters (rescaled values) during the minimization. The gray shaded area indicates the 400 randomly selected points in the free parameter space, which were sampled initially to create the first surrogate function.

new evaluations of the cost function at the poll point and the positively spanning neighbors, until no new minima are located on the current mesh. If the polling routine does not locate a new minimum, then the poll was unsuccessful, and the mesh is refined. The kriging and searching process then repeats iteratively with the polling process until convergence is reached.

Overall, SMF combines both approximation modeling of the cost function (with the surrogate functions) and pattern search methods (by polling near the minimum cost function values) to minimize the cost function. In the example at Torrey Pines Beach alongshore section T2, the gray shaded area in Figure C.2 indicates the 400 initial locations (Figure C.2c) at which the cost function was evaluated (Figure C.2a) to develop the initial surrogate function. The searching and polling routines then iteratively tested each possible minimum and the neighboring points, selecting each new minimum value found in this process (Figure C.2b). The mesh refinements often caused boundary points to be detected as minima (causing large variability in the values tested as possible minima in Figure C.2c). The mesh was refined no further when the mesh size reached a minimum spacing ($spc = 2000$, which is a minimum grid spacing of approximately 0.05). The best fit free parameters are the final location of the minimum cost function evaluation on the current mesh (e.g. Table C.3, SMF for T2).

Table C.2: Model RMS errors [m] with simulated annealing- (SA) and SMF-derived free parameters at each alongshore section at Torrey Pines.

	T1	**T2**	**T3**	**T4**	**T5**	**T6**	**T7**	**T8**
SA	3.3	4.0	4.2	3.8	4.2	5.1	4.6	5.8
SMF	3.3	4.0	4.0	3.6	3.8	4.7	4.4	5.2

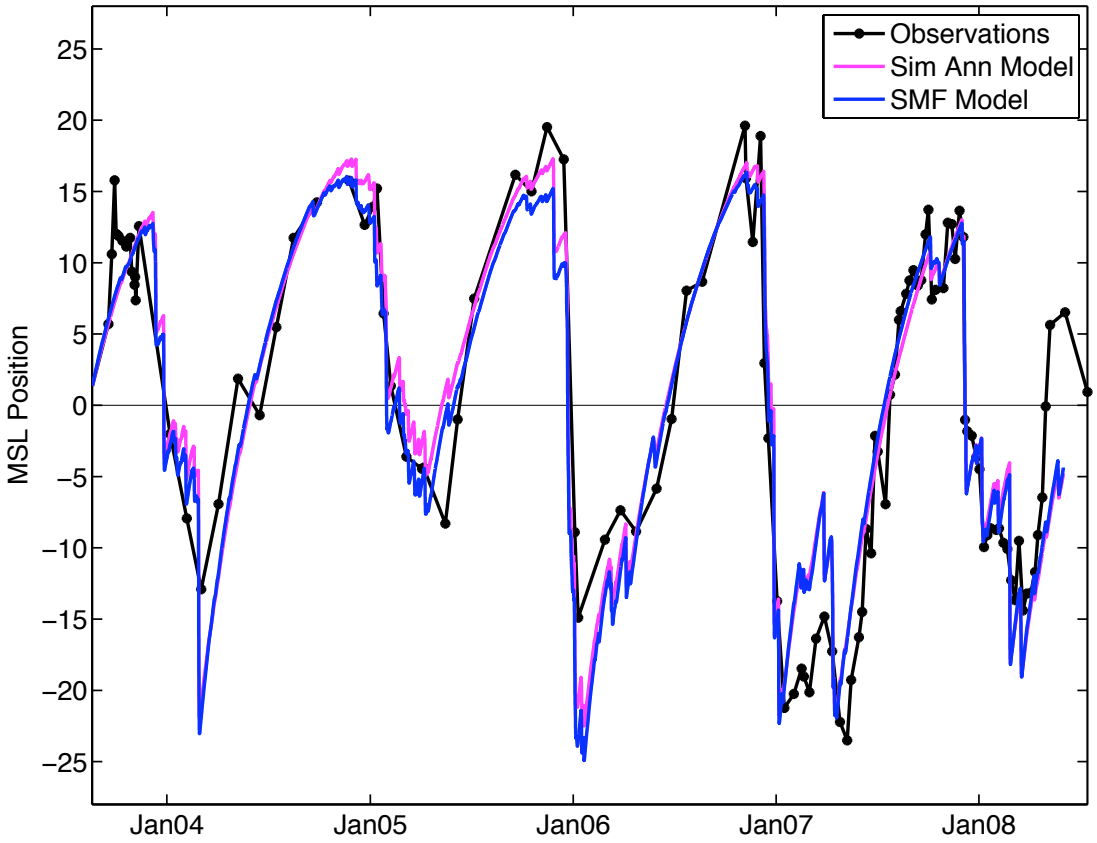

Figure C.3: Comparison of the observations (black) and the model results when the simulated annealing (magenta) and SMF (blue) optimization techniques are used to determine the model free parameters at alongshore section T2. The RMS errors between the observations and models are approximately 4.0 m for both cases.

C.3 Selecting an optimization technique

The model behavior, using the free parameters determined by simulated annealing and SMF, is very similar, with only small differences in the RMSE between the observations and model results (Table C.2). Figure C.3 (alongshore section T2) demonstrates the qualitatively similar model results, showing only small differences in the maximum eroded and accreted MSL position achieved due to differences in the model free parameters (Table C.3). While the four-dimensional free parameter space has many local minima, changes to the equilibrium slope a and change rate parameters $C^{\pm}$ can have compensating effects (discussed in section

Table C.3: The magnitudes of the four model free parameters for alongshore section T2, using simulated annealing (SA) and SMF. The model output is very similar (Figure C.3) using the free parameters determined by the two optimization techniques, with RMS errors of approximately 4.0 m in both cases.

	$\boldsymbol{a}$ (m^2/m)	$\boldsymbol{b}$ (m^2)	$\boldsymbol{C^+}$ ($m^{-1}s^{-1}$)	$\boldsymbol{C^-}$ ($m^{-1}s^{-1}$)
SA	-0.0037	0.14	-0.38	-1.37
SMF	-0.0035	0.12	-0.53	-1.23

4.6.2), causing only small quantitative changes in the model behavior. For example, the simulated annealing optimization technique found a minimum with a slightly steeper equilibrium slope a (Table C.3), which decreases the number of erosion events and lessens their impact (and increases the number of accretion events and their impact). The rate change coefficients compensated for the steeper slope with a slightly larger erosion rate coefficient C^- and a slightly smaller accretion rate coefficient C^+, causing little change in the model results (Figure C.3).

In general, the free parameters determined using the SMF algorithm produced smaller model RMS errors, and SMF was more computationally efficient, requiring many fewer cost function evaluations. At alongshore section T2, the simulated annealing optimization required approximately 5000 cost function evaluations (Figure C.1), while SMF required approximately 600 cost function evaluations (Figure C.2) to reach approximately the same cost function minimum. Thus, SMF was used in this analysis to determine the model free parameters due to the computational and time efficiency, and its ability to avoid getting trapped in local minima, thereby optimizing the model behavior and producing the smallest RMS errors.

References

Anthony, E., 1998: Sediment-wave parametric characterization of beaches. *J. Coastal Res.*, **14**(1), 347–352.

Aubrey, D., 1979: Seasonal patterns of onshore/offshore sediment movement. *J. Geophys. Res.*, **84**, 6347–6354.

Aubrey, D., Inman, D., and Winant, C., 1980: The statistical prediction of beach changes in southern California. *J. Geophys. Res.*, **85**, 3264–3276.

Bailard, J., 1981: An energetics total load sediment transport model for a plane sloping beach. *J. Geophys. Res.*, **86**, 938–954.

Barth, N., and Wunsch, C., 1990: Oceanographic experiment design by simulated annealing. *J. Phys. Ocean.*, **20**, 1249–1263.

Bascom, W., 1951: The relationship between sand size and beach-face slope. *Transactions, American Geophysical Union*, **32**(6), 866–874.

Battjes, J., 1974: Surf similarity. In *Proc. 14th Conference of Coastal Engineering*, 466–480. Copenhagen, Denmark, American Society of Civil Engineers.

Bodge, K., Olsen, E., and Creed, C., 1993: Performance of beach nourishment at Hilton Head Island, South Carolina. In *Proc. Coastal Zone '93*, 16–30. New York, American Society of Civil Engineers.

Booker, A., J.E., D., P.D., F., Serafini, D., Torczon, V., and M.W., T., 1999: A rigorous framework for optimization of expensive functions by surrogates. *Struct. Opt.*, **17**, 1–13.

Brock, J., Wright, C., Sallenger, A., Krabill, W., and Swift, R., 2002: Basis and methods of NASA Airborne Topographic Mapper lidar surveys for coastal studies. *J. Coastal Res.*, **18**, 1–13.

Browder, A., and Dean, R., 2000: Monitoring and comparison to predictive models of the Perdido Key beach nourishment project, Florida, USA. *Coast. Eng.*, **39**, 173–191.

Browder, A., and McNinch, J., 2006: Linking framework geology and nearshore morphology: Correlation of paleo-channels with shore-oblique sandbars and gravel outcrops. *Mar. Geol.*, **231**, 141–162.

Bruun, P., 1954: Coastal erosion and development of beach profiles. Technical Memorandum No. 44, U.S. Army Corps of Engineers, Washington.

Bryant, E., 1982: Behavior of grain size characteristics on reflective and dissipative foreshores, Broken Bay, Australia. *J. Sediment. Petrol.*, **52**(2), 431–450.

Capobianco, M., Hanson, H., Larson, M., Steetzel, H., Stive, M., Chatelus, Y., Aarninkhof, S., and Karambas, T., 2002: Nourishment design and evaluation: applicability of model concepts. *Coast. Eng.*, **47**, 113–135.

Carter, R., and Orford, J., 1984: Coarse clastic barrier beaches: A discussion of the distinctive dynamic and morphosedimentary characteristics. *Mar. Geol.*, **60**, 377–389.

CDBW and SCC, 2002: California beach restoration study. Technical report, California Department of Boating and Waterways and State Coastal Conservancy, Sacramento, CA.

Clarke, D., and Eliot, I., 1982: Description of littoral, alongshore sediment movement from empirical eigen-function analysis. *Journal of the Geological Society of Australia*, **29**, 327–341.

Cowell, P., Roy, P., and Jones, R., 1995: Simulation of large-scale coastal change using a morphological behaviour model. *Mar. Geol.*, **126**, 45–61.

CRA, 1997: California's ocean resources: An agenda for the future. Technical report, California Resources Agency, Sacramento, CA.

Creaser, G., Davis Jr., R., and Haines, J., 1993: Relationships between wave climate and performance of a recently n ourished beach, Indian Rocks Beach, Pinellas County, Florida. In *Proc. Coastal Zone '93*, 43–56. New York, American Society of Civil Engineers.

Dalrymple, R., 1992: Prediction of storm/normal beach profiles. *J. Wat., Port, Coast, Ocean Eng.*, **118**, 193–200.

Dean, R., 1973: Heuristic models of sand transport in the surf zone. In *Proc. Conference on Engineering Dynamics in the Surf Zone, Sydney, N.S.W.*, 208–214.

Dean, R., 1977: Equilibrium beach profiles: U.S. Atlantic and Gulf coasts. Technical Report No. 12, Department of Civil Engineering, University of Delaware.

Dean, R., 1991: Equilibrium beach profiles: Characteristics and applications. *J. Coastal Res.*, **7**, 53–84.

Dean, R., 2002: *Beach Nourishment: Theory and Practice*. World Scientific, River Edge, N.J.

Dong, P., and Zhang, K., 2002: Intense near-bed sediment motions in waves and currents. *Coastal Engineering*, **45**, 75–87.

Drake, T., and Calantoni, J., 2001: Discrete particle model for sheet flow sediment transport. *Journal of Geophysical Research*, **106**(C9), 19859–19868.

Dubois, R., 1990: Barrier-beach erosion and rising sea level. *Geology*, **18**, 1150–1152.

Edelman, T., 1968: Dune erosion during storm conditions. In *Proc. 11th Conf. Coast. Eng.*, 719–722. London.

Emery, K., 1961: A simple method of measuring beach profiles. *Limnology and Oceanpgraphy*, **6**(1), 90–93.

Farris, A., and List, J., 2007: Shoreline change as a proxy for subaerial beach volume change. *J. Coast. Res.*, **23**(3), 740–748.

Folk, R., 1974: *Petrology of sedimentary rocks*. Hemphill Publishing Company, Austin, Texas.

Gallagher, E., Elgar, S., and Guza, R., 1998: Observations of sand bar evolution on a natural beach. *Journal of Geophysical Research*, **103**(C2), 3203–3215.

Gares, P., Wang, Y., and White, S., 2006: Using LIDAR to monitor a beach nourishment project at Wrightsville Beach, North Carolina, USA. *J. Coastal Res.*, **22**, 1206–1219.

Gibeaut, J., Gutierrez, R., and Kyser, J., 1998: Increasing the accuracy and resolution of coastal bathymetric surveys. *J. Coastal Res.*, **14**(3), 1082–1098.

Guenther, G., Cunningham, A., LaRocque, P., and Reid, D., 2000: Meeting the accuracy challenge in airborne lidar bathymetry. In *Proc. 20th EARSeL Symposium: Workshop on Lidar Remote Sensing of Land and Sea*, CD–ROM, 1. Dresden, Germany, European Association of Remote Sensing Laboratories.

Haas, J., 2006: *Grain size and mineralogical characteristics of beach sand in the Oceanside Littoral, Southern California: implications for sediment provenance*. Master's thesis, University of California, San Diego.

Hamm, L., Capobianco, M., Dette, H., Lechuga, A., Spanhoff, R., and Stive, M., 2002: A summary of European experience with shore nourishment. *Coast. Eng.*, **47**, 237–264.

Hanson, H., Brampton, A., Capobianco, M., Dette, H., Hamm, L., Laustrup, C., Lechuga, A., and Spanhoff, R., 2002: Beach nourishment projects, practices, and objectives - a European overview. *Coast. Eng.*, **47**, 81–111.

Hapke, C., Reid, D., Richmond, B., Ruggiero, P., and List, J., 2006: National assessment of shoreline change:part 3: Historical shoreline changes and associated coastal land loss along sandy shoreline of the California coast. Open-file report 2006-1219, U.S. Geological Survey.

Haxel, J., and Holman, R., 2004: The sediment response of a dissipative beach to variations in wave climate. *Mar. Geol.*, **206**, 73–99.

Hoefel, F., and Elgar, S., 2003: Wave-induced sediment transport and sandbar migration. *Science*, **299**, 1885–1887. doi:10.1126/science.1081448.

Hogarth, L., Babcock, J., Driscoll, N., Le Dantec, N., J.K., H., Inman, D., and Master, P., 2007: Long-term tectonic control on Holocene shelf sedimentation offshore La Jolla, California. *Geol.*, **35**(3), 275–278. doi:10.1130/G23234A.1.

Holman, R., 1986: Extreme value statistics for wave run-up on a natural beach. *Coast. Eng.*, **9**, 527–544.

Houser, C., Hapke, C., and Hamilton, S., 2008: Controls on coastal dune morphology, shoreline erosion and barrier island response to extreme storms. *Geomorphology*, **100**, 223–240.

Hsu, T.-J., Jenkins, J., and Liu, P.-F., 2004: On two-phase sediment transport: Sheet flow of massive particles. *Proc. Roy. Soc. Lond. (A)*, **460**, 2223–2250. doi:10.1098/rspa.2003.1273.

Inman, D., Elwany, M., and Jenkins, S., 1993: Shorerise and bar-berm profiles on ocean beaches. *J. Geophys. Res.*, **98**(C10), 18181–18199.

Jackson, D., Cooper, J., and del Rio, L., 2005: Geological control of beach morphodynamic state. *Mar. Geol.*, **216**, 297–314.

Jiménez, J., Guillén, J., and Falqués, A., 2008: Comment on the article "morphodynamic classification of sandy beaches in low energetic marine environment" by gómez-pujol, l., orfila, a., cañellas, b., alvarez-ellacuria, a., méndez, f.j., medina, r. and tintoré, j. *Marine Geology*, 242, pp. 235-246, 2007. *Mar. Geol.*, **255**, 96–101.

Kamphius, J., 1991: Alongshore sediment transport rate. *J. Water., Port, Coast., Ocean Eng.*, **117**(6), 624–640.

Kirkpatrick, S., Gelatt, C., Jr., and Vecchi, M., 1983: Optimization by simulated annealing. *Science*, **220**(4598), 671–680.

Komar, P., 1998: *Beach Processes and Sedimentation*. Prentice Hall, Upper Saddle River, NJ, 2 edition.

Krabill, W., Wright, C., Swift, R., Frederick, E., Manizade, S., Yungel, J., Martin, C., Sonntag, J., Duffy, M., Hulslander, W., and Brock, J., 2000: Airborne laser mapping of Assateague National Seashore Beach. *Photogramm. Eng. Remote Sens.*, **66**, 65–71.

Kriebel, D., and Dean, R., 1993: Convolution method for time-dependent beach profile response. *J. Waterw. Port Coastal Ocean Eng.*, **119**, 204–226.

Larson, M., and Kraus, N., 1989: SBEACH: Numerical model for simulating storm-induced beach change. CERC, Technical Report CERC-89-9, U.S. Army Corps of Engineers, Vicksburg, Mississippi.

Larson, M., M. Capobianco, and Hanson, H., 2000: Relationship between beach profiles and waves at Duck, North Carolina, determined by canonical correlation analysis. *Mar. Geol.*, **160**, 275–288.

Lee, G., Nicholls, R., and Birkemeier, W., 1998: Storm-driven variability of the beach-nearshore profile at Duck, North Carolina, USA, 1981-1991. *Mar. Geol.*, **148**, 163–177.

List, J., and Farris, A., 1999: Large-scale shoreline response to storms and fair weather. In *Proc. Coastal Sediments '99, Amer. Soc. of Civil Eng. Reston, VA*, 1324–1338.

List, J., Farris, A., and Sullivan, C., 2003: Large-scale response of foreshore slope to storm events. In *Proc. Coastal Sediments 2003*. World Scientific Publishing Corp. and East Meets West Productions, Corpus Christi, Texas. ISBN 981-238-422-7. CD-ROM.

List, J., Farris, A., and Sullivan, C., 2006: Reversing storm hotspots on sandy beaches: Spatial and temporal characteristics. *Mar. Geol.*, **226**, 261–279.

Longuet-Higgins, M., 1970: Longshore currents generated by obliquely incident sea waves .1. *J. Geophys. Res.*, **75**, 6778–6790.

Lophaven, S., Nielsen, H., and Søndergaard, J., 2002: DACE: A Matlab kriging toolbox. Technical Report IMM-TR-2002-12, Technical University of Denmark, Kgs. Lyngby, Denmark.

Marine Board, 1995: *Beach Nourishment and Protection*. National Academy Press, Washington, D.C.

Marsden, A., Wang, M., Dennis, J., and Moin, P., 2004: Optimal aerocoustic shape design using the surrogate management framework. *Optimization and Engineering*, **5**, 235–262.

Masselink, G., and Short, A., 1993: The effect of tide range on beach morphodynamics and morphology: A conceptual beach model. *J. Coastal Res.*, **9**(3), 785–800.

McKay, M., Beckman, R., and Conover, W., 1979: A comparison of three methods for selecting values of input variables in the analysis of output from a computer code. *Technometrics*, **21**(2), 239–245.

McNinch, J., 2004: Geologic control in the nearshore: shore-oblique sandbars and shoreline erosional hotspots, Mid-Atlantic Bight, USA. *Mar. Geol.*, **211**, 121–144.

Metropolis, N., Rosenbluth, A., Rosenbluth, M., Teller, A., and Teller, E., 1953: Equation of state calculations by fast computing machines. *J. Chem. Phys.*, **21**(6), 1087–1092.

Miller, J., and Dean, R., 2004: A simple new shoreline change model. *Coast. Eng.*, **51**, 531–556.

Miller, J., and Dean, R., 2007a: Shoreline variability via empirical orthogonal function analysis: Part I temporal and spatial characteristics. *Coast. Eng.*, **54**, 111–131.

Miller, J., and Dean, R., 2007b: Shoreline variability via empirical orthogonal function analysis: Part II relationship to nearshore conditions. *Coast. Eng.*, **54**, 133–150.

Miselis, J., and McNinch, J., 2006: Calculating shoreline erosion potential using nearshore stratigraphy and sediment volume: Outer Banks, North Carolina. *J. Geophys. Res.*, **111**, F02019.

Mobley, C., 1994: *Light and Water: Radiative Transfer in Natural Waters*. Academic Press.

Morton, R., Gibeaut, J., and Paine, J., 1995: Meso-scale transfer of sand during and after storms: implications for prediction of shoreline movement. *Mar. Geol.*, **126**, 161–179.

Morton, R., Leach, M., Paine, J., and Cardoza, M., 1993: Monitoring beach changes using GPS surveying techniques. *J. Coastal Res.*, **9**, 702–720.

Muñoz Péréz, J., Medina, R., and Tejedor, B., 2001: Evolution of longshore beach contour lines determined by the E.O.F. method. *Scientia Marina*, **65**, 393–402.

Niedoroda, A., Reed, C., Swift, D., Arato, H., and Hoyanagi, K., 1995: Modeling shore-normal large-scale coastal evolution. *Mar. Geol.*, **126**, 181–199.

Nordstrom, K., 1989: Downdrift coarsening of beach foreshore sediments at tidal inlets: An example from the coast of New Jersey. *Earth Surf. Proc. Land.*, **14**, 691–701.

O'Reilly, W., and Guza, R., 1998: Assimilating coastal wave observations in regional swell predictions. part i: Inverse methods. *J. Phys. Oceanogr.*, **28**, 679–691.

O'Reilly, W., Seymour, R., Guza, R., and D., C., 1993: Wave monitoring in the southern california bight. In *Proc. 2nd International Symposium Ocean Wave Measurement and Analysis, New Orleans, LA*, 448–457.

Özkan Haller, H., and Brundidge, S., 2007: Equilibrium beach profile concept for Delaware beaches. *J. Wat., Port, Coast, Ocean Eng.*, **133**(2), 147–160. doi: 10.1061/(ASCE)0733-950X(2007)133:2(147).

Pawka, S., 1983: Island shadows in wave directional spectra. *J. Geophys. Res.*, **88**, 2571–2591.

Plant, N., Holman, R., and Freilich, M., 1999: A simple model for interannual sandbar behavior. *J. Geophys. Res.*, **104**(C7), 15755–15776.

Quartel, S., Kroon, A., and Ruessink, B., 2008: Seasonal accretion and erosion patterns on a microtidal sandy beach. *Mar. Geol.*, **250**, 19–33. doi: 10.1016/j.margeo.2007.11.003.

Raubenheimer, B., Guza, R., and Elgar, S., 2001: Field observations of wave-driven setdown and setup. *J. Geophys. Res.*, **106**, 4629–4638.

Revell, D., Komar, P., and Sallenger, A., 2002: An application of LIDAR to analyses of El Niño erosion in the Netarts littoral cell, Oregon. *J. Coastal Res.*, **18**, 792–801.

Robertson, W., Zhang, K., and Whitman, D., 2007: Hurricane-induced beach change derived from airborne laser measurements near Panama City, Florida. *Mar. Geol.*, **237**, 191–205.

Roelvink, J., and Stive, M., 1989: Bar-generating cross-shore flow mechanisms on a beach. *J. Geophys. Res.*, **94**, 4785–4800.

Ruessink, B., van Enckevort, I., Kingston, K., and Davidson, M., 2000: Analysis of observed two- and three-dimensional nearshore bar behaviour. *Mar. Geol.*, **169**, 161–183.

Ruggiero, P., Komar, P., McDougal, W., Marra, J., and Beach, R., 2001: Wave runup, extreme water levels and the erosion of properties backing beaches. *J. Coastal Res.*, **17**, 407–419.

Sallenger, A., Krabill, W., Brock, J., Swift, R., Manizade, S., and Stockdon, H., 2002: Sea-cliff erosion as a function of beach changes and extreme wave runup during the 1997-1998 El Niño. *Mar. Geol.*, **187**, 279–297.

Sallenger, A., Krabill, W., Swift, R., Brock, J., List, J., Hansen, M., Holman, R., Manizade, S., Sontag, J., Meredith, A., Morgan, K., Yunkel, J., Frederick, E., and Stockdon, H., 2003: Evaluation of airborne topographic lidar for quantifying beach changes. *J. Coastal Res.*, **19**, 125–133.

Saye, S., van der Wal, D., Pye, K., and Blott, S., 2005: Beach-dune morphological relationsips and erosion/accretion: An investigation at five sites in England and Wales using LIDAR data. *Geomorphology*, **72**, 128–155.

Schupp, C., McNinch, J., and List, J., 2006: Nearshore shore-oblique bars, gravel outcrops, and their correlation to shoreline change. *Mar. Geol.*, **233**, 63–79.

Self, R., 1997: Longshore variation in beach sands, Nautla area, Veracruz, Mexico. *J. Sediment. Petrol.*, **47**, 1437–1443.

Serafini, D., 1998: *A framework for managing models in nonlinear optimization of computationally expensive functions.* Ph.D. thesis, Rice University.

Seymour, R., Guza, R., O'Reilly, W., and Elgar, S., 2005: Rapid erosion of a small southern California beach fill. *Coast. Eng.*, **52**, 151–158.

Shepard, F., 1950: Beach cycles in southern California. Technical report, U.S. Army Corps of Engineers, Washington, D.C.,.

Sherman, D., 1991: Gravel beaches. *National Geographic Research and Exploration*, **7**, 442–452.

Shrestha, R., Carter, W., Sartori, M., Luzum, B., and Slatton, K., 2005: Airborne laser swath mapping: Quantifying changes in sandy beaches over time scales of weeks to years. *Photogramm. Eng. Remote Sens.*, **59**, 222–232.

Sonu, C., and James, W., 1973: A Markov model for beach profile changes. *J. Geophys. Res.*, **78**(9), 1462–1471.

Sorensen, R., Douglass, S., and Weggel, J., 1988: Results from the Atlantic City, NJ Beach Nourishment Monitoring Program. In *Proc. 21st Int. Conf. on Coastal Engineering*, 2806–2817. American Society of Civil Engineers, New York.

Stauble, D., and Kraus, N., 1993: Project performance: Ocean City, Maryland, proceedings of beach nourishment engineering and management considerations. In *Proc. Coastal Zone '93*, 1–15. New York, American Society of Civil Engineers.

Stive, M., Nicholls, R., and de Vriend, H., 1991: Sea-level rise and shore nourishment: a discussion. *Coast. Eng.*, **16**, 147–163.

Stockdon, H., Holman, R., Howd, P., and Sallenger, A., 2006: Empirical parameterization of setup, swash, and runup. *Coast. Eng.*, **53**, 573–588.

Stockdon, H., Sallenger, A., List, J., and Holman, R., 2002: Estimation of shoreline position and change using airborne topographic lidar data. *J. Coastal Res.*, **18**, 502–513.

Swart, D., 1974: Offshore sediment transport and equilibrium beach profiles. Technical Report Publ. No. 131, Delft Hydraulics Lab., Delft Univ. Technol.

Thomson, J., Elgar, S., Raubenheimer, B., Herbers, T., and Guza, R., 2006: Tidal modulation of infragravity wave via nonlinear energy losses in the surfzone. *Geophys. Res. Lett.*, **33**. doi:10.1029/2005GL025514. L05601.

Wehr, A., and Lohr, U., 1999: Airborne laser scanning - an introduction and overview. *Photogramm. Eng. Remote Sens.*, **54**, 68–82.

Wijnberg, K., and Terwindt, J., 1995: Extracting decadal moephological behavior from high-resolution, long-term bathymetric surveys along the holland coast using eigenfunction analysis. *Mar. Geol.*, **126**, 301–330.

Winant, C., Inman, D., and Nordstrom, C., 1975: Description of seasonal beach changes using empirical eigenfunctions. *J. Geophys. Res.*, **80**, 1979–1986.

Woolard, J., and Colby, J., 2002: Spatial characterization, resolution, and volumetric change of coastal dunes using airborne LIDAR: Cape Hatteras, North Carolina. *Geomorphology*, **48**, 269–287.

Work, P., 1993: Monitoring the evolution of a beach nourishment project. In *Proc. Coastal Zone '93*, 57–70. New York, American Society of Civil Engineers.

Wright, L., and Short, A., 1984: Morphodynamic variability of surf zones and beaches: A synthesis. *Mar. Geol.*, **56**, 93–118.

Wright, L., Short, A., and Green, M. O., 1985: Short-term changes in the morphodynamic states of beaches and surf zones: An empirical predictive model. *Mar. Geol.*, **62**, 339–364.

Yates, M., Guza, R., Gutierrez, R., and Seymour, R., 2008: A technique for eliminating water returns from lidar beach elevation surveys. *J. Atmos. Oc. Tech.*, **25**(9), 1671–1682.

Young, A., and Ashford, S., 2006: Application of airborne LIDAR for seacliff volumetric change and beach-sediment budget contributions. *J. Coastal Res.*, **22**, 307–318.

Zhang, K., Whitman, D., Leatherman, S., and Robertson, W., 2005: Quantification of beach changes caused by Hurricane Floyd along Florida's Atlantic Coast using airborne laser surveys. *J. Coastal Res.*, **21**, 123–134.